TECH LIBRARY KAFB, NM

0060709

NASA CONTRACTOR REPORT

NASA CR-1523

NASA CR-15

c. 1

EVALUATION OF THE GUST-ALLEVIATION CHARACTERISTICS AND HANDLING QUALITIES OF A FREE-WING AIRCRAFT

by Richard F. Porter and Joe H. Brown, Jr.

Prepared by
BATTELLE MEMORIAL INSTITUTE
Columbus, Ohio
for U. S. Army Aeronautical Research Laboratory
Ames Research Center

NATIONAL AERONAUTICS AND SPACE ADMINISTRATION • WASHINGTON, D. C. • APRIL 1970

TABLE OF CONTENTS

TABLE OF CONTENTS
(Continued)

SUMMARY

An analytical investigation was performed to evaluate the dynamic characteristics of aircraft employing an unconventional wing, free to pivot freely about a spanwise axis forward of its aerodynamic center and subject only to aerodynamic moments imposed by lift and drag forces and a trailing-edge control tab. The left and right wing panels operate independently, with symmetrical tab displacement being used to control the angle of attack and differential tab deflections causing asymmetric panel deflections for lateral control.

Three hypothetical subsonic aircraft were considered, ranging in gross weight from 3000 to 50,000 pounds. The influence of the free-wing concept was determined by comparing the turbulence penetration performance and handling qualities for each free-wing aircraft and the equivalent conventional aircraft.

It was found that the free-wing concept has natural gust-alleviation characteristics which greatly reduce the perturbations in atmospheric turbulence. The most dramatic reductions are in normal load-factor increments, vertical path displacements, and roll disturbances.

While longitudinal handling qualities appear to be satisfactory, an artificial roll damper was found to be beneficial to the lateral control characteristics because of inherent low roll damping and spiral divergence. With the roll damper augmentation, the lateral-directional control characteristics are excellent. The very powerful roll control provided by differential panel displacements, and the reduced gust sensitivity, would be particularly beneficial during low-speed approaches in rough air.

INTRODUCTION

Background

Operation in atmospheric turbulence is an inescapable fact of life for any aircraft. Although turbulence severe enough to endanger the structure is rare and avoidable, milder regions of rough air are present in even the finest weather. The unavoidable turbulence is frequently found at lower levels and is caused by thermal drafts or mechanical mixing of the air over rough terrain.

The frequency and extent of exposure to turbulence depends strongly, of course, on the nature of the aircraft's mission. For high performance aircraft engaged in flights over longer distances, the low-level turbulence is encountered only during climb-out and approach. Furthermore, these aircraft are characterized by high wing loadings which attenuate much of the ride discomfort. By contrast, many military and commercial flight operations are conducted at relatively low altitudes and with aircraft having low wing loadings. Examples of the latter type are aircraft for military observation and liaison missions and commercial pipeline-patrol flights.

Although professional crew members may develop a high tolerance for ride discomfort, prolonged operation in the turbulent environment is physically exhausting and mission performance seems certain to be degraded. Furthermore, an encounter with gusty air during landing approach forces the pilot to adopt higher approach speeds which compromise the short-field capabilities of the aircraft. In particular, the degradation of lateral control power has been a limitation on the maximum performance capability of some STOL aircraft in rough-air approaches.

Attempts have been made to provide artificial gust alleviation by sensing flow changes and actuating either conventional or special control surfaces. This attack on the problem has merit but has not been completely explored; however, available results indicate that the more effective gust-alleviation systems may require considerable mechanical and electronic complexity.

The unconventional wing concept explored in this study is a more fundamental approach to the gust-alleviation problem in that no sensing devices or special control actuators are employed. Instead, the free-wing concept makes use of the natural alleviation caused by the fact that a stable lifting surface tends to maintain a prescribed lift coefficient by responding to natural pitching moments which accompany changes in flow direction.

The Free-Wing Concept

As defined in this report, a free-wing aircraft differs from a conventional airplane in that the two panels of the fuselage-mounted wing are free to move independently about a spanwise axis and are controlled by means of trailing-edge control tabs. Each wing panel is completely free to rotate about its spanwise axis, subject to aerodynamic moments but otherwise unrestricted by mechanical constraints. To provide static pitching stability, the axis of rotation is located forward of the chordwise center of pressure of the wing

panel, as shown in Figure 1. The wing is brought to an equilibrium angle of attack through a balance of moments created by the trailing-edge tab, which is controlled by the pilot, and the torques produced by the lift and drag forces.

Longitudinally, the pitching motion of the wing is mechanically uncoupled from the rest of the aircraft, and the vehicle may be considered a "flying wing" with all parts of the aircraft, except the wing itself, hanging freely from the spanwise axis of rotation. For lateral-directional motion, no analogy to any other type of aircraft exists, since the left and right wing panels are free to rotate independently.

The basic concept of the free wing was disclosed in U. S. Patent No. 2,347,230, now expired, issued in 1944 to Mr. Daniel R. Zuck, who built a small prototype aircraft in 1945 as a private venture. This aircraft was never successfully flown, and no analytical work to predict the dynamic behavior of such an aircraft is known to have been performed.

Several potential benefits of the free-wing design were cited by the inventor and these can be supported by intuitive arguments. The most significant claim is that of reduced sensitivity to atmospheric turbulence.

All stable aircraft tend to relieve the normal load-factor response to vertical gusts, for example, by pitching into the relative wind to maintain the equilibrium lift coefficient. The rapidity of the alleviating motion depends upon the pitching moment of inertia. Although reflecting a somewhat oversimplified view, it may be argued that significant normal load-factor increments do not occur at frequencies below the natural short-period frequency since these components are attenuated by the pitching of the aircraft.

The wing alone will certainly have a much lower moment of inertia in pitch than the entire aircraft; consequently, its natural frequency will be much higher, and a greater portion of the gust spectrum will be alleviated. In addition, the energy content of the spectral components of the atmospheric turbulence falls off sharply with frequency. This is seen in Figure 2 which represents a typical power spectral density (PSD) function for vertical gust velocity.

The PSD function may be regarded as the relative portion of the total turbulence energy which is contained in an infinitesimal bandwidth about a given wavelength corresponding to the value of the spatial frequency, Ω. Figure 2 displays the characteristic, common to all such atmospheric turbulence models, of sharply reduced energy content at the higher frequencies.

On the basis of the preceding information, it is logical to expect the free-wing aircraft to exhibit reduced vertical turbulence responses.
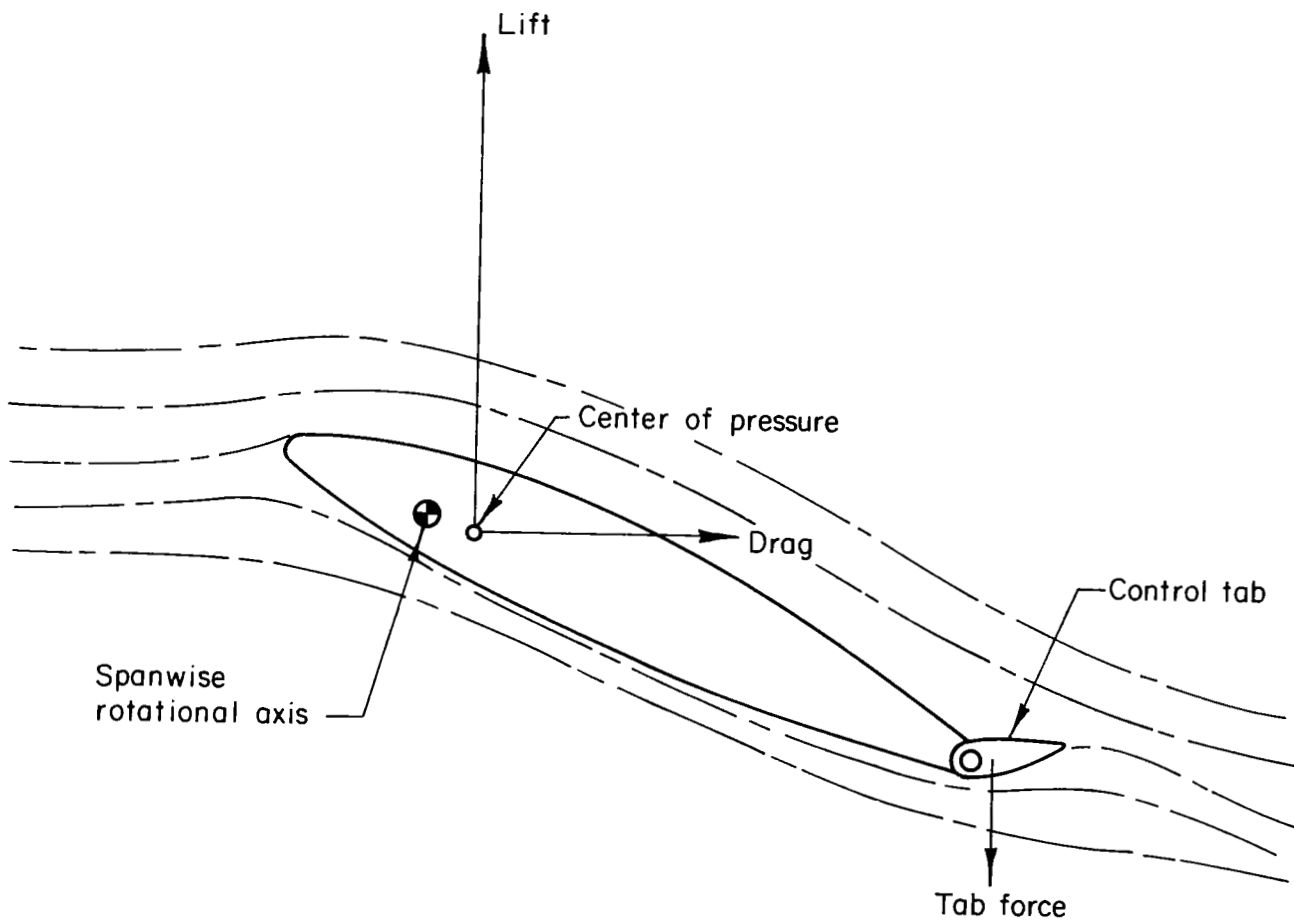
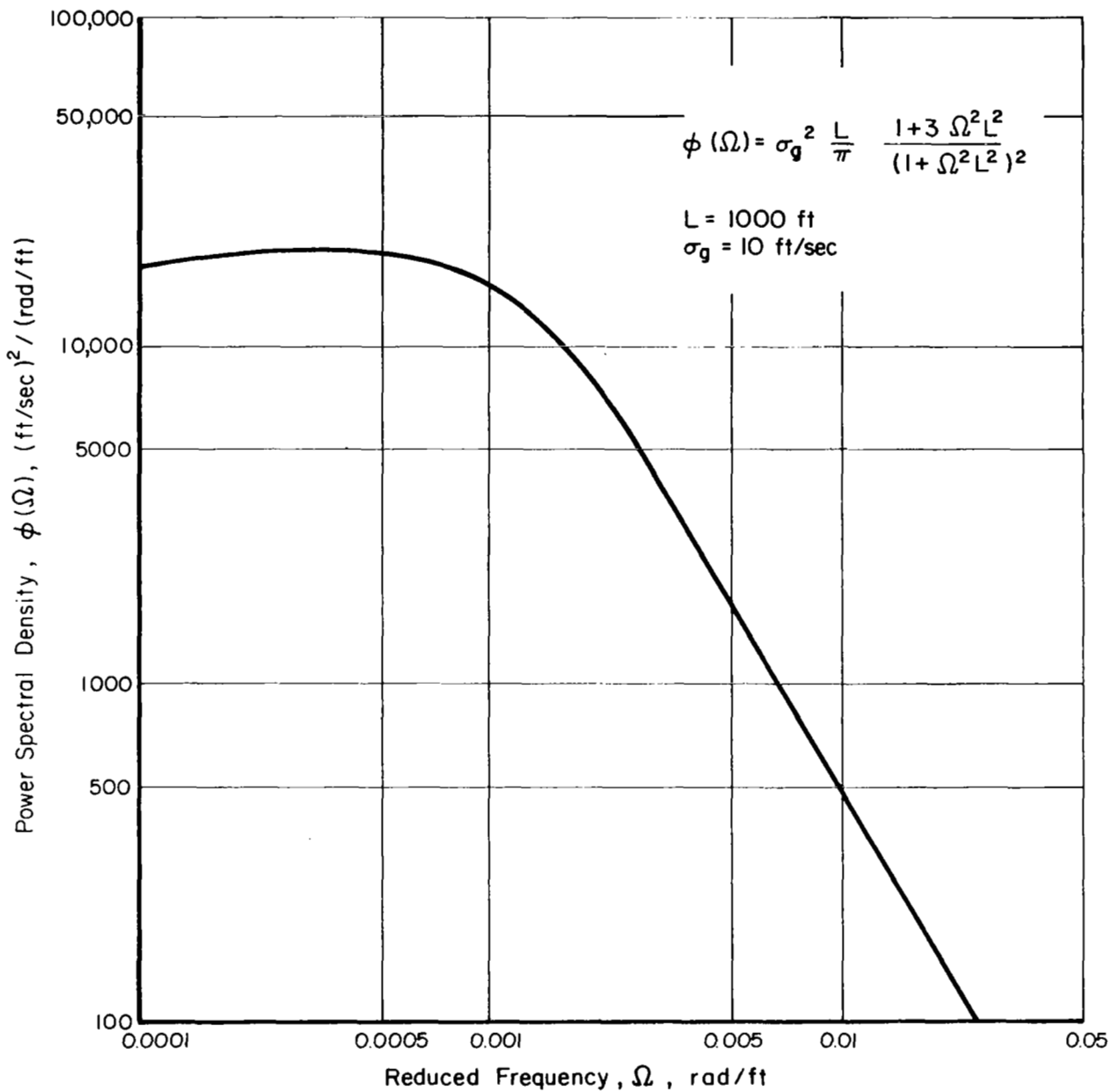FIGURE 1. CROSS-SECTIONAL ILLUSTRATION OF THE FREE WING

FIGURE 2. POWER SPECTRAL DENSITY REPRESENTATION OF
ATMOSPHERIC TURBULENCE

Additional benefits which might be expected are improved maneuvering capability because of the rapid panel responses and differential deflections, possible beneficial stall behavior because the tab may not be capable of developing a full wing stall, and various configuration improvements made possible by the removal of direct pitch coupling between the fuselage and wing.

It should also be noted at this point that some variations of the basic free-wing concept may have merit, although they are not explored in this study. In particular, it is possible that some beneficial effects may be obtained by a partial restraint of the wing rotation, in the form of a spring or a damper device. Additional variations might include the use of physical interconnects between wing and tail surfaces.

On the debit side, some penalties may be inherent in the free-wing concept. These might include the weight and drag increments caused by the structural complexity of the pivot supports, and the induced drag penalties caused by imperfect sealing of the wing-fuselage gap.

Scope

The research effort described in this report is an analysis of the primary effects of the free-wing concept upon turbulence operation and gross handling qualities, designed to provide a first-order evaluation of some of the potential benefits described above and to expose any inherent eccentricities which might offset these advantages.

Attention was confined to linear analyses of turbulence responses and certain handling qualities, for both longitudinal and lateral-directional motion. No evaluation was made of nonlinear phenomena such as stall characteristics, nor was consideration given to performance effects or possible unique design features.

The turbulence responses were evaluated by computing root-mean-square (rms) values of pertinent output variables in response to continuous atmospheric turbulence, but no attempt was made to evaluate, directly, the riding qualities as affected by human tolerance factors.

Only those handling qualities phenomena which are inherently affected by the free-wing aircraft were evaluated. These factors include the stability of characteristic modes and the nature of certain open- and closed-loop control behavior, but exclude consideration of control force gradients.

6

SYMBOLS

The following symbols are used in the main body of this report; additional symbols are defined in each appendix, as required.

$\bar{c}$ = mean aerodynamic chord, feet

C_{l_p} = roll-damping-stability derivative

$C_{l_{\delta_P}}$ = slope of roll-moment coefficient vs. right-wing-panel displacement

$C_{m_{L_{\delta_P}}}$ = slope of left-panel pitching-moment coefficient vs. right-panel displacement

$C_{m_{R_p}}$ = slope of right-panel pitching-moment coefficient vs. non-dimensional roll rate

$C_{m_{R_{\delta_P}}}$ = slope of right-panel pitching-moment coefficient vs. right-panel displacement

C_{m_β} = slope of right-wing-panel pitching moment vs. slideslip angle

C_{n_p} = slope of yawing-moment coefficient vs. nondimensional roll rate

$C_{n_{\delta_P}}$ = slope of yawing-moment coefficient vs. right-wing-panel displacement

C_p = gain constant, aileron deflection per unit roll rate, seconds

C_φ = gain constant, aileron deflection per unit roll angle

D_y = lateral path displacement, feet

g = acceleration of gravity, feet/$\sec^2$

h = vertical path displacement, feet

I_{XX_T} = total moment of inertia about roll axis, slug-ft^2

I_{XY_P} = X-Y product of inertia of right wing panel, slug-ft^2

I_{XZ_T} = X-Z total product of inertia, slug-ft^2

$I_{y'}$ = moment of inertia of each wing panel about hinge axis, slug-ft^2

I_{YZ_P} = Y-Z product of inertia of right wing panel, slug-ft^2

I_{ZZ_T} = total moment of inertia about yaw axis, slug-ft^2

j = unit imaginary number, $\sqrt{-1}$

K_θ = gain constant, elevator deflection per unit pitch angle

L = scale length of atmospheric turbulence, feet

L_p = roll damping coefficient, 1/second

L_{p_w} = wing contribution to roll damping coefficient, 1/second

L_r = coefficient of roll moment due to yaw rate, 1/second

L_{δ_P} = coefficient of roll moment due to right-wing-panel displacement, 1/second^2

$L_{\delta_{t_R}}$ = coefficient of roll moment due to right-control-tab displacement, 1/second^2

L_β = coefficient of roll moment due to sideslip, 1/second^2

m_p = mass of one wing panel, slugs

M_q = fuselage pitch damping coefficient, 1/second

M_{R_p} = coefficient of right-wing-panel pitching moment due to roll rate, 1/second

M_{R_β} = coefficient of right-wing-panel pitching moment due to sideslip, 1/second^2

$M_{R_{\delta_P}}$ = coefficient of right-wing-panel pitching moment due to right-panel displacement, 1/second^2

$M_{R_{\delta_L}}$ = coefficient of right-wing-panel pitching moment due to left-panel displacement, 1/second^2

$M_{R_{\delta_{t_R}}}$ = coefficient of right-wing-panel pitching moment due to right-tab displacement, $1/\text{second}^2$

$M_{R_{\delta_{t_L}}}$ = coefficient of right-wing-panel pitching moment due to left-tab displacement, $1/\text{second}^2$

$M_{R_{\dot{\delta}}}$ = coefficient of right-wing-panel pitching moment due to angular rate, $1/\text{second}$

M_{α} = fuselage pitching-moment coefficient due to angle of attack, $1/\text{second}^2$

$M_{\dot{\alpha}}$ = fuselage pitching-moment coefficient due to angle of attack rate, $1/\text{second}$

M_{δ_P} = fuselage pitching moment due to symmetric panel displacement, $1/\text{second}^2$

$M_{\ddot{\delta}_P}$ = fuselage pitching moment due to panel rotational acceleration

M_{v_g} = fuselage pitching moment due to vertical gust velocity, $1/\text{feet-second}$

$M_{\dot{v}_g}$ = fuselage pitching moment due to vertical-gust acceleration, $1/\text{feet}$

N_p = coefficient of yawing moment due to roll rate, $1/\text{second}$

N_{p_w} = wing contribution to N_p, $1/\text{second}$

N_r = yaw damping coefficient, $1/\text{second}$

N_{β} = coefficient of yawing moment due to sideslip, $1/\text{second}^2$

N_{δ_P} = coefficient of yawing moment due to right-wing-panel displacement, $1/\text{second}^2$

$N_{\delta_{t_R}}$ = coefficient of yawing moment due to right-control-tab displacement, $1/\text{second}^2$

P = area of each free-wing panel, feet^2

P_q = panel-pitching-moment coefficient due to pitch rate, $1/\text{second}$

$P_{\dot{q}}$ = panel-pitching-moment coefficient to pitch acceleration

9

$P_{\dot{u}}$ = panel-pitching-moment coefficient due to longitudinal acceleration, 1/second

P_{v_g} = panel-pitching-moment coefficient due to vertical gust velocity, 1/feet-second

P_{α} = panel-pitching-moment coefficient due to angle of attack, $1/\text{second}^2$

$P_{\dot{\alpha}}$ = panel-pitching-moment coefficient due to angle of attack, rate, 1/second

P_{δ_e} = panel-pitching-moment coefficient due to symmetrical tab displacement, $1/\text{second}^2$

P_{δ_P} = panel-pitching-moment coefficient due to symmetrical panel displacement, 1/second

$P_{\dot{\delta}_P}$ = panel-pitching-moment coefficient due to panel displacement rate, 1/second

$P_{\ddot{\delta}_P}$ = panel-pitching-moment coefficient due to panel acceleration

p = roll rate, radians/second except when indicated

r = yaw rate, radians/second except when indicated

U = true airspeed, feet/second

u = dimensionless airspeed variable, $\Delta U/U$

V_g = vertical-gust velocity, feet/second

X_u = longitudinal force coefficient due to airspeed, 1/second

X_{v_g} = longitudinal force coefficient due to vertical-gust velocity, 1/feet

X_{α} = longitudinal force coefficient due to angle of attack, 1/second

X_{θ} = longitudinal force coefficient due to pitch angle, 1/second

X_{δ_P} = longitudinal force coefficient due to wing-panel displacement, 1/second

X'_{cg} = position of wing-panel center of gravity forward of hinge axis, in percent of $\bar{c}$

Y_p = coefficient of side force due to roll rate, 1/second

Y_r = coefficient of side force due to yaw rate, 1/second^2

Y_β = coefficient of side force due to sideslip, 1/second^2

Y_{δ_P} = coefficient of side force due to asymmetric panel displacement, 1/second^2

Z_q = coefficient of normal force due to pitch rate, 1/second

$Z_{\dot{q}}$ = coefficient of normal force due to pitch acceleration

Z_u = coefficient of normal force due to airspeed, 1/second^2

Z_{v_g} = coefficient of normal force due to vertical gust velocity, 1/feet-second

Z_α = coefficient of normal force due to angle of attack, 1/second^2

$Z_{\dot{\alpha}}$ = coefficient of normal force due to angle of attack rate, 1/second

Z_{δ_e} = coefficient of normal force due to symmetrical tab displacement, 1/second^2

Z_{δ_P} = coefficient of normal force due to symmetrical wing-panel displacement, 1/second^2

$Z_{\dot{\delta}_P}$ = coefficient of normal force due to panel rate, 1/second

$Z_{\ddot{\delta}_P}$ = coefficient of normal force due to panel acceleration

α_f = inertial angle of attack of fuselage angle between longitudinal axis and projection of inertial velocity vector in plane of symmetry, radians

β = inertial sideslip angle, angle between longitudinal axis and projection of inertial velocity vector in horizontal plane, radians

β_g = sideslip gust velocity, lateral gust velocity divided by airspeed

δ_a = aileron deflection, or asymmetric tab deflection, numerically equal to displacement of right tab, radians

δ_e = elevator deflection, or symmetrical tab deflection, radians

δ_P = displacement angle of right wing panel with respect to fuselage axis, radians

θ = pitch angle of longitudinal fuselage axis with respect to horizon, radians

λ = Laplace operator, 1/second

ρ = atmospheric density, slugs/feet^3

σ_g = rms gust intensity, feet/second

τ_R = roll-mode time constant, seconds

φ = roll angle, radians

$\dot{\varphi}_g$ = rolling gust, 1/second

Φ = power spectral density of gust velocity, (feet/second)^2/(radians/foot)

Φ_{n_z} = power spectral density of normal acceleration, (g units)^2/(radians/foot)

Φ_{n_y} = power spectral density of lateral acceleration, (g units)^2/(radians/foot)

$\Phi_{\dot{\varphi}}$ = power spectral density of roll rate (radians/sec)^2/(radians/foot)

$\Phi_{\dot{\psi}}$ = power spectral density of yaw rate (radians/sec)^2/(radians/foot)

Ψ = yaw angle, radians

Ω = reduced, or spatial, frequency, radians/foot.

PROCEDURE

Free-Wing Static and Dynamic Characteristics

An initial decision was made to include unsteady aerodynamic effects in the longitudinal motion of the free wings, but to limit the lateral-directional aerodynamic representation to that provided by conventional stability derivatives augmented by new derivatives peculiar to the split free wing.

As a first step, an assessment was made of the necessary control-tab geometry required to provide trim lift coefficients throughout the expected linear range. The chosen geometry was then held constant for the remainder of the program.

Transfer functions were developed to approximate the unsteady aerodynamic effects on wing panels undergoing symmetrical pitching and plunging, and a brief study was made of the dynamics of the wing free only in pitch. This cursory examination illustrated the effect of the unsteady aerodynamics on the natural frequency in pitch and provided a rational basis for the quasi-static panel damping derivative (panel pitching moment per unit angular rate) in the lateral-directional equations which follow.

Except for the aforementioned damping derivative, the lateral-directional-stability derivatives of the split free wing were computed from classical lifting line theory, using a finite trigonometric series to describe the spanwise circulation distribution, and an iterative procedure to determine the series coefficients which satisfied the boundary conditions. The desired stability derivatives were then computed from the series coefficients, including new derivatives which occur because of the panel rotational degrees of freedom. Details of the tasks described above are given in Appendix B.

Hypothetical Aircraft

To provide a direct assessment of the effects of the free-wing concept, three basic hypothetical aircraft were chosen and each was examined in two versions: as a free-wing aircraft and as a conventional fixed-wing airplane.

The aircraft were chosen to represent light observation and transport vehicles ranging in weight from 3000 pounds to 50,000 pounds. Furthermore, two flight conditions were considered for each aircraft: one representative of cruise flight for that class of airplane, and the other an approach condition at roughly 1.3 stall speed. These aircraft are described in more detail in

13

Appendix C, but some of the gross characteristics are given in Table I. A subscript attached to each aircraft designates its wing planform, two aspect ratios and two taper ratios being considered.

TABLE I. HYPOTHETICAL AIRCRAFT

| Desig-nation | Description | Aspect Ratio | Taper Ratio | Span, ft | Gross Weight, lb | Wing loading, lb/ft^2 | Cruise | | Approach | |
							Alt., ft	True Speed, knots	Alt., ft	True Speed, knots
A_1	Light obser-vation	8.	1.0	41.4	3,000	14.	5,000	118.	1,000	74
A_2	"	8.	0.6	41.4	3,000	14.	5,000	118.	1,000	74
A_3	"	6.	1.0	35.8	3,000	14.	5,000	118.	1,000	74
A_4	"	6.	0.6	35.8	3,000	14.	5,000	118.	1,000	74
B_1	Utility trans-portation	8.	1.0	54.6	12,500	33.5	10,000	197.	1,000	115
B_2	"	8.	0.6	54.6	12,500	33.5	10,000	197.	1,000	115
B_3	"	6.	1.0	47.3	12,500	33.5	10,000	197.	1,000	115
B_4	"	6.	0.6	47.3	12,500	33.5	10,000	197.	1,000	115
C_1	Light freighter	8.	1.0	116.3	50,000	29.6	20,000	219.	1,000	108
C_2	"	8.	0.6	116.3	50,000	29.6	20,000	219.	1,000	108
C_3	"	6.	1.0	100.7	50,000	29.6	20,000	219.	1,000	108
C_4	"	6.	0.6	100.7	50,000	29.6	20,000	219.	1,000	108

Equations of Motion

The complete nonlinear equations of motion were developed as described in Appendix A. With each wing panel free to move independently, the complete equations described a dynamic system with eight degrees of freedom. These eight degrees of freedom are related to the eight independent variables required to identify the instantaneous state of the system: six conventional

variables to define the spatial position and orientation of the fuselage assembly, and two additional variables to define the respective left- and right-wing-panel displacements with respect to the fuselage.

The complete set of equations were then linearized about a straight and level equilibrium flight condition. The linearization process permitted the separation of the equations into two uncoupled sets describing the lateral-directional and longitudinal motions separately; made possible the direct computation of characteristic roots which greatly simplified the assessment of handling qualities; and permitted the use of conventional power spectral density techniques for turbulence-response calculations.

The linearized set of equations describing the longitudinal motion of the aircraft in response to vertical gust velocities is given in Equation (1).

$$[A] \begin{bmatrix} \alpha_f \\ \theta \\ \delta_P \\ u \\ \delta_e \\ h \end{bmatrix} = \begin{bmatrix} -Z_{v_g} \\ -M_{\dot{v}_g}\lambda - M_{v_g} \\ -P_{v_g} \\ -X_{v_g} \\ 0 \\ 0 \end{bmatrix} V_{g_v} \tag{1}$$

where the matrix of coefficients is:

$$[A] = \begin{bmatrix} (-Z_{\dot{\alpha}}\lambda + Z_\alpha) & (Z_{\dot{q}}\lambda^2 + Z_q\lambda) & (Z_{\ddot{\delta}_P}\lambda^2 + Z_{\dot{\delta}_P}\lambda + Z_{\delta_P}) & Z_u & Z_{\delta_e} & 0 \\ (M_{\dot{\alpha}}\lambda + M_\alpha) & (-\lambda^2 + M_q\lambda) & (M_{\ddot{\delta}_P}\lambda^2 + M_{\delta_P}) & 0 & 0 & 0 \\ (P_{\dot{\alpha}}\lambda + P_\alpha) & (P_{\dot{q}}\lambda^2 + P_q\lambda) & [(-1 + P_{\ddot{\delta}_P})\lambda^2 + P_{\dot{\delta}_P}\lambda + P_{\delta_P})] & P_u\lambda & P_{\delta_e} & 0 \\ X_\alpha & X_\theta & X_{\delta_P} & -\lambda + X_u & 0 & 0 \\ 0 & K_\theta & 0 & 0 & -1 & 0 \\ -U & U & 0 & 0 & 0 & -\lambda \end{bmatrix}$$

$$\tag{2}$$

15

These equations are written with respect to a stability axis system with origin at the center of gravity of the aircraft. The first four equations of the set represent the translational motion normal to the longitudinal axis, pitching motion of the fuselage, wing-panel pitching about the hinge axis, and longitudinal acceleration. The fifth equation of the set permits feeding back a pitch-angle signal to elevator deflection (symmetrical tab displacement), while the last equation represents the kinematic relationship between inertial flight-path angle and rate of climb.

The set of equations is more complex than Equation (2) indicates because eight of the coefficients, namely, Z_α, Z_q, $Z_{\dot\delta P}$, $Z_{\delta P}$, P_α, P_q, $P_{\dot\delta P}$ and $P_{\delta P}$, contain a first-order transfer function representing the lag in the circulatory lift buildup following a change in angle of attack. This complication required a special technique for the numerical expansion of the determinant of the coefficients to obtain the characteristic equation. This is discussed further in Appendix E.

Only the vertical component of turbulence was considered for longitudinal motion, since the head-on component has little influence except at very low frequencies.

When represented as a polynomial in the operator λ, the determinant of the coefficients of Equation (2) became a ninth-order expression. One of the roots of this characteristic equation was always zero, leaving eight roots to describe the longitudinal modes of the system.

As derived in Appendix A, the lateral-directional motion of the aircraft system was permitted to be perturbed by spanwise gradients of vertical gust velocity, and by lateral gust velocities and gradients. Mathematically the gust disturbances appear as rolling gusts and sideslip gusts as shown in Equation (3).

$$
[B]
\begin{bmatrix}
\varphi \\
\Psi \\
\beta \\
\\
\delta_P \\
\delta_a \\
D_y
\end{bmatrix}
=
\begin{bmatrix}
-L_{P_w} \\
-N_{P_w} \\
0 \\
\\
-M_{R_p} \\
0 \\
0
\end{bmatrix}
\dot\varphi_g
+
\begin{bmatrix}
-L_\beta \\
-N_\beta - N_r \lambda \\
-Y_\beta \\
\\
-2M_{R_\beta} \\
0 \\
0
\end{bmatrix}
\beta_g
\qquad (3)
$$

16

where the matrix of coefficients of the homogeneous equations, $[B]$, is given by:

$$
[B] = \begin{bmatrix}
(-\lambda^2 + L_p\lambda) & (\dfrac{I_{XZ_T}}{I_{XX_T}}\lambda^2 + L_r\lambda) & L_\beta & 2(\dfrac{I_{XY_P}}{I_{XX_T}}\lambda^2 + L_{\delta_P}) & 2L_{\delta_{t_R}} & 0 \\[2ex]
(\dfrac{I_{XZ_T}}{I_{ZZ_T}}\lambda^2 + N_p\lambda) & (-\lambda^2 + N_r\lambda) & N_\beta & 2(\dfrac{I_{YZ_P}}{I_{ZZ_T}}\lambda^2 + N_{\delta_P}) & 2N_{\delta_{t_R}} & 0 \\[2ex]
(Y_p\lambda + \dfrac{g}{U}) & (Y_r - 1)\lambda & (-\lambda + Y_\beta) & 2Y_{\delta_P} & 0 & 0 \\[2ex]
(\dfrac{I_{XY_P}}{I_{y'}}\lambda^2 + M_{R_p}\lambda) & \dfrac{I_{YZ_P}}{I_{y'}}\lambda^2 & 2M_{R_\beta} & (-\lambda^2 + M_{R_{\dot\delta}}\lambda + M_{R_{\delta_P}} - M_{R_{\delta_L}}) & (M_{R_{\delta_{t_R}}} - M_{R_{\delta_{t_L}}}) & 0 \\[2ex]
(C_p\lambda + C_\varphi) & 0 & 0 & 0 & -1 & 0 \\[2ex]
0 & U & U & 0 & 0 & -\lambda
\end{bmatrix}
$$

(4)

The first three of the equations of this set are very similar to the ordinary rolling, yawing, and lateral translation equations of conventional aircraft. The fourth equation describes the asymmetric motion of the wing panels, the fifth permits the use of a closed-loop control of aileron in response to bank angle and roll rate, while the last is the kinematic relationship for lateral path displacement.

The expansion of the determinant of the coefficients of Matrix B yielded an eighth-order characteristic equation, but for stick-fixed motion, two of the roots were zero, leaving six nonzero roots to describe the lateral-directional characteristic modes.

Equations (1) and (3) required the estimation of numerous aerodynamic coefficients and nondimensional stability derivatives of the complete aircraft. The estimation procedure is outlined in Appendix D.

Handling-Qualities Evaluation

The primary reference for handling-qualities requirements was the revised military handling-qualities specification, Reference 1. For longitudinal motion, the phugoid damping and the short-period frequency and damping were compared with the specification requirements. In addition, the ability of the

pilot to damp long-period oscillations by monitoring fuselage attitude was examined. This feature is not specifically required by Reference 1, but was incorporated in this study because of the unconventional nature of the free-wing aircraft.

For lateral-directional motion, the characteristic roots were used to check compliance with dutch-roll damping requirements, roll-mode time-constant specifications and permissible rates of divergence in the spiral mode. In addition, the closed loop roll control characteristics were evaluated using a simple pilot transfer function.

Responses to Atmospheric Turbulence

The responses of the aircraft to atmospheric turbulence were computed using the power spectral density techniques outlined in Appendix E. Except in selected instances, all responses were computed for stick-fixed motion to provide a simple basis for comparison.

For the purpose of comparing the free-wing and fixed-wing statistical responses, the rms values of selected variables were computed from truncated spectra which eliminated all harmonic components below a temporal frequency of 0.3 radians per second. These low-frequency disturbances are easily controlled by pilot action, and in some cases, a static instability of the spiral mode would have rendered the output spectrum meaningless at zero frequency.

For longitudinal disturbances, only vertical gust components were considered, and the Dryden PSD function of Figure 2 was used, with a scale length of 1000 feet, and an rms gust intensity of 1 foot per second.

For lateral-directional motion, the combined effects of uncorrelated rolling and side gusts were computed, and these were based upon the same basic spectral density function as was used for the longitudinal motion.

18

DISCUSSION OF RESULTS

Isolated Free-Wing Characteristics

Static Characteristics

A necessary first step in this study was an investigation of control-tab requirements, and a cursory examination of the dynamic characteristics of the free wing to identify possible difficulties caused by pitching-mode instabilities of the wing itself. The details of this work are found in Appendix B.

Considering the static characteristics, it was found that no difficulty would be encountered in providing sufficient control power for symmetrical pitching. The effects of a 10 percent chord, sealed, plain-flap control were examined in detail, using two-dimensional characteristics from Reference 2, and a symmetrical airfoil section with zero pitching moment at zero lift. Only operation in the linear lift curve range was considered.

The control deflection required for trim is shown in Figure 3 for a wing of infinite aspect ratio, for several values of hinge margin. The hinge margin used here is the distance, in percent of chord, that the hinge axis is forward of the quarter-chord line.

In Figure 4, the same information is shown for finite wings with aspect ratios of 8 and 6 and taper ratios of 0.6 and 1. Although these data are idealized in that the flattening of the lift curve near the stall is ignored and the tab effectiveness is independent of angle of attack, it seems clear that no problems are likely to be encountered in providing sufficient control power for the free-wing panels.

Dynamic Characteristics

The dynamic characteristics of the free-wing panels are quite complicated. As mentioned earlier in this report, the evaluation of the stall characteristics was outside the scope of this study, but there is evidence that a possibility exists of single-degree-of-freedom torsion flutter near the stall. Rainey (Reference 3), for example, examined the characteristics of a two-dimensional wing oscillating about its midchord axis and found large regions of reduced frequency and angle of attack near the stall, where negative damping exists.
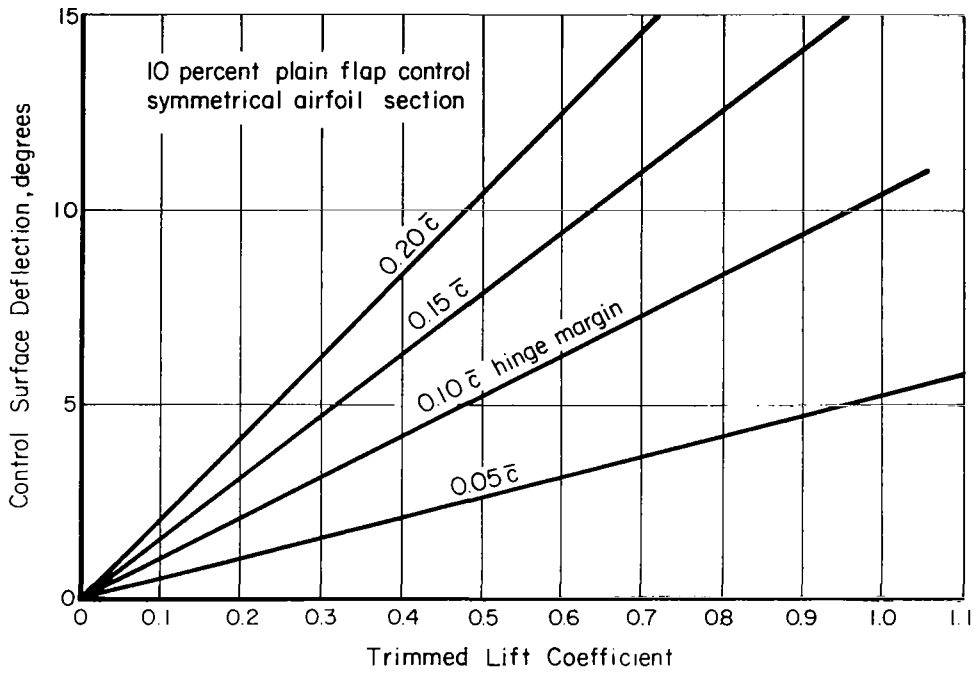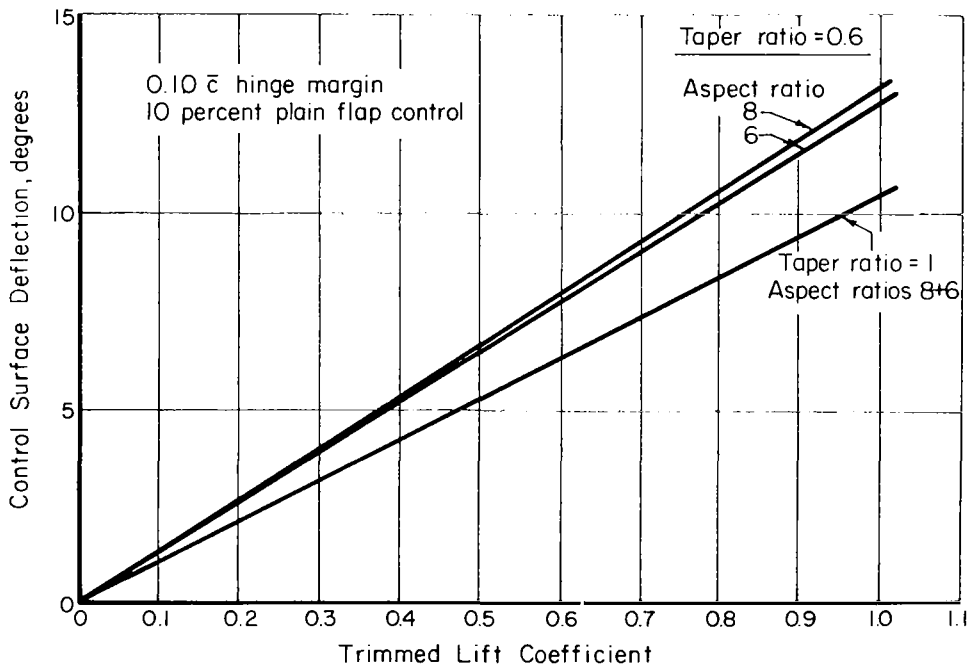
FIGURE 3. TWO-DIMENSIONAL TRIM CHARACTERISTICS

FIGURE 4. FINITE WING TRIM CHARACTERISTICS

On the other hand, available data, such as that contained in Reference 4, indicates that single-degree-of-freedom torsion flutter is no threat at mean angles of attack in the linear range for the mass parameters and hinge-axis locations envisioned for free-wing aircraft.

Aside from flutter considerations, the pitching dynamics of the free wing are interesting because of the effect of short-period natural frequency upon the response to vertical gusts. The importance of the natural frequency prompted an examination of the influence of unsteady aerodynamic forces upon the pitching mode.

Following Jones (Reference 5), a wing with an aspect ratio of 6 was considered to be free to rotate in pitch about a spanwise axis forward of the aerodynamic center. The lift force on the wing was composed of circulatory contributions and virtual mass forces. Using Jones' exponential approximation to the indicial lift growth function, a transfer function was derived relating circulatory lift coefficient to angle of attack, as outlined in Appendix B.

The characteristic equation of the wing free only in pitch was derived assuming that the pitching moment was caused by both the circulatory and apparent mass components of the lifting forces acting through their respective moment arms. This equation is given in Appendix B as Equation B-22. The dimensionless roots of this characteristic equation, a cubic, were found to be functions of two parameters only, the static hinge margin and a mass parameter as shown in Figure 5. The static hinge margin is the distance, in percent of chord, that the hinge axis is located forward of the wing aerodynamic center. Aside from the oscillatory mode shown, a stable real root also exists for all cases studied. It should be mentioned that the hinge margin and mass parameter are not independent for an actual wing because the pitching moment of inertia is a function of pivot location.

To assess the importance of the unsteady aerodynamic forces, the frequencies of oscillation for a hinge margin of 10 percent were compared with those obtained by ignoring all forces but that caused by multiplying the instantaneous angle of attack by the static lift curve slope. This comparison is shown in Figure 6, and the importance of unsteady aerodynamic forces is evident when the mass parameter is small.

The mass parameters of the free wings used in this study were typically about 10, so the conclusion was reached that unsteady aerodynamic effects were necessary to describe the longitudinal wing motion. These effects were incorporated into the derivation of the complete longitudinal equations. For lateral-directional motion, unsteady aerodynamic effects, as such, were not used, but the wing-panel damping coefficients were based upon the damping observed in the longitudinal motion.

Dimensionless root = a ± jb

To dimensionalize, multiply roots by $\frac{2U}{\bar{c}}$

0.25 $\bar{c}$ hinge margin

Values of mass parameter

Aspect ratio 6

0.10 $\bar{c}$

0.05 $\bar{c}$

Mass parameter = $\frac{8I_{y'}}{\rho P \bar{c}^3}$

Imaginary Axis

Real Axis a
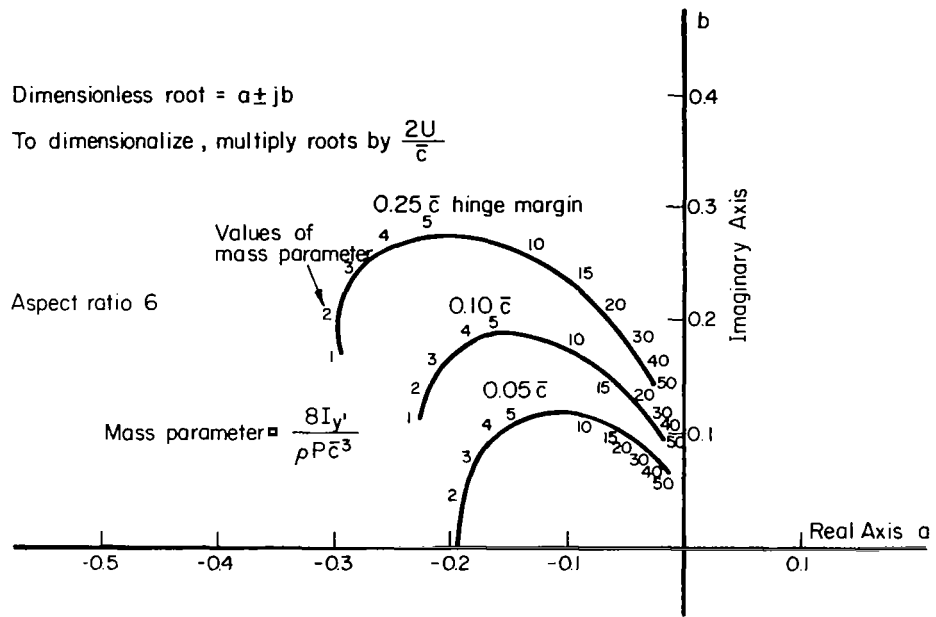
FIGURE 5. ONE-DEGREE-OF-FREEDOM OSCILLATORY MODE ROOTS

0.10 $\bar{c}$ hinge margin
Aspect ratio 6

Static lift force only

With unsteady aerodynamics

Imaginary Component of Dimensionless Root

Mass Parameter, $\frac{8I_{y'}}{\rho P \bar{c}^3}$
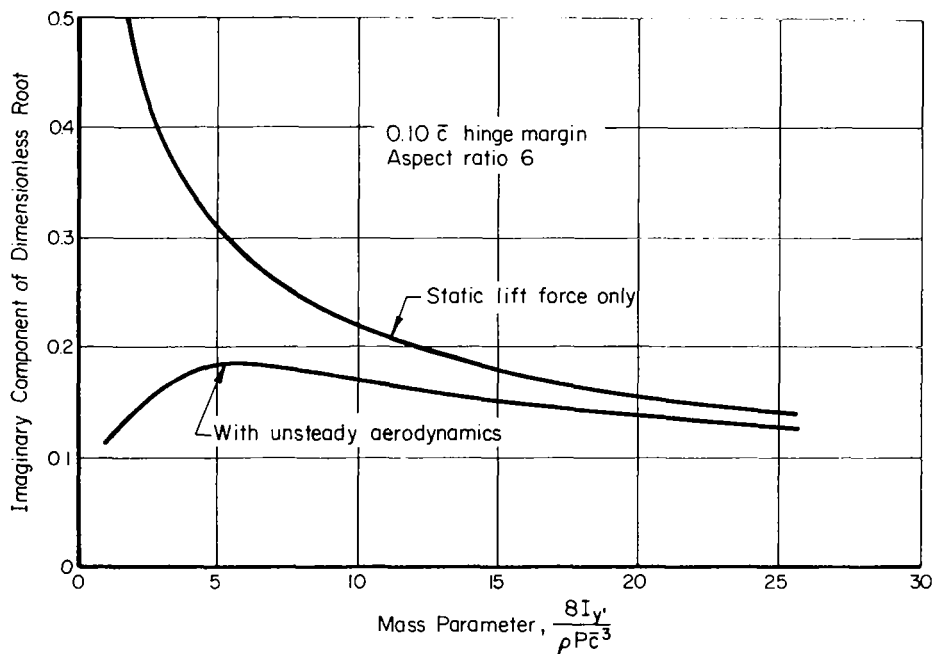
FIGURE 6. EFFECT OF UNSTEADY AERODYNAMICS ON
NATURAL FREQUENCY

22

Longitudinal Motion

Free-Wing Characteristic Modes

Additional Modes. The longitudinal motion of a conventional rigid aircraft with controls fixed is adequately described by a set of equations yielding four characteristic roots. These four roots are typically divided into two complex pairs: one defining the long period phugoid mode, and the other pair representing the longitudinal short period motion. In contrast, as derived in Appendix A, the linearized set of equations describing the longitudinal dynamics of the free-wing aircraft will generally yield four additional characteristic roots. In addition to the phugoid and short-period mode, a rapid oscillatory mode and two heavily damped aperiodic modes appear for the free wing with unsteady aerodynamic effects included.

The nature of these modes can be illustrated by considering a particular example. Table II lists the characteristic roots for the light, observation class aircraft with an aspect ratio of 6, in the cruise condition. The fixed-wing aircraft can be compared with three versions of the free-wing aircraft obtained by varying the hinge axis location and the horizontal tail volume.

TABLE II. LONGITUDINAL CHARACTERISTIC ROOTS

Aircraft A_3, Cruise

Mode	Fixed Wing	10% Panel Margin Nominal Tail Volume	10% Panel Margin 1/2 Tail Volume	20% Panel Margin Nominal Tail Volume
Phugoid	$-0.0228 \pm j\,0.180$	$-0.0239 \pm j\,0.226$	$-0.0239 \pm j\,0.226$	$-0.0240 \pm j\,0.226$
Short period	$-4.41 \pm j\,2.73$	$-2.89 \pm j\,6.65$	$-1.49 \pm j\,5.01$	$-3.11 \pm j\,6.87$
Symmetric Wing-Panel Mode		$-8.90 \pm j\,12.2$	$-8.60 \pm j\,12.04$	$-10.5 \pm j\,16.4$
Aperiodic		-22.3	-22.9	-23.4
		-20.5	-20.1	-20.5

The phugoid mode is little affected by the free-wing concept, as would be expected in view of the relatively minor effect of short-term pitching dynamics on this long-period motion.

The short period roots are changed in magnitude when comparing fixed-wing and free-wing versions, and, more importantly, the function of the short-period mode described by these roots is changed considerably. The free-wing short-period roots describe a motion which is largely confined to pitching of the fuselage assembly about the hinge axis, with only a minor normal-load-factor contribution caused by aerodynamic forces associated with pitch-rate-induced aerodynamic forces on the horizontal tail. The short-period mode of a conventional aircraft dominates the normal-load-factor response to turbulence and control inputs; in the free-wing aircraft, this function is assumed by the symmetrical wing-panel mode.

Sample Longitudinal Responses. Figure 7 illustrates time histories of the control responses of the fixed-wing aircraft of Table II and its free-wing counterpart with 10 percent panel margin and 1/2 the fixed-wing horizontal tail volume. The most striking effect of the free wing in these motions is the greatly reduced time required to reach the peak load factor. As mentioned above, this is a consequence of the fact that the symmetric wing-panel mode dominates the initial response. As seen in Table II, the natural frequency of the wing-panel mode is more than four times as high as the fixed-wing short period mode. Consequently, peak load factor is reached in approximately one-fourth the time.

The wing-panel-deflection history in Figure 7 appears to contain a residual damped oscillation in the short period mode. This is rather misleading since the panel deflection is measured with respect to the fuselage, and it is the residual pitching motion of the fuselage which gives this appearance to this trace. The wing-panel displacement with respect to a fixed horizontal reference does not contain a significant component in the short-period mode.

The reduction in the damping ratio of the free-wing short period mode is caused primarily by the loss of the Z_α damping effect which contributes significantly to the fixed-wing short-period damping.

Another interesting observation from Figure 7 is the fact that the angle of attack of the free-wing aircraft's fuselage assembly responds to longitudinal control exercised through the wing control tabs even though no mechanical pitch coupling between wing and fuselage exists. This phenomenon is a result
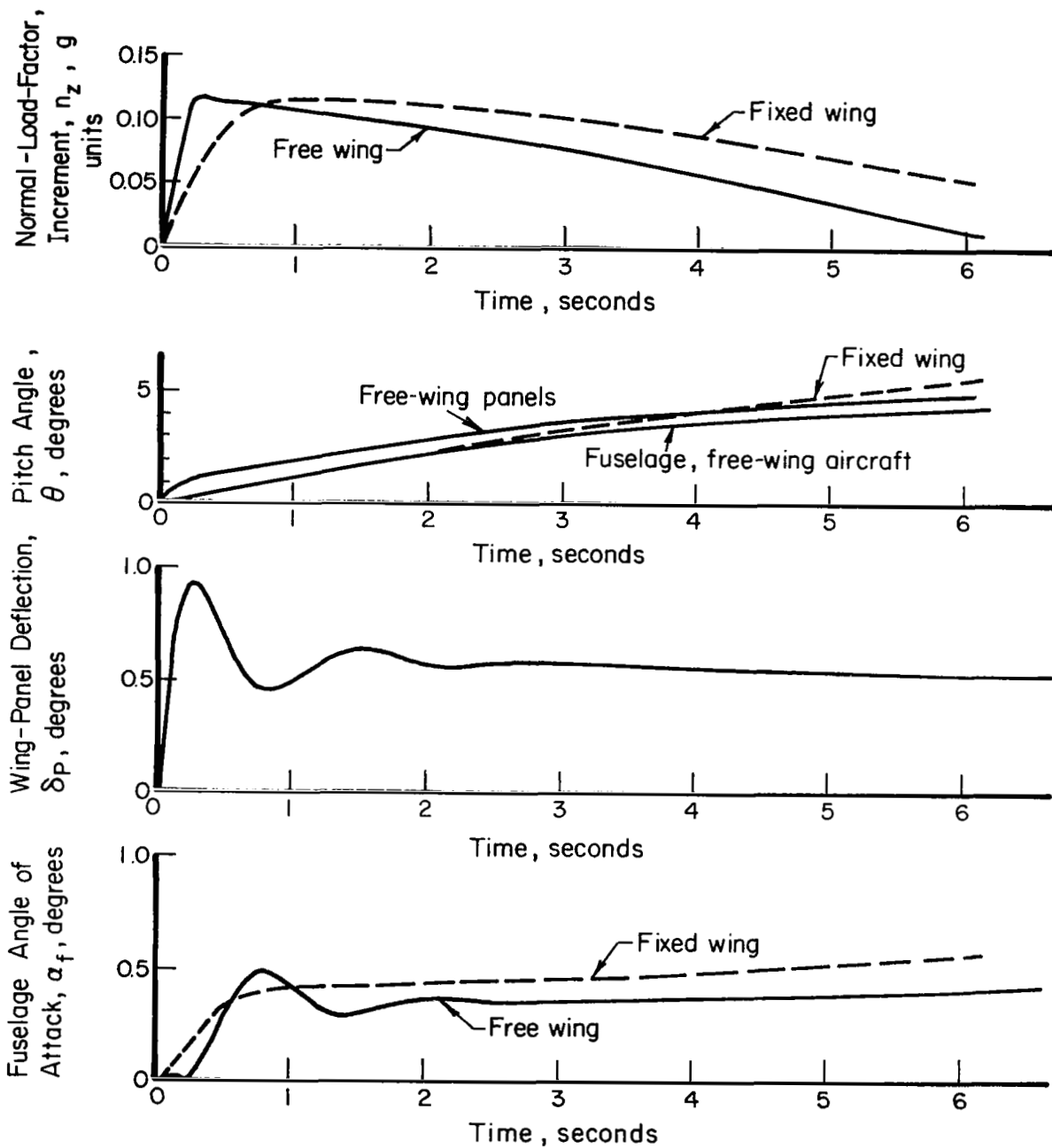
FIGURE 7. COMPARISON OF RESPONSES TO STEP
LONGITUDINAL CONTROL INPUT

Aircraft A₃, Cruise

of the increase in the downwash angle at the horizontal tail when the lift coefficient of the wing is increased. This is a beneficial effect, from the handling qualities standpoint, and will be discussed later.

Further insight into the longitudinal behavior can be obtained from Figure 8 which demonstrates the effect of the free-wing on the encounter with an isolated vertical gust. The assumed gust has the commonly used "1-cosine" shape with a period of 1 second, corresponding to a 200-foot wavelength, and a peak velocity of 10 feet per second.

The dramatic reduction in load-factor response is apparent, as is the reason — the ability of the wing panel to deflect rapidly into the updraft as opposed to the relative sluggishness of the fixed-wing aircraft pitch angle response. The net result is a reduction of over 4 to 1 in the positive load-factor peak and an attenuation of better than 2.5 to 1 in the negative transient.

Once again, it should be noted that the wing-panel deflection plotted in Figure 8 is measured with respect to the fuselage whose pitch-angle oscillation is also shown. After the gust has subsided, it should be observed that the fuselage pitch angle and wing-panel deflection traces are virtually equal and opposite, demonstrating that the true wing panel motion has subsided and the predominant motion is in fuselage pitching.

Effect of Parameter Variations. With regard to the fuselage pitching motion, it was found that the frequency and damping of the oscillation (the free-wing short period mode) are strongly influenced by the horizontal tail volume. In some cases, reducing the tail volume to 1/4 the nominal value gave better turbulence response than that obtained with either the nominal or 1/2 nominal values. In other cases, 1/2 nominal tail volume seemed best. A number of possibilities exist for improving the pitch response. Fixed auxiliary damping surfaces, mechanical interconnects between wing deflection and tail surface displacement, wing pivot restraints by means of springs or dashpots, or a simple pitch rate SAS operating through the horizontal tail could be investigated in any particular design. Again referring to Table II, and comparing the nominal tail volume roots with those for the 1/2-tail-volume case, the evidence is clear that changing the free-wing short period mode characteristics has a negligible effect on the other modes. Because of this, artificial improvement in the fuselage pitching motion would not be expected to have any adverse effects on other motions. In fact, since the short-period mode does appear somewhat in the residual normal load-factor response as seen in Figure 8, any artificial improvement in fuselage pitch damping would be expected to improve the overall response characteristics.
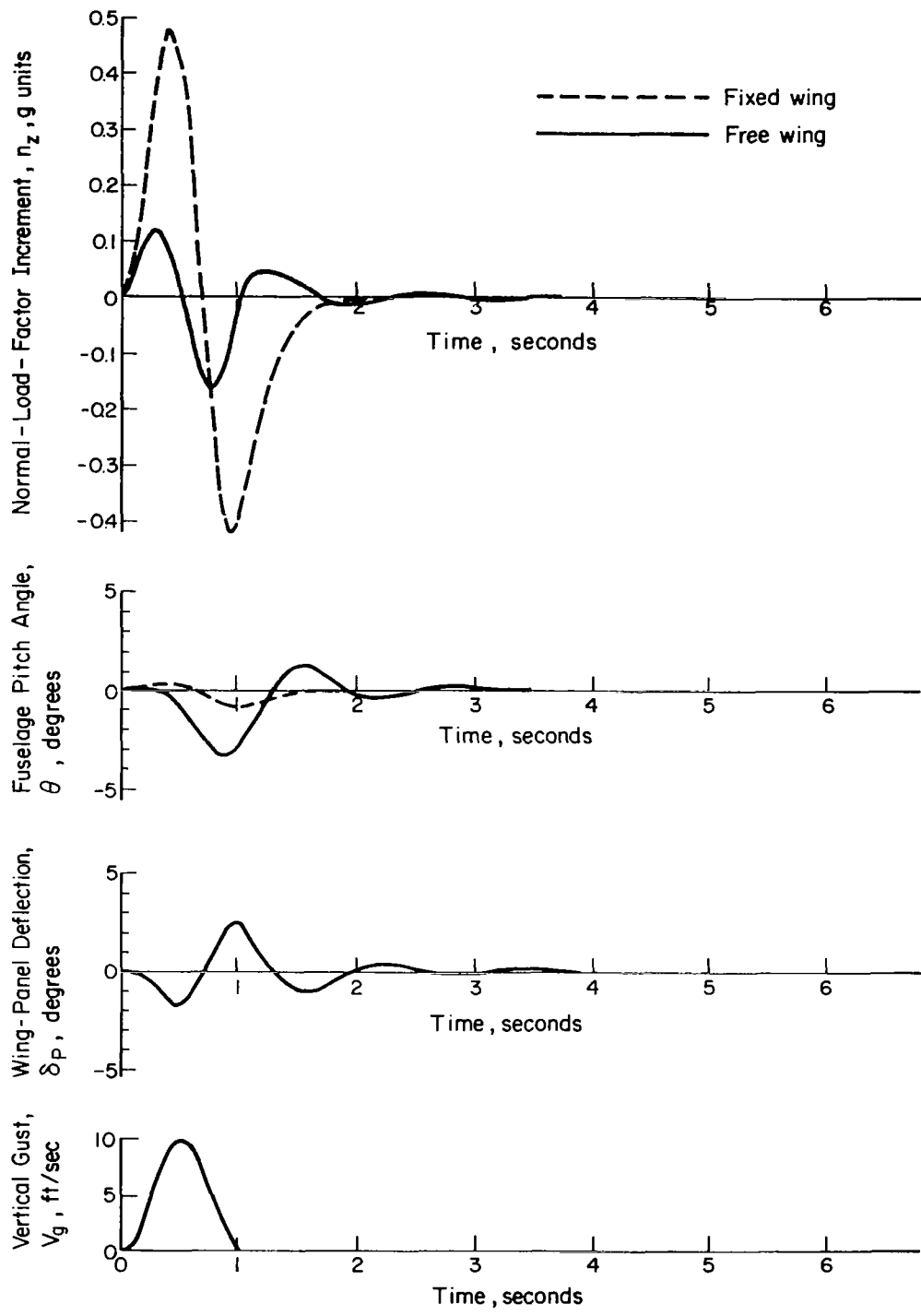
FIGURE 8. COMPARISON OF RESPONSES TO A DISCRETE GUST

Aircraft A3, Cruise

The effect of a forward movement of the hinge axis location is to increase the frequency of both the short period and wing panel modes. Time histories are not shown for the 20 percent panel-margin case of Table II, but further improvement in load-factor turbulence response and control deflection response time could be expected. In fact, the spectral turbulence responses to be discussed later show improved load-factor responses because of the increased natural frequency of the wing panel mode with the 20 percent margin. Offsetting this advantage somewhat is the increased control power required with the greater hinge margin, as was illustrated in Figure 3. The greater tab deflection requirements reduce the trimmed lift curve slope of the wing panels and would have an adverse effect on trim drag.

Several other parameters were varied to assess their impact upon the longitudinal modes. Specifically, the characteristic roots were examined for sensitivity to aspect ratio, fuselage center of gravity with respect to hinge axis, and wing-panel imbalance with respect to hinge axis.

With regard to aspect ratio, values of 6 and 8 were examined, and aside from the expected increase in wing panel mode frequency caused by the larger lift-curve slope with an aspect ratio of 8, no particularly significant differences were noted. No variation of taper ratio was explored because its impact on longitudinal motion could be expected to be smaller than the aspect ratio effects.

Similarly, the effect of locating the center of gravity of the fuselage assembly off the hinge axis was insignificant for reasonable locations, either for vertical or longitudinal displacements. Since the assumption of the initial equilibrium state demands that steady mass imbalance effects be trimmed, the primary effect of displacing the center of gravity reduces to a slight alteration in the pitching moment of inertia of the fuselage assembly.

Displacement of the wing panel center of gravity was found to influence the frequency of the wing panel oscillatory mode almost exclusively. Deviations of the wing panel center of gravity ranging from 0.1 $\bar{c}$ forward to 0.25 $\bar{c}$ aft of the hinge axis were permitted. Intuitively, it had been expected that such imbalances would result in pronounced effects, perhaps undesirable, in the longitudinal characteristics. Consequently, root loci were computed for all three basic aircraft, with both aspect ratios, for both cruise and approach flight conditions. Rather surprisingly, the effect was mild considering the extent of the permitted imbalance, and, furthermore, all cases were quite similar.

The relatively minor effect of panel imbalance is probably related to the fact that the ratio of wing mass to fuselage assembly mass is small. If this

ratio were large, a panel center-of-gravity location aft of the wing quarter-chord line could be expected to produce a purely divergent motion.

As mentioned previously, for an actual wing the pitching moment of inertia and the location of the pitching axis are not independent without structural mass changes. For simplicity, however, the assumption was made in this part of the study that the pitching moment of inertia is constant about an axis through the center of gravity, regardless of its location. Consequently, the moment of inertia about the hinge axis is a minimum for the nominal case, $X'_{cg} = 0$, and increases parabolically for center-of-gravity offsets in either direction.

A typical root locus illustrating the effect of wing panel imbalance on the wing-panel symmetric mode is shown in Figure 9 for Aircraft C_1 in the cruise condition. Forward center of gravity locations cause an increase in mode frequency, while aft locations reduce the mode frequency at a relatively constant damping ratio. The effect on other characteristic roots is insignificant, although some increase in phugoid frequency was observed for aft panel center of gravity locations. As discussed in a later portion of this report, the lateral-directional modes are much more strongly affected by wing panel imbalance, and, therefore, no further discussion of longitudinal effects is warranted.

Longitudinal Handling Qualities

Evaluation of the longitudinal handling qualities was confined to long-term path control and maneuvering characteristics, and then only to the extent that these features might be modified by the inherent nature of the free-wing concept. Specifically, attention was given to (1) the stability of the phugoid oscillation and the pilot's ability to damp this mode, and (2) the short-term response to longitudinal control inputs.

With regard to phugoid characteristics, Table III contains period and damping-ratio data for all cases considered. It may be noted that the free-wing version of each aircraft exhibits a reduction in period and a slight deterioration in damping ratio except for Aircraft B_1 and B_3 in the approach condition. In any event, the damping ratio exceeds the standard of Reference 1, which prescribes a minimum damping ratio of 0.04 for Level 1, the highest level of acceptability.

In a conventional fixed-wing aircraft, oscillations in the phugoid mode are usually damped by the pilot's control of pitch attitude through elevator displacement. It seems highly desirable, therefore, that the free-wing aircraft phugoid oscillation should be controllable by similar pilot action,
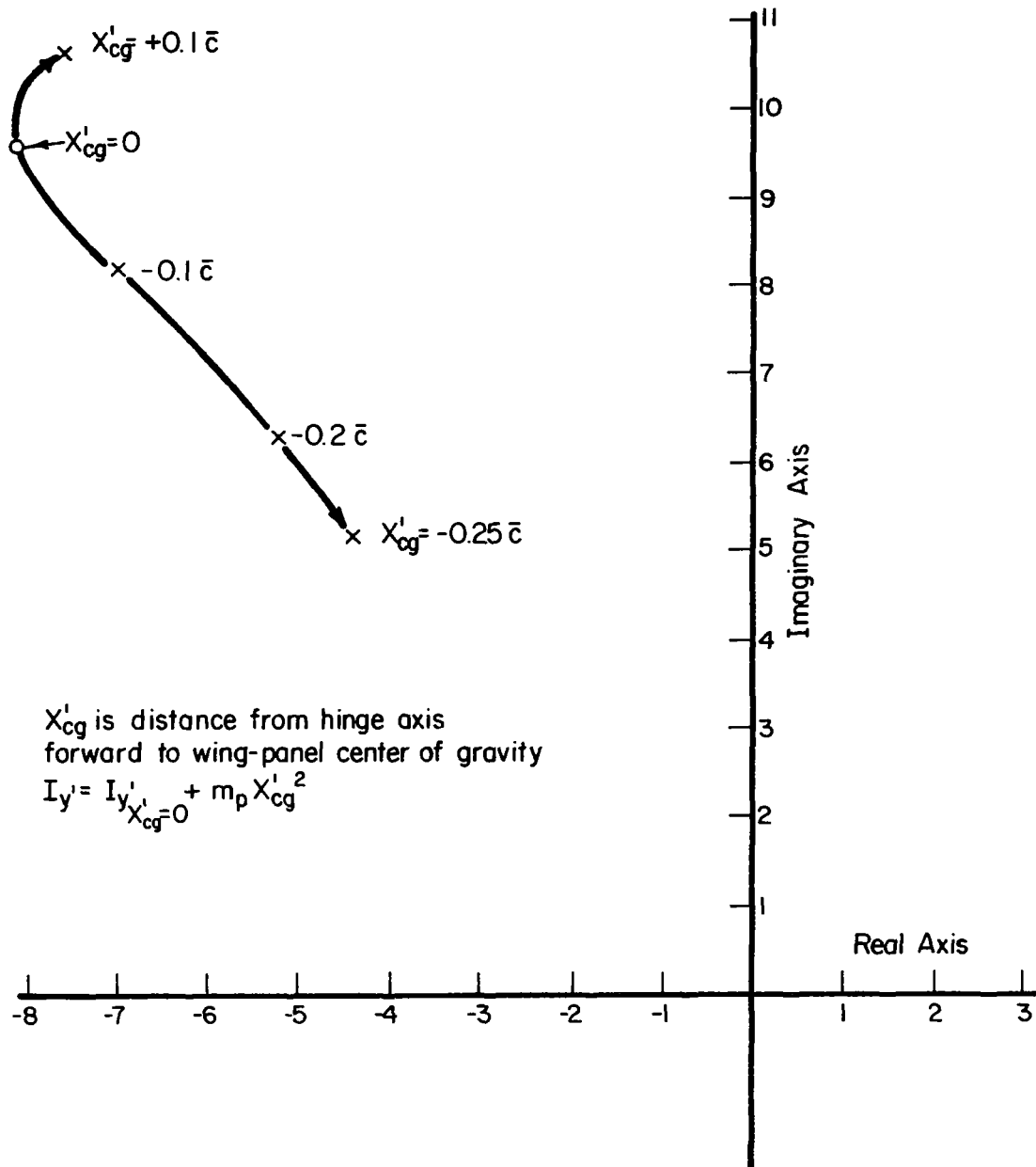
29

FIGURE 9. EFFECT OF PANEL CENTER-OF-GRAVITY LOCATION
ON WING-PANEL SYMMETRIC MODE

Aircraft C_1, Cruise

although no mechanical pitch coupling exists between the lifting surfaces and the fuselage assembly, and despite the fact that the longitudinal control is exercised through the trailing-edge control tabs instead of the horizontal tail surface.

TABLE III. STICK-FIXED PHUGOID CHARACTERISTICS

| Aircraft | Flight Condition | Fixed Wing | | Free Wing | |
		Period, seconds	Damping Ratio	Period, seconds	Damping Ratio
A_1	Cruise	34.7	0.120	27.8	0.100
A_1	Approach	22.6	0.088	17.3	0.072
A_3	Cruise	34.8	0.126	27.8	0.106
A_3	Approach	22.8	0.102	17.3	0.085
B_1	Cruise	52.0	0.105	46.1	0.100
B_1	Approach	31.8	0.070	26.9	0.076
B_3	Cruise	51.9	0.111	46.1	0.106
B_3	Approach	32.0	0.084	26.9	0.089
C_1	Cruise	61.5	0.163	51.5	0.100
C_1	Approach	34.7	0.096	25.3	0.071
C_3	Cruise	62.1	0.121	51.5	0.107
C_3	Approach	34.9	0.110	25.4	0.084

To determine whether such control was possible, several root loci were computed in which fuselage pitch attitude was fed back to the free-wing control tabs. A typical root locus in Figure 10 shows the path of the phugoid mode root as the feedback gain is increased. Notice that the oscillation can be completely damped in this manner, just as in a conventional aircraft.

An explanation of this fortuitous behavior lies in the fact that the fuselage tends to align itself with the flight path through the fuselage angle-of-attack stability provided by the horizontal tail surface. As a result, the fuselage pitch attitude behavior is very similar to that of a fixed-wing aircraft for long period motions. In addition, for shorter term motions, the pilot is provided some pitch-angle response to his control inputs by the changes in downwash at the horizontal tail caused by changes in wing lift coefficient.
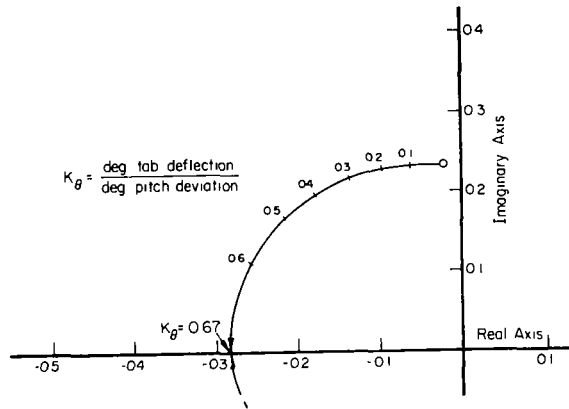
FIGURE 10.   ROOT LOCUS OF PHUGOID MODE AS AFFECTED BY
            FUSELAGE PITCH-ANGLE FEEDBACK TO
            CONTROL TABS

With regard to short term maneuvering response to control inputs, the
typical response time history in Figure 7 indicates several excellent attri-
butes for the free-wing aircraft. The response in normal load factor is much
more rapid than with the fixed-wing aircraft, while the fuselage pitch-attitude
and angle-of-attack histories are very similar.

The handling qualities specification, Reference 1, places limits upon
both the minimum and maximum short-period frequencies as functions of the
ratio of normal load factor to angle of attack in response to rapid longitudinal
control displacement. Taken literally, the free-wing responses would fall
within the allowable range of frequencies; but because of the unconventional
nature of these aircraft, direct application of the specification may not be
valid. In the free-wing aircraft, it is the symmetrical panel mode which
governs normal load-factor response, and not the short period mode, and
the panel mode frequencies are always higher than the maximum acceptable
"short period" frequency of the specification. On the other hand, fuselage
pitching motion is not dominated by the panel mode, but takes place predomi-
nantly in the short period mode which is not greatly different in frequency
than that of the fixed-wing aircraft. Because of this paradox, it can only be
surmised that the rapid load-factor response to control displacement is

entirely beneficial from the pilot's standpoint; a moving-base piloted simulation might be required to provide a definitive answer to this question.

With regard to short period damping ratios, the free-wing aircraft can meet the requirements of Section 3.2.2.1.2 of Reference 1 if either the wing-panel mode or the short period mode is considered to be appropriate, assuming that the horizontal tail volume is sized properly or that wing-fuselage interconnects or a suitable pitch damper is provided to augment the free-wing short-period mode.

Longitudinal Turbulence Responses

As discussed previously, the prospect of reduced turbulence responses is, perhaps, the strongest justification for a consideration of the free-wing concept. In particular, intuitive arguments were advanced in a preceding section which would suggest substantial improvements in turbulence flying, particularly with regard to the load-factor response to vertical gust velocities.

To evaluate the promised advantages, the power-spectral-density approach was employed, as described in Appendix E. For longitudinal disturbances, only the vertical gust component was considered, and the power spectrum of this component was assumed to be adequately represented by the one-dimensional Dryden model. A plot of this function was presented earlier in Figure 2, and a scale length, L, of 1000 feet was used for all cases.

To prevent the stick fixed phugoid mode from contributing significantly to the computed responses, all power spectra were truncated at a reduced frequency, Ω, corresponding to a temporal frequency of 0.3 radian per second. It was reasoned that disturbances in this low-frequency range could be easily controlled and should not be permitted to influence the computed rms perturbations.

Since the rms value of each output variable is computed by evaluating the square root of the area under its spectral density curve, a finite upper limit of integration was needed and was chosen as the reduced frequency corresponding to a temporal frequency of 40 radians per second.

Typical power spectral density functions of the load-factor responses to vertical gust disturbances of unit intensity are shown in Figure 11 for Aircraft B_1 in cruise for the fixed-wing aircraft and two versions of the free-wing counterpart. The tremendous reductions in the load-factor responses of the free-wing aircraft certainly support the intuitive arguments presented earlier.
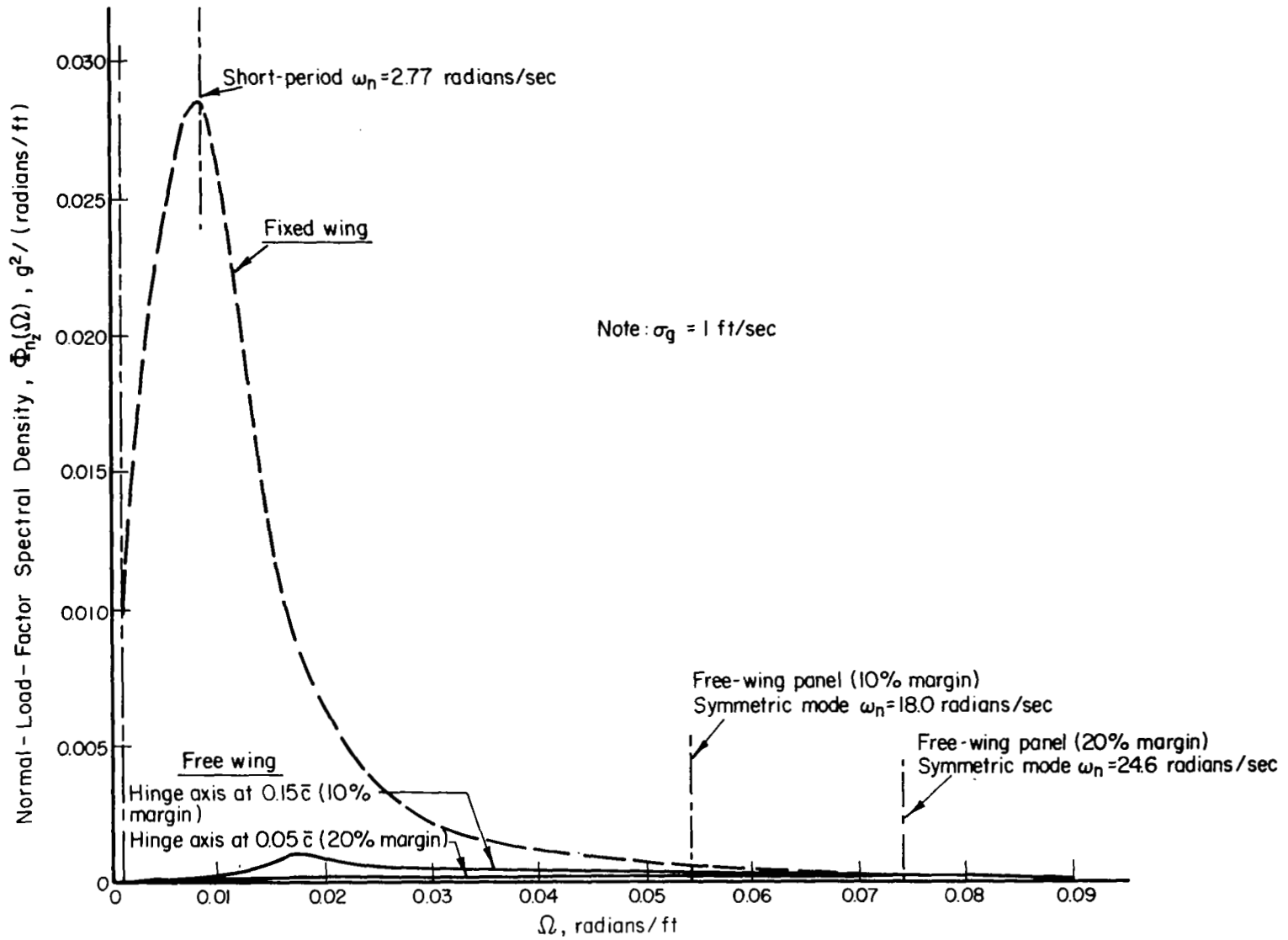
FIGURE 11. COMPARISON OF NORMAL-LOAD-FACTOR OUTPUT SPECTRA

Aircraft B_1, Cruise

The fixed-wing aircraft exhibits the customary response peak at the short-period frequency (although the peak actually occurs at a slightly lower frequency because of the slope of the input disturbance as shown in Figure 2). The response of the free-wing aircraft, on the other hand, is governed by the symmetric wing-panel mode which occurs at a much greater frequency where the input power is greatly reduced. At all lower frequencies, the ability of the wing panels to adapt to the random vertical drafts counteracts the increased turbulence energy. The slight bump in the 10 percent margin response spectrum is located near the free-wing short period frequency and is probably caused by vertical loads on the horizontal tail caused by fuselage pitching in this mode. A similar slight bump occurs in the 20 percent margin spectrum but it is not apparent in the scale of Figure 11.

Integration of the output spectra of Figure 11 yielded an rms normal-load-factor response of 0.0206 g's for the fixed-wing aircraft as compared with 0.00588 for the 10 percent margin free-wing aircraft and 0.00365 g's for the 20 percent margin. Expressed another way, the load-factor responses have been attenuated by a factor of 3.5 and 5.65, respectively.

The reduction of vertical path displacement is even more pronounced, since the rms altitude deviation for the fixed wing case was 0.659 feet as compared to 0.054 and 0.041 feet, respectively, for the two free-wing aircraft.

On the adverse side, the pitch-rate and pitch-acceleration rms responses are larger for the free-wing aircraft, each being over three times as high for the free-wing aircraft as for the fixed-wing version. As discussed previously, however, it is clear that fuselage pitching oscillations can be improved through reductions in horizontal tail size or other passive or active means with no adverse effects.

Figure 12 displays the rms load-factor, pitch-rate, pitch-acceleration, and path-displacement responses to unit turbulence intensity for all three aircraft with rectangular wing planforms and aspect ratio of 8. The fixed-wing responses are shown for comparison with the free-wing results. The free-wing aircraft shown have a 10 percent hinge axis margin and a horizontal tail volume one-fourth that of their fixed-wing counterparts. It can be seen that attenuation of load-factor responses by a factor of about three can easily be achieved. A greater reduction in normal load factor could have been displayed if the 20 percent hinge margin cases were used, but the 10 percent value may be more practical because of other penalties associated with the greater control power requirements of the larger hinge margin.
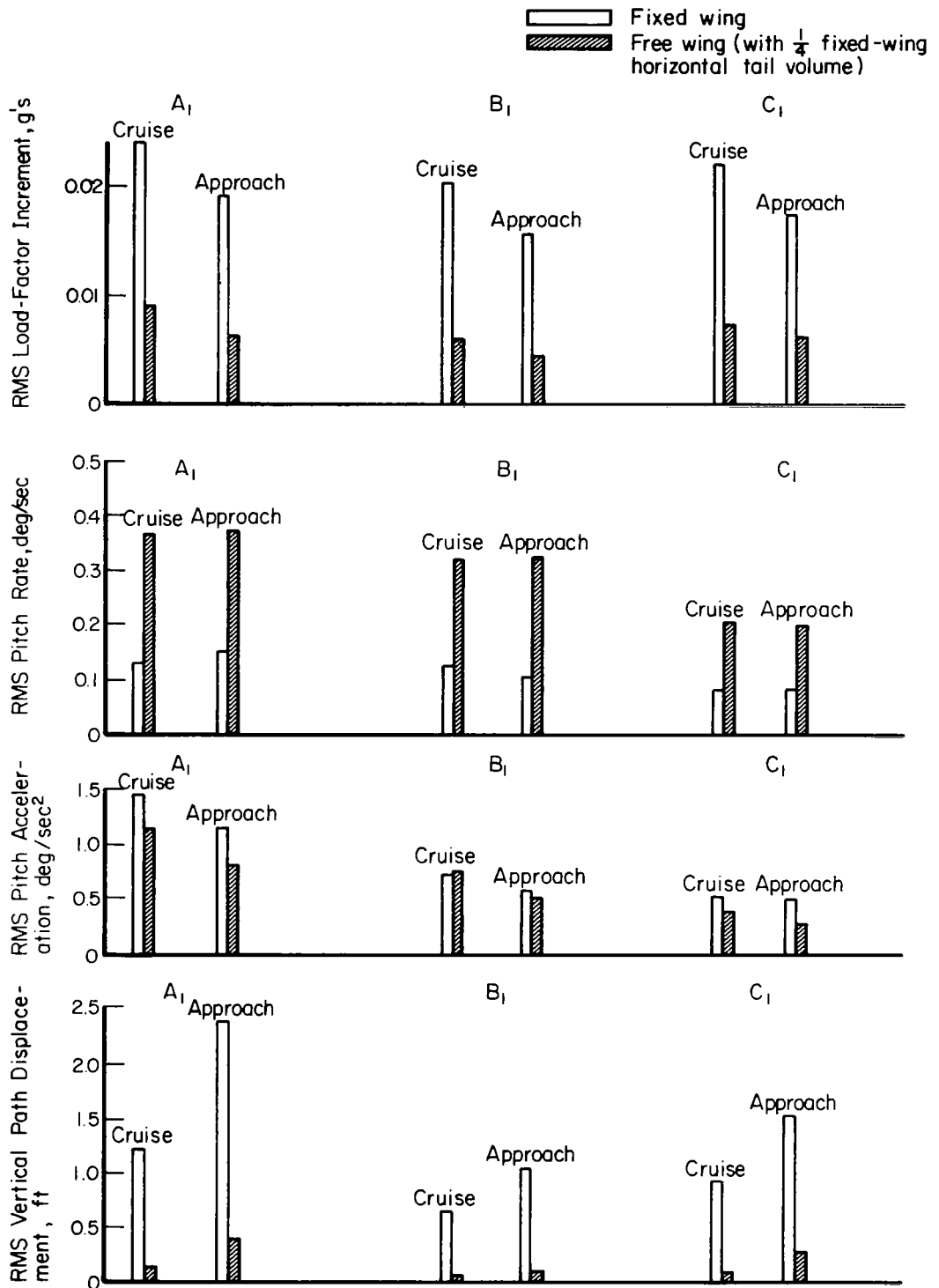
FIGURE 12. COMPARISON OF LONGITUDINAL
TURBULENCE RESPONSES

The reduced tail volume of the free-wing aircraft has an effect which is significant only in the pitch-rate and pitch-acceleration responses, and these could be improved greatly by an artificial fuselage pitch damper as mentioned previously.

The rms responses for the aircraft with aspect ratio of 6 are quite similar to those displayed in Figure 12. Although these are not shown graphically, they are tabulated numerically with the other data contained in Appendix F.

Lateral-Directional Motion

Free-Wing Characteristic Modes

Comparison With Fixed-Wing Aircraft. As with the longitudinal motion, the lateral-directional characteristics of a conventional fixed-wing aircraft are adequately described by a set of differential equations of fourth order. The four characteristic roots typically are found to include one complex pair, associated with the dutch roll mode, and two real roots defining the aperiodic roll and spiral modes.

For a free-wing aircraft, an additional complex pair of roots is obtained which describes an asymmetric mode of wing panel deflection. In addition, the aperiodic roll and spiral modes are significantly modified; the roll mode becoming far less heavily damped and the spiral mode tending towards instability. The dutch-roll mode roots are not substantially altered by the free-wing concept.

A nominal configuration for each free-wing aircraft was employed in the study of lateral-directional motion. This configuration featured a 10 percent panel hinge margin with the panel center of gravity on the hinge axis, a fuselage assembly center of gravity directly below the hinge axis, and a vertical tail volume identical to the fixed-wing equivalent aircraft.

Lateral-directional motion was analyzed for Aircraft A_1, B_1, C_1, A_2, B_2, C_2, A_3, B_3, and C_3 for both the cruise and approach flight conditions. For clarity, only the characteristic modes of A_1, B_1, and C_1 will be discussed in detail. Some indication of the effects of wing planform variations are discussed later, and all results are tabulated in Appendix F.

Considering first the dutch roll mode, a comparison is presented in Table IV which illustrates the fact that the free-wing concept has virtually no effect upon this oscillation.

TABLE IV.   COMPARISON OF DUTCH ROLL MODES

Aircraft	Flight Condition	Fixed Wing		Free Wing	
		Period, seconds	Damping Ratio	Period, seconds	Damping Ratio
A_1	Cruise	1.75	0.202	1.75	0.202
A_1	Approach	2.58	0.210	2.57	0.179
B_1	Cruise	1.83	0.156	1.82	0.154
B_1	Approach	2.66	0.167	2.67	0.139
C_1	Cruise	2.76	0.198	2.76	0.198
C_1	Approach	4.07	0.258	4.00	0.212

For the spiral mode, on the other hand, the effect of the free-wing is quite pronounced and is detrimental. As seen in Table V, the fixed-wing aircraft have slightly stable spiral modes in the cruise condition and mildly instable characteristics in the approach. The free-wing aircraft exhibit spiral instability at all flight conditions examined, and although the rates of divergence are mild during cruise, they become quite pronounced during approach.

TABLE V.   COMPARISON OF SPIRAL MODES

Aircraft	Flight Condition	Fixed Wing		Free Wing	
		Stable	Unstable	Stable	Unstable
		Time to 1/2 Amp, sec	Time to Double, sec	Time to 1/2 Amp, sec	Time to Double, sec
A_1	Cruise	4,780	--	--	28.2
A_1	Approach	--	20.7	--	3.76
B_1	Cruise	12,000	--	--	44.7
B_1	Approach	--	31.6	--	5.25
C_1	Cruise	8,800	--	--	50.5
C_1	Approach	--	30.1	--	5.3

It should be mentioned that the dihedral effect parameter, L_β, has a pronounced effect upon the fixed-wing spiral stability. Because of this, some caution was required in selecting the fixed-wing dihedral parameter which would permit a legitimate comparison with the free-wing aircraft. The resulting fixed-wing spiral characteristics are believed to be representative.

The free-wing concept also has an important and deleterious effect upon the roll mode because of the reduction in roll damping. A comparison is made in Table VI, where the roll mode root is given along with its reciprocal, the roll-mode time constant.

TABLE VI. COMPARISON OF ROLL MODES

Aircraft	Flight Condition	Fixed Wing		Free Wing	
		Root, sec^{-1}	Time Constant, sec	Root, sec^{-1}	Time Constant, sec
A_1	Cruise	-6.58	0.152	-0.639	1.56
A_1	Approach	-4.68	0.213	-0.783	1.28
B_1	Cruise	-5.35	0.129	-0.554	1.81
B_1	Approach	-4.15	0.241	-0.675	1.48
C_1	Cruise	-5.73	0.175	-0.497	2.01
C_1	Approach	-5.16	0.194	-0.600	1.66

The additional oscillatory mode, peculiar to the free-wing aircraft, describes an asymmetric mode of wing panel displacement, as listed in Table VII. This mode is characterized by a much higher frequency than the dutch-roll oscillation, and is well damped.

TABLE VII. ASYMMETRIC WING PANEL MODE CHARACTERISTICS

Aircraft	Flight Condition	Period, sec	Damping Ratio
A_1	Cruise	0.422	0.591
A_1	Approach	0.642	0.617
B_1	Cruise	0.312	0.614
B_1	Approach	0.490	0.685
C_1	Cruise	0.531	0.690
C_1	Approach	0.895	0.820

Sample Lateral-Directional Responses. Figure 13 shows the motion of the fixed-wing and free-wing versions of Aircraft A_1, with controls fixed, in the approach condition, following release from a steady slip. The initial condition was with wings level, but with the nose of the aircraft displaced 10 degrees to the left of the flight path.

In some respects, the motion of both aircraft is similar: the initial yawing motion is virtually identical, and after an initial roll to the left, both aircraft eventually assume a right turn. The disimilarities which exist are clearly caused by the much more rapid spiral divergence of the free-wing aircraft. In fact, referring to Table V, the rate of divergence of the free-wing aircraft is more than seven times as rapid.

These time histories also indicate that the wing panel mode is largely confined to motion of the wing panels themselves, as evidenced by the initial transient in the panel deflection trace, which is not apparent in the other variables.

Effect of Parameter Variations. The sensitivity of the stick-fixed lateral-directional characteristic modes of the free-wing was examined for variations in several of the parameters. Specifically, the influence of wing planform, fuselage center-of-gravity location, wing panel imbalance, hinge axis location, vertical tail volume, and wing pitching moments due to sideslip were examined.

With regard to wing planform variations, the primary effect of reducing the aspect ratio from 8 to 6 was to cause a reduction in the magnitude of the roll root, and a reduction in the rate of spiral divergence. These trends are similar to those observed for fixed-wing aircraft. A change in taper ratio from 1.0 to 0.6 had a similar beneficial effect on spiral divergence rate, and also improved the roll damping somewhat. Table VIII is a listing of these results for the light observation class of aircraft. Since the wing panel mode does not couple with the other modes for the nominal configuration, it is not contained in the table but the roots, tabulated in Appendix F, show that the primary effect of planform is on the frequency of this mode.

The variation of the fuselage center of gravity with respect to the hinge axis revealed that neither vertical nor longitudinal displacements had a pronounced effect on any of the modes, but the effect of wing panel center-of-gravity displacements can be dramatic.

To investigate the effects of mass imbalance on the wing panels, the panel center of gravity was varied from 20 percent of the chord length forward
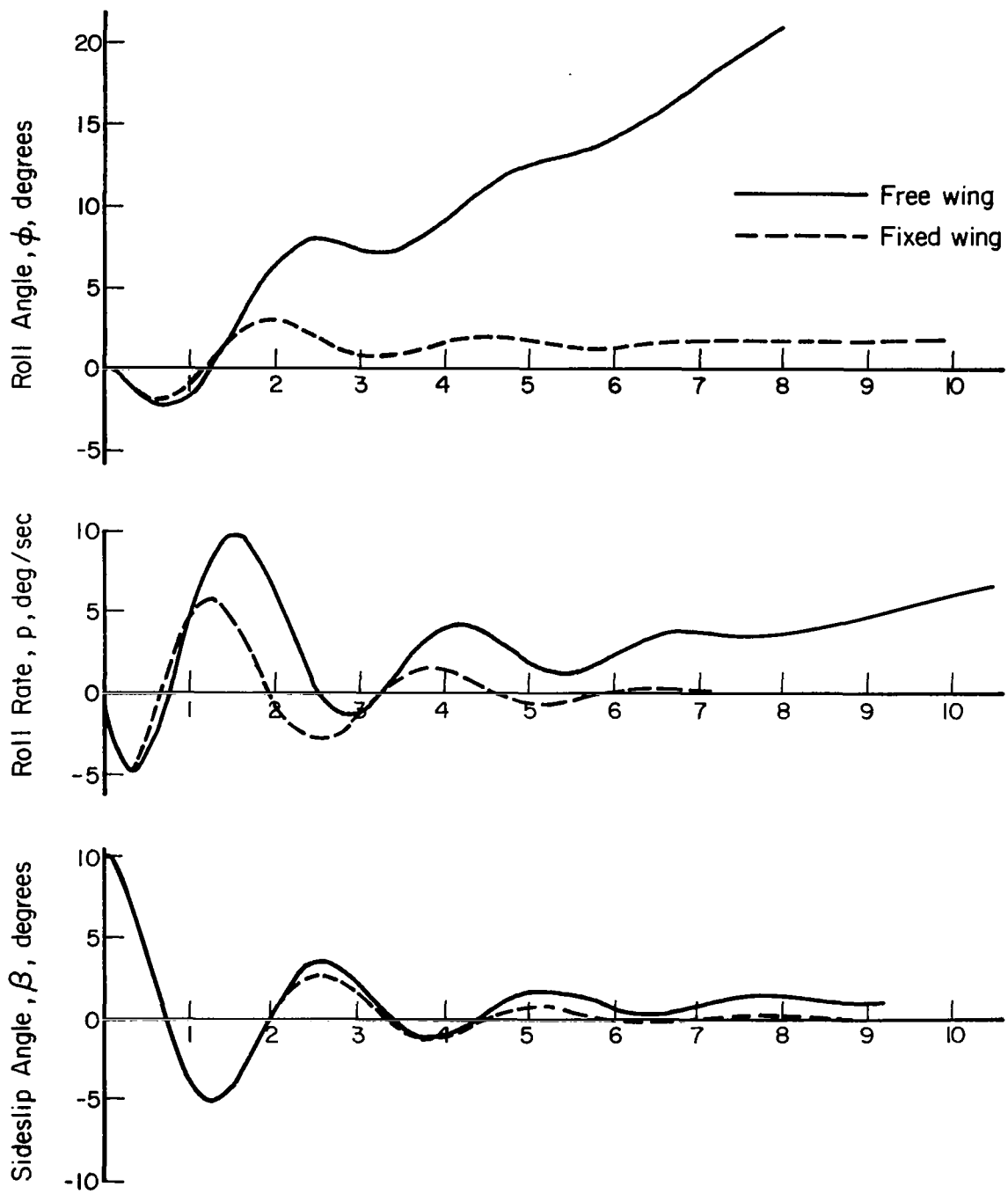
FIGURE 13. TIME HISTORY OF RELEASE FROM SIDESLIP
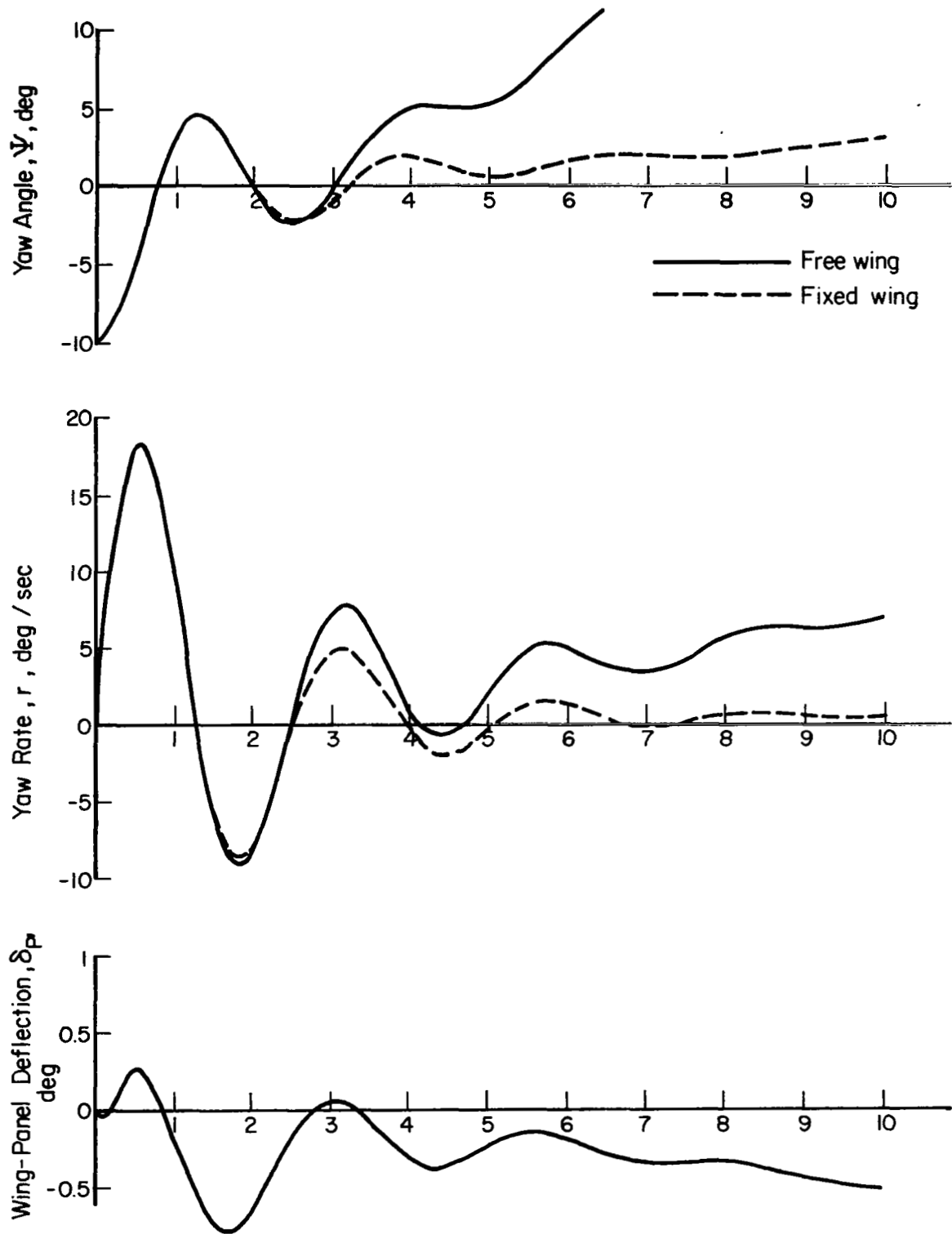
Aircraft A_1, Approach

FIGURE 13. CONCLUDED

of the hinge axis to 30 percent rearward. These extreme changes had a neg-ligible effect upon the dutch roll mode, and only a minor effect upon the spiral divergence. On the other hand, an interesting coupling between the roll con-vergence and panel mode roots was found to exist at large aft center-of-gravity location is shown in Figure 14 for Aircraft A_1 in cruise, and the same phe-nomenon was found to exist for all of the aircraft and flight conditions.

TABLE VIII. EFFECT OF WING PLANFORM ON LATERAL-DIRECTIONAL FREE-WING MODES

Aircraft	Flight Condition	Planform		Dutch Roll		Spiral Divergence Time to Double Amp, sec	Roll Mode	
		Aspect Ratio	Taper Ratio	Period, sec	Damping Ratio		Root	Time Constant, sec
A_1	Cruise	8	1.0	1.75	0.202	28.2	-0.639	1.56
A_1	Approach	8	1.0	2.57	0.179	3.76	-0.783	1.28
A_2	Cruise	8	0.6	1.70	0.215	38.2	-0.717	1.40
A_2	Approach	8	0.6	2.49	0.181	4.02	-0.860	1.16
A_3	Cruise	6	1.0	1.76	0.182	31.2	-0.463	2.16
A_3	Approach	6	1.0	2.60	0.138	4.05	-0.662	1.51

It can be seen that moving the panel center of gravity progressively aft of the hinge axis causes the wing panel mode to diminish in frequency and split into two aperiodic modes. One of these new roots tends to merge with the roll root to form an oscillatory mode which then becomes dynamically unstable. Computed time histories of the divergent oscillations show that the mode is one in which rolling motion is predominant.

Although the coupled mode is technically interesting, its importance should not be overemphasized since the instability can be avoided by re-stricting the permissible panel center-of-gravity range.

Movement of the hinge axis has no significant effect on any of the modes except the wing panel mode itself, whose frequency increases with increasing hinge margin as would be expected. This relative invariance is more readily understood by examining a simplified mathematical model of the aircraft. Con-sider, for example, the net roll damping and adverse yaw characteristics that may be computed for a quasi-static condition of pure rolling velocity and pitching equilibrium on each panel. Beginning with Equation (3), if the total pitching moment on each panel is set to zero and the equilibrium panel dis-placements are found in terms of roll rate, these displacements may be
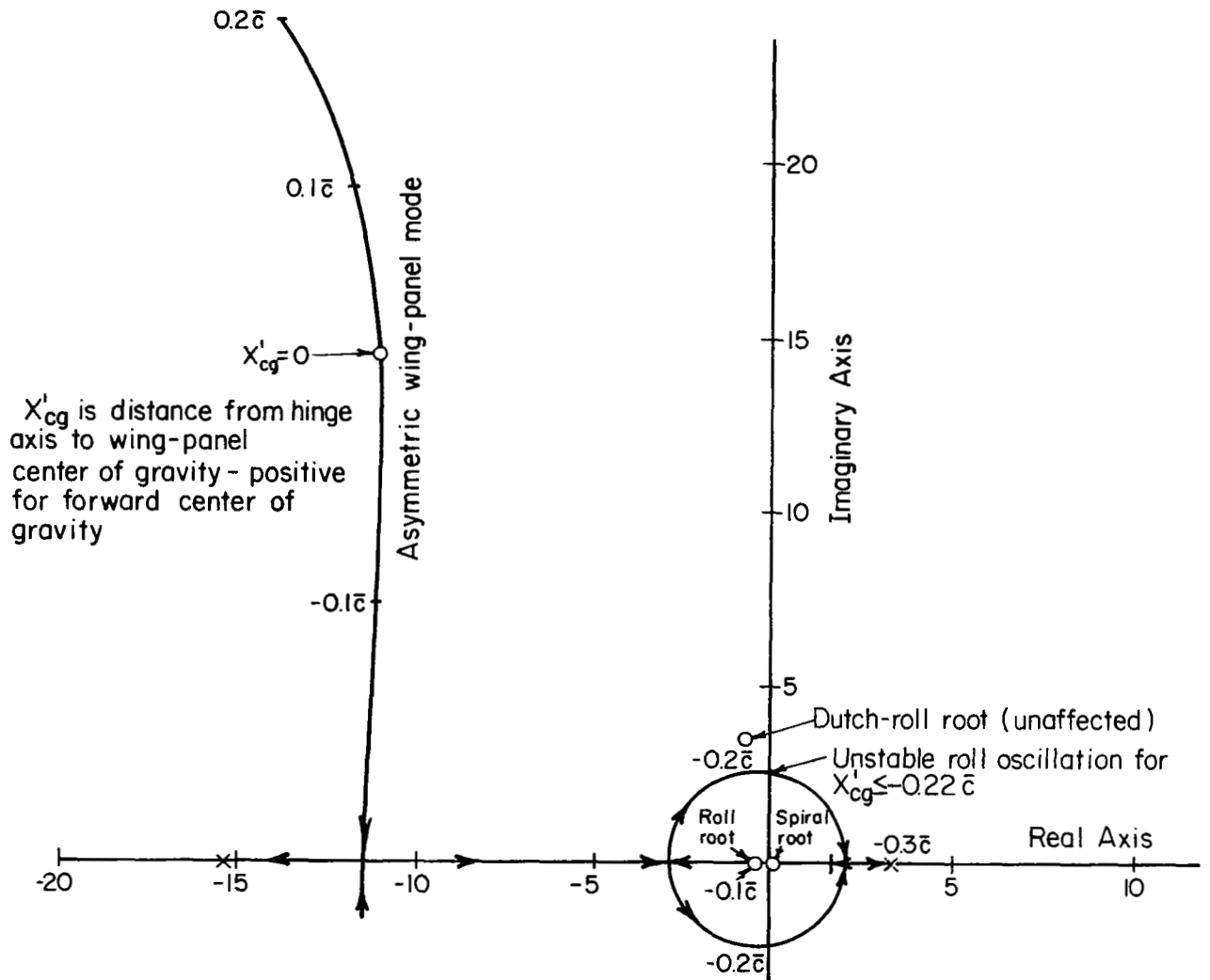
FIGURE 14. EFFECT OF WING-PANEL CENTER OF GRAVITY ON
LATERAL-DIRECTIONAL MODES

Aircraft A_1, Cruise

44

substituted into the rolling- and yawing-moment equations to arrive at quasi-static effective stability derivatives. The equivalent roll-damping derivative is

$$\text{Effective } C_{\ell_p} = C_{\ell_p} + \frac{2\, C_{\ell_{\delta P}}\, C_{m_{R_p}}}{C_{m_{L_{\delta P}}} - C_{m_{L_{\delta P}}}} \quad . \tag{5}$$

Similarly, the equivalent yawing-moment derivative due to roll rate is

$$\text{Effective } C_{n_p} = C_{n_p} + \frac{2\, C_{n_{\delta P}}\, C_{m_{R_p}}}{C_{m_{L_{\delta P}}} - C_{m_{R_{\delta P}}}} \quad . \tag{6}$$

The significant result of this is that both the numerator and the denominator of the additional terms are directly proportional to the distance between the hinge axis and the quarter-chord line. Values of these derivatives are tabulated in Appendix B. It follows that the effective changes in roll damping and yaw due to roll in this prescribed quasi-static condition are independent of wing-panel hinge margin. Similar arguments can be advanced for other stability parameters, supporting the observed fact that hinge margin has little effect on any of the lateral-directional modes except the asymmetric panel mode itself.

The effects of changes in the vertical tail size were mostly confined to a reduction in both the frequency and damping ratio of the dutch roll mode as the tail size was reduced. Some minor improvement was noted in the roll mode root for reduced tail size, but the spiral mode roots were less sensitive to the parameter than one might expect from fixed-wing experience. For fixed-wing aircraft, an increase in vertical tail size would invariably be detrimental to spiral stability; but, in the free-wing aircraft, the vertical tail contribution to net dihedral effect is very significant and may tend to counter-act the destabilizing influence of the increased weather-vane effect.

An aerodynamic parameter peculiar to the free-wing aircraft is the wing panel pitching moment, about the hinge axis, caused by sideslip. If the wing has a positive dihedral effect with the wing panels restrained, positive sideslip (to the right) will cause an increase in the lift on the right wing and a decrease on the left. Intuitively, then, the incremental pitching moments about the hinge axis will be negative on the right wing and positive on the left, resulting in an asymmetric panel deflection in a direction which would reduce the dihedral effect. An accurate determination of these pitching moments would require a theory which could provide chordwise, as well as spanwise,

normal force distributions. This capability is beyond the simple lifting line theory used in this study, so an arbitrary value of the pitching-moment derivative, C_{m_β}, was established for each flight condition, and a sensitivity analysis was conducted to evaluate the influence of this unknown parameter.

The nominal value of C_{m_β} was selected as the magnitude required to eliminate the wing contribution to the rolling moment, in the presence of a steady sideslip. In the steady state, then, with the wing panels in equilibrium, the total aircraft dihedral effect is completely dependent upon other components of the aircraft, particularly the vertical tail.

Figure 15 illustrates the locus of the affected roots as C_{m_β} is varied through both positive and negative values with absolute magnitudes up to more than three times the nominal value. The nominal value of C_{m_β} is negative since the sign is governed by the right wing panel, and larger negative values than the nominal can be seen to aggravate the spiral divergence. Some improvement in the roll mode may also be noted, but the roll convergence root remains quite small by comparison with that for fixed-wing aircraft. Although positive values of C_{m_β} are not expected, the trend in the positive direction is a coupling of the roll and spiral roots into a low-frequency oscillatory mode. Such coupling would be unacceptable from the handling-qualities standpoint, as discussed later; but, if attention is confined to the expected negative values of C_{m_β}, the most significant influence of this derivative is upon the spiral-mode stability.
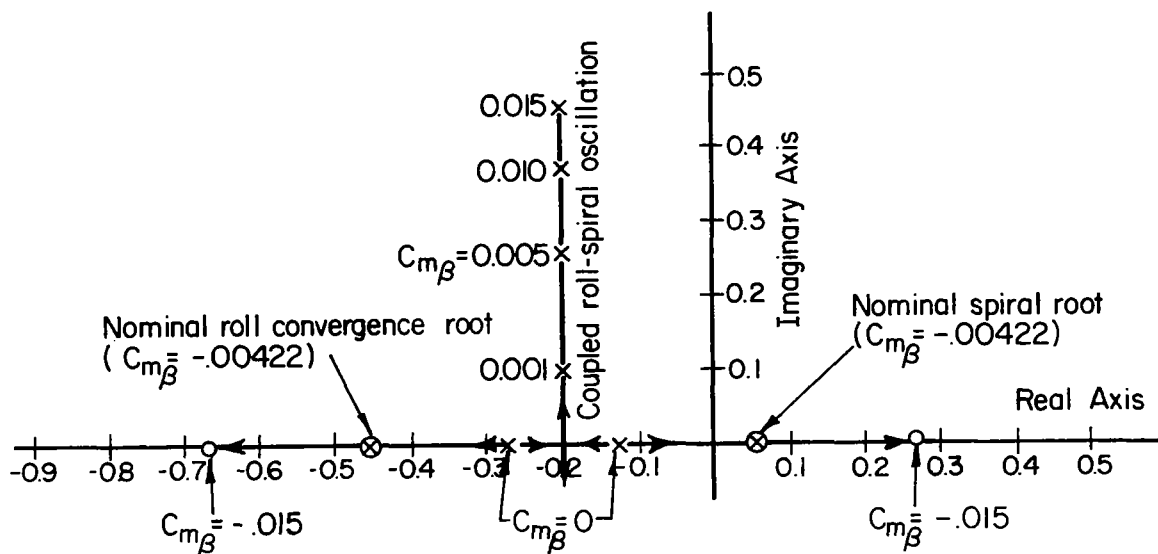

FIGURE 15. EFFECT OF PANEL PITCHING MOMENT DUE TO SIDESLIP ON THE ROLL AND SPIRAL MODES

Aircraft A1, Cruise

46

Lateral-Directional Handling Qualities

Free-Wing Lateral Dynamics. From the pilot's viewpoint, a primary lateral-directional control task is to establish and maintain a prescribed bank angle. This function is required to maintain level flight in the presence of disturbances, and to achieve coordinated turns for heading control.

While not explicitly stated in the handling qualities specifications, evidence suggests that the pilot prefers a lateral control system which commands a pure rolling motion at a rate of roll proportional to control deflection.

Figure 16 shows time histories of response to step lateral-control deflection for both the fixed-wing and free-wing versions of Aircraft A_1, for both the approach and cruise conditions. It should be noted that the fixed-wing behavior is very near the ideal, in that a relatively steady rate of roll is quickly achieved. The free-wing behavior, on the other hand, is far from ideal; the control deflection appears to command not a roll rate, but a rolling acceleration yielding a monotonic increase in roll rate. This unfortunate behavior can be attributed to the combination of low roll damping and spiral divergence of the free-wing configuration.

The significance of the roll-mode time constant listed in Table VI lies in the fact that if an aircraft is assumed to be constrained to pure rolling motion in response to a step control displacement, the roll rate is given by

$$p = \left[\tau_R L_{\delta_a} \left(1 - e^{-\frac{t}{\tau_R}} \right) \right] \delta_a \quad . \tag{7}$$

Equation (7) is derived in many texts, for example, Chapter XVIII of Reference 6. This equation describes a simple first-order exponential rise to the steady-state rolling velocity. The roll-mode time constant is a direct indication of the time required to achieve the steady rate because when the elapsed time equals this value, the idealized aircraft will reach approximately 63 percent of the steady roll rate regardless of the aileron deflection.

According to Figure 16, the simplified model of Equation (7) describes the actual time history very well for the fixed-wing aircraft, but the free-wing responses appear quite differently. The roll-mode time constants are appreciably longer for the free wing, and it appears that the divergent spiral mode begins to dominate the response, particularly in approach, soon after the time exceeds τ_R.

Reference 1 specifically disallows any outright coupling of the spiral and roll mode roots, such as the so-called lateral phugoid oscillation seen in
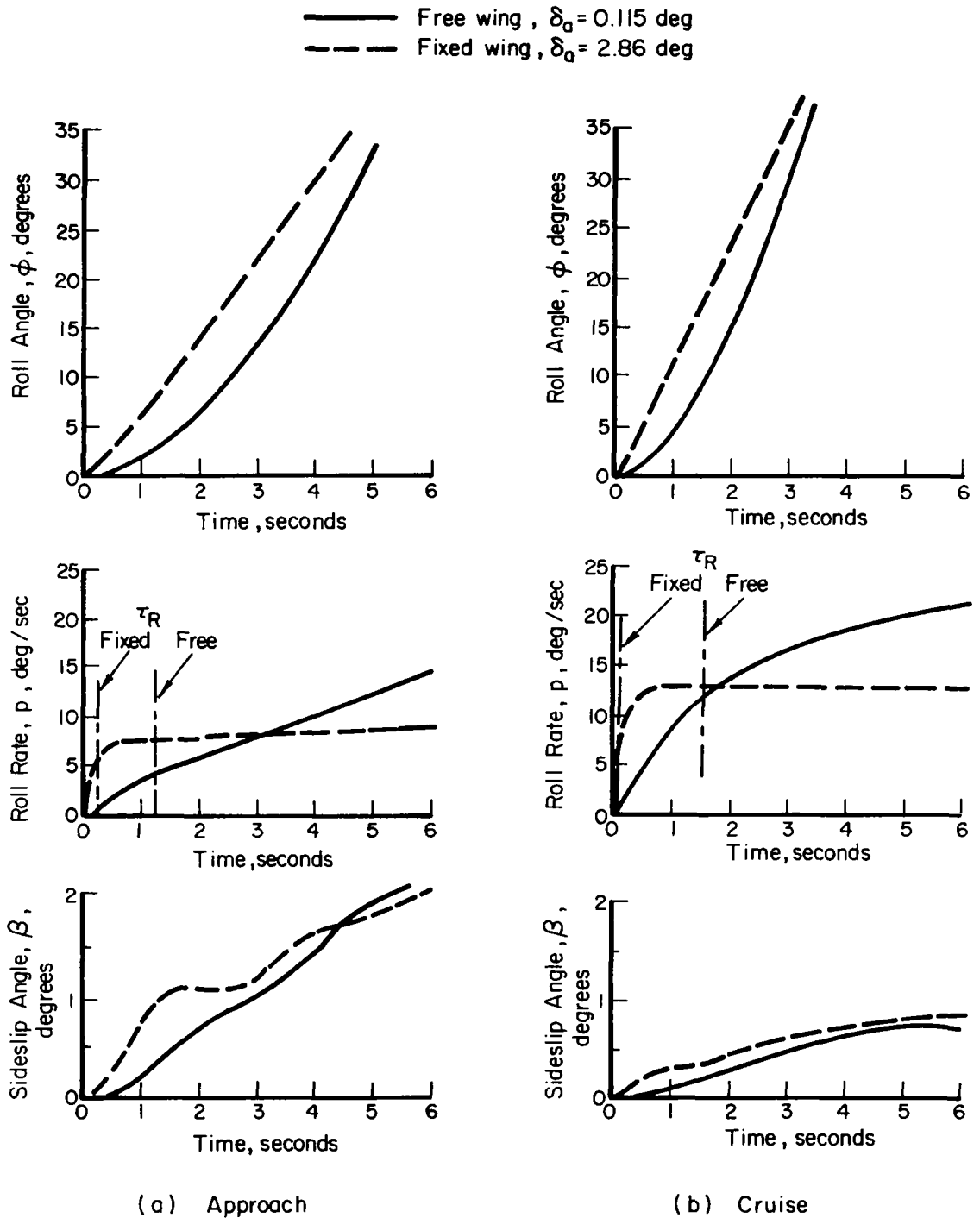
FIGURE 16. RESPONSES TO STEP LATERAL CONTROL INPUTS

Aircraft A_1

Figure 15 for positive C_{m_β}, but no explicit combined effects are covered if the roots remain real. Evidence suggests, however, that the ratio of absolute values of these real roots should be at least 30, according to Reference 7. Intuitively, this would seem to be particularly true if the spiral mode is unstable, if the synergistic effects in Figure 16 are to be avoided.

The standards of Reference 1 were examined for the roll and spiral modes separately, using the mode data in Tables V and VI. Concerning the spiral mode, all three aircraft exceeded the standards for Level 1* during cruise, but in approach none were able to satisfy Level 2 requirements and Aircraft A_1 was unable to meet even Level 3 specifications. This is the aircraft in Figure 16.

For the roll-mode time constant, the standards are not met for Level 1 operation at all, but are within Level 2 standards during cruise for all three aircraft. For approach, Aircraft A_1 meets Level 2 requirements, but B_1 and C_1 fall to Level 3.

Closed-Loop Bank-Angle Control. It is instructive to examine the closed-loop behavior of the pilot aircraft system if the pilot is assumed to act as a pure gain, feeding back a lateral control displacement in response to a deviation in bank angle. In practice the pilot is able to adjust his transfer function considerably to compensate for aircraft dynamic deficiencies. More will be said of this later, but the use of a "pure-gain" pilot illustrates basic differences between the fixed- and free-wing aircraft.

For the data in Figure 17, the pilot gain relating aileron deflection to bank-angle error was given by the magnitude of C_φ. With the fixed-wing aircraft, increasing the feedback gain caused the roll and spiral roots to combine into a stable oscillatory mode. The dutch roll roots were practically unaffected. By contrast, the free-wing case showed a dynamic instability, if C_φ were sufficiently large, caused by movement of the dutch roll root to the positive half plane. Even with lower gains, the coupled roll spiral oscillatory mode would be poorly damped.

---

*Reference 1 defines three levels of acceptability:
  Level 1. Flying qualities clearly adequate.
  Level 2. Flying qualities adequate to accomplish the mission...but some increase in pilot work load or degradation in mission effectiveness exists.
  Level 3. Flying qualities such that the airplane can be controlled safely, but pilot work load is excessive or mission effectiveness is inadequate, or both.
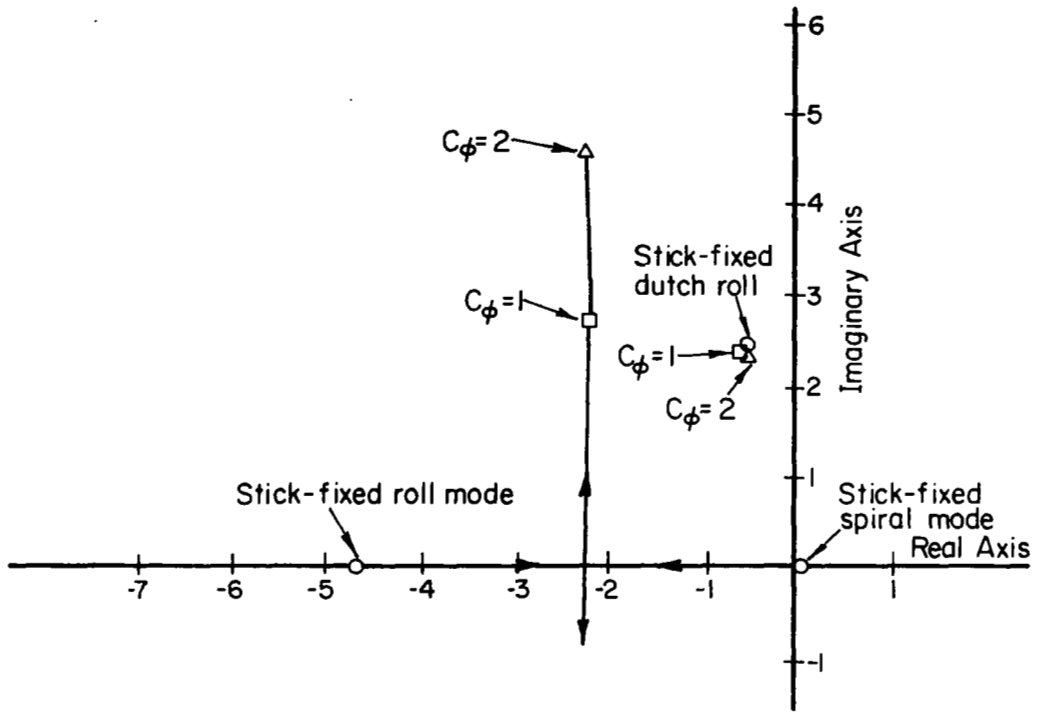
(a) Fixed-Wing Aircraft
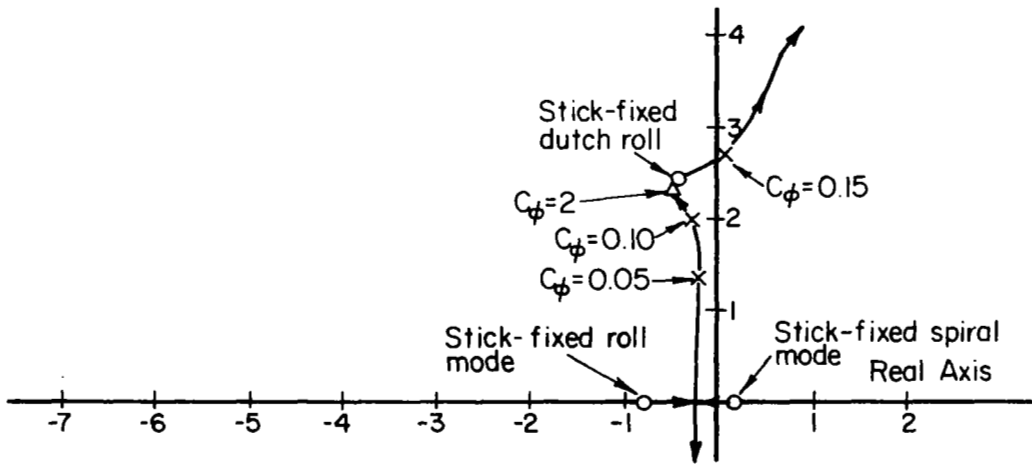
(b) Free-Wing Aircraft

FIGURE 17. EFFECT OF ROLL-ANGLE FEEDBACK TO AILERON

Aircraft A_1, Approach

Since the fundamental problem appears to be the small value of the roll-mode root, artificial stability augmentation in the form of a roll damper was evaluated. It is likely that other possible solutions may exist, such as a spring restraint on wing panel asymmetric displacement, but only the roll damper was evaluated. A system with no actuator lags was conceived which fed back an aileron deflection in response to a rolling rate. In particular, the feedback gain of this damper was selected to yield a roll mode time constant for the augmented free-wing aircraft equal to that of the fixed-wing aircraft. The closed-loop root loci as a function of pilot gain is shown in Figure 18.

The closed-loop behavior of the augmented aircraft is clearly superior to the basic free-wing configuration, even though a dynamic instability is still possible if C_φ is sufficiently large. A range of values of C_φ exists which should provide reasonably tight control with good damping.

As mentioned previously, the actual behavior of a human pilot is variable, in that he can adapt his control technique to a wide range of situations. The matter of defining human transfer functions has been the subject of considerable research effort, and a particular representation was chosen to obtain a better understanding of the roll control features of the free wing.

In Reference 8 an instability in roll of the aircraft-pilot combination for the X-15 was successfully explained using the transfer function:

$$\frac{L_{\delta_a} \delta_a(\lambda)}{\varphi(\lambda)} = -5 - 2.9\lambda \quad . \tag{8}$$

The evidence cited in Reference 8 suggests that this transfer function provides a good description of the pilot performing a stabilization control task near the limits of pilot controllability. Notice that the roll power characteristics of the aircraft do not enter into Equation (8) since it prescribes a rolling moment per unit bank-angle error rather than merely a control deflection.

To apply Equation (8) to the free-wing aircraft, an effective roll power must be derived. From Equation (3), if the wing panel is in static pitching-moment equilibrium under the influence of tab deflection and panel displacement only, the resulting panel displacement is:

$$\delta_P = \frac{-(M_{R_{\delta_{t_R}}} - M_{R_{\delta_{t_L}}})}{M_{R_{\delta_P}} - M_{R_{\delta_L}}} \delta_a \tag{9}$$

51
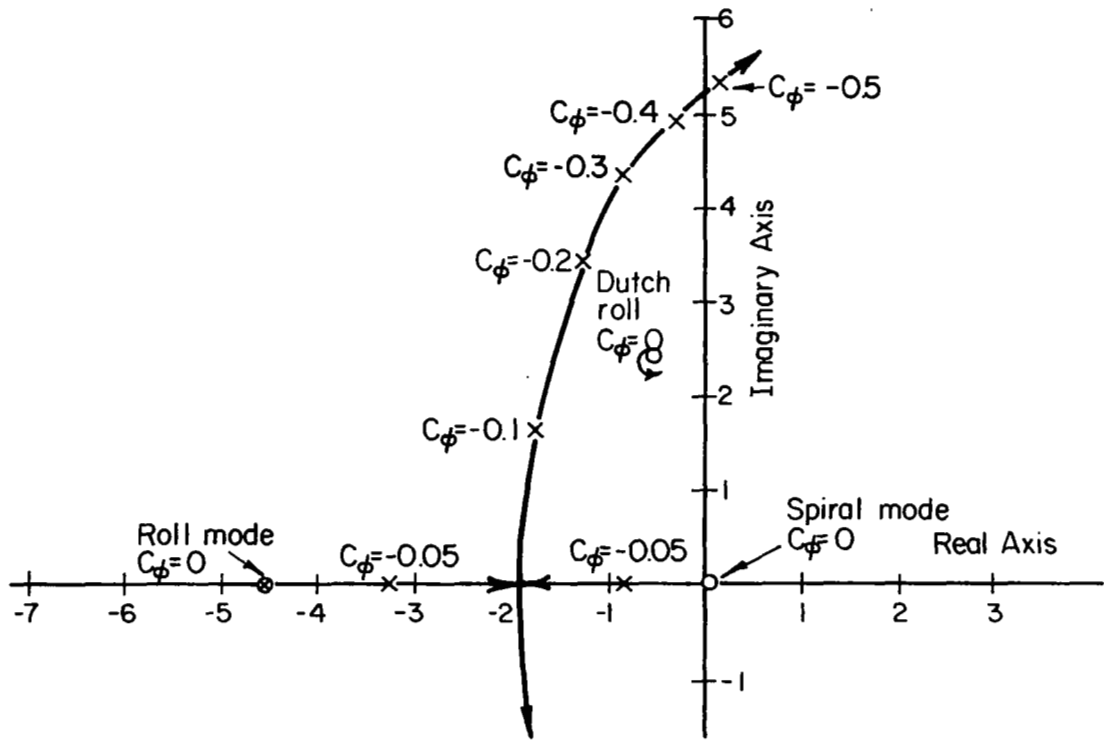
FIGURE 18. EFFECT OF ROLL ANGLE FEEDBACK TO AILERON

Aircraft A_1, Free Wing With Augmentation

Substituting into the rolling-moment equation, the effective roll power derivative is

$$\text{Effective } L_{\delta_a} = 2 L_{\delta_P} \frac{(M_{R_{\delta_{t_L}}} - M_{R_{\delta_{t_R}}})}{M_{R_{\delta_P}} - M_{R_{\delta_L}}} + 2 L_{\delta_{t_R}} \quad . \tag{10}$$

Using appropriate numerical data to compute the effective L_{δ_a} and substituting into Equation (8) produces the desired feedback function

$$\delta_a = C_\varphi \, \varphi + C_p \, p \quad . \tag{11}$$

Using these procedures for the free-wing versions, the time histories in Figure 19 were computed to illustrate the human pilot's ability to recover from an initial bank-angle error in both approach and cruise. The corresponding behavior with the fixed-wing version of the aircraft is also shown for comparison.

It should be noted that the unaugmented free-wing aircraft is not only controllable, but the pilot is able to remove the bank-angle error in less time than with the fixed-wing aircraft. The smoothness of his recovery with the fixed-wing aircraft is much better, however.

Lateral-Control Responses With Stability Augmentation. Figure 20 displays the time histories of response to step lateral control deflection for the free-wing aircraft with roll rate damping augmentation. This figure may be compared with Figure 16 to demonstrate the tremendous improvement in lateral-control characteristics afforded by the roll-rate damper.

The rate damper not only permits a roll rate response which has a nearly ideal shape, but the spiral mode is made stable and the augmented free-wing aircraft displays a roll rate capability, per unit aileron deflection, which is nearly independent of airspeed. This latter feature could be quite important during approach, where available roll rates are reduced for conventional aircraft as seen in the fixed-wing traces in Figure 16.

Returning to Equation (7), and recalling that the dimensional roll damping derivative, L_p, is simply the negative of the reciprocal of τ_R, the steady-state roll rate response is, ideally:

$$p = -\frac{L_{\delta_a}}{L_p} \, \delta_a \quad . \tag{12}$$

53
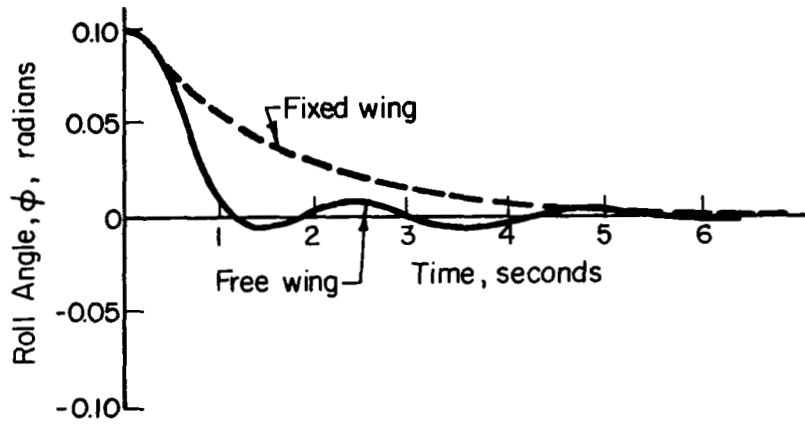
Approach
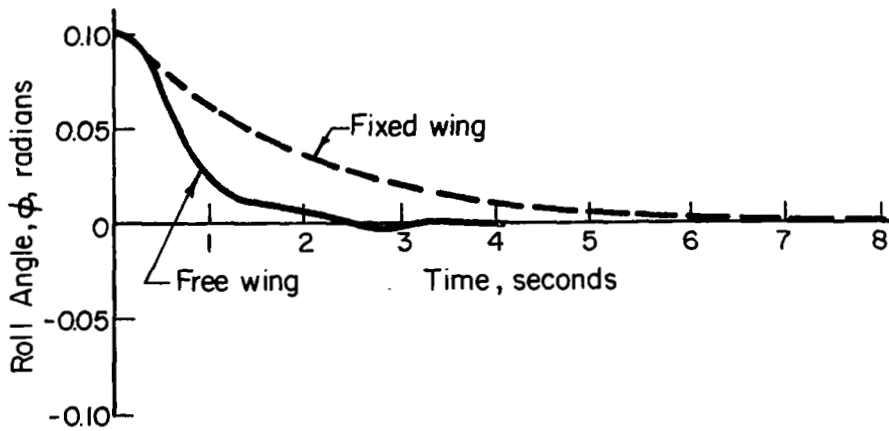
Cruise

FIGURE 19. PILOTED RECOVERY FROM ROLL-ANGLE DISPLACEMENT
Aircraft A_1

(a) Approach

(b) Cruise
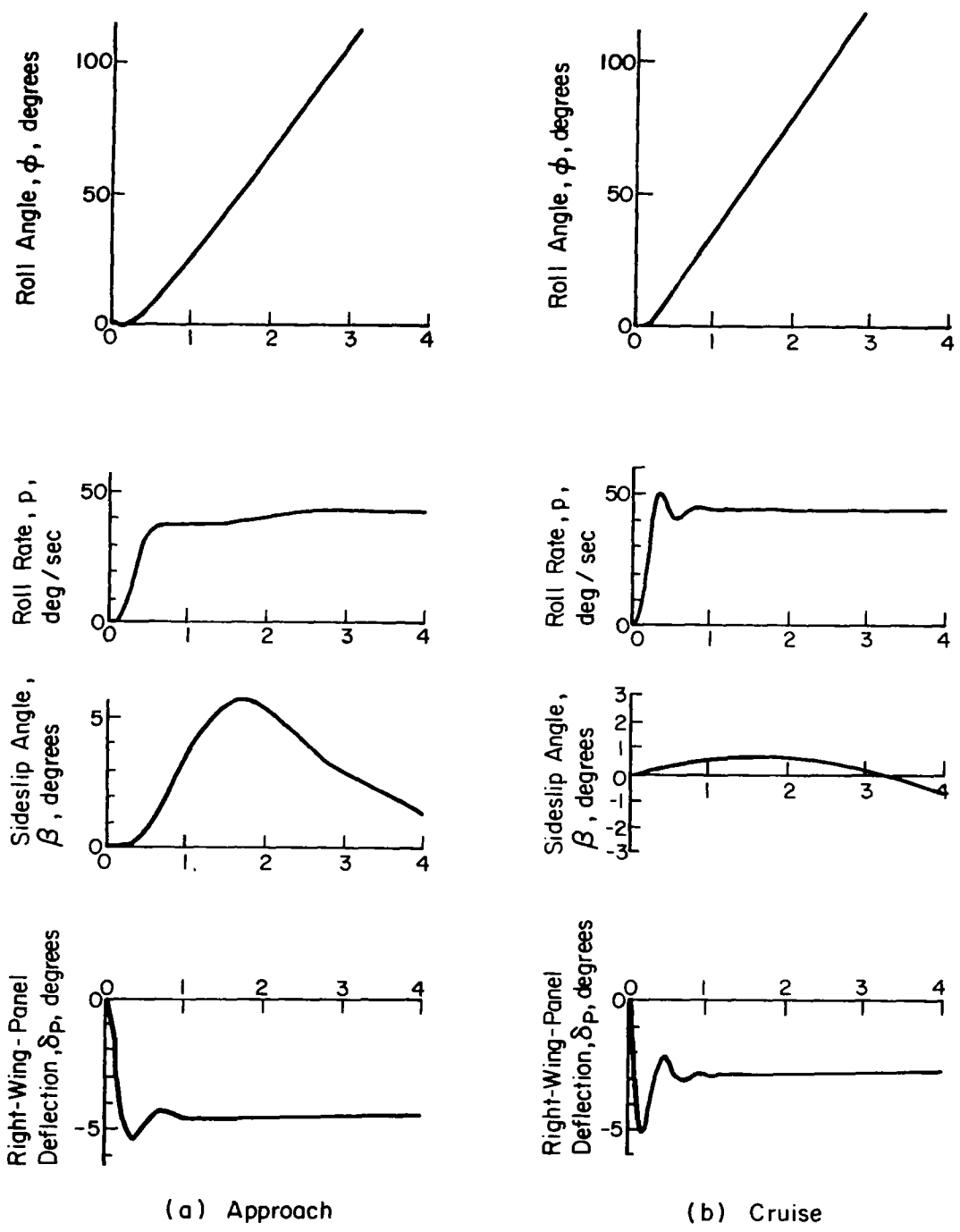
FIGURE 20. RESPONSES TO STEP AILERON WITH
ROLL-RATE AUGMENTATION

Aircraft A_1, δ_a = 2. 86 degrees.

55

If all roll damping is provided by natural aerodynamic means, the ratio of dimensional derivatives is proportional to true airspeed, all other things being equal. It follows that the maximum rate of roll will also then tend to vary directly with speed.

For the augmented free-wing aircraft, however, the greatest portion of the effective roll damping is artifically produced and the roll rate per unit aileron deflection tends to be constant. Furthermore, the effectiveness of the control tab, in displacing the wing panels for roll control, is very powerful. It may be surmised, in view of these facts, that any desired roll-rate capability within practical limits could be provided down to very low approach speeds.

Lateral-Directional Turbulence Responses

The lateral-directional turbulence responses were computed for the combined effects of uncorrelated side and rolling gusts using the power spectral density techniques described in Appendix E. Typical power spectral density functions for selected variables are shown in Figure 21 for Aircraft A_1 in cruise. When a comparison is made with the fixed-wing aircraft, the effect of the free-wing configuration in reducing roll rate response is very pronounced, but the effect on yaw rate is very small, with the free-wing response being slightly larger.

As with the longitudinal responses, the output spectra were truncated to include frequency components only within the temporal frequency range from 0.3 to 40 radians/sec. The rms values are based upon integrating the output spectra in this interval.

A comparison of rms responses is shown graphically in Figure 22 for Aircraft A_1, B_1, and C_1. In addition to decreasing the rolling motion, the free-wing aircraft shows a marked reduction in lateral path displacement and lateral load factor. No really significant differences were observed for the other planforms, although some responses were slightly greater for the reduced aspect ratio cases. These data are tabulated in Appendix F.

Finally, the performance of the stability augmented free-wing aircraft should be noted. Table IX is a comparison of the responses of the aircraft, with roll rate damping, to the behavior of the unaugmented free-wing and fixed-wing aircraft.

Despite the fact that roll damper gain, C_p, was sized to make the roll mode time constant equal to that of the fixed-wing aircraft, the augmented free-wing aircraft shows great improvement in lateral turbulence responses.
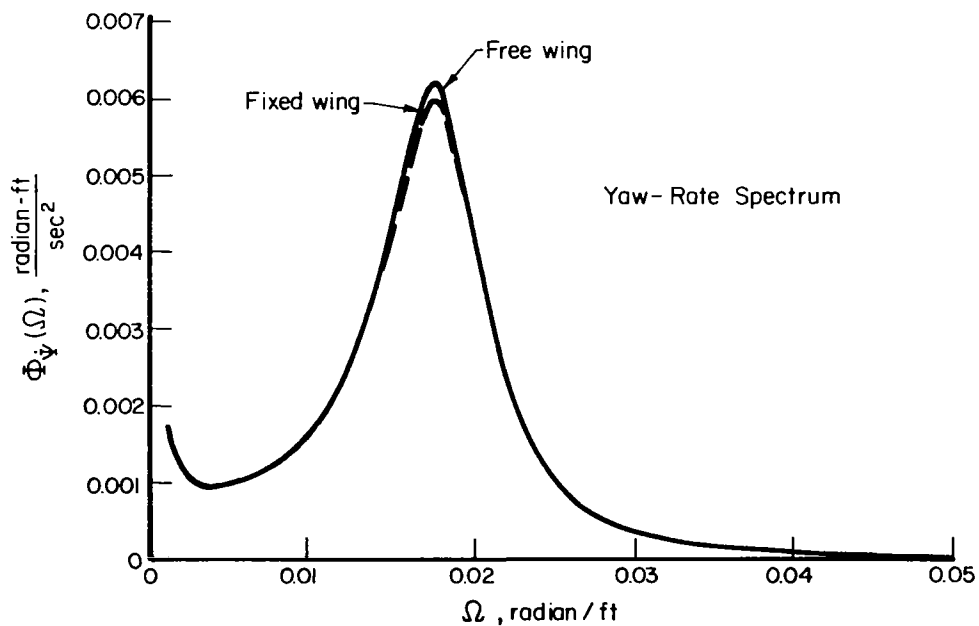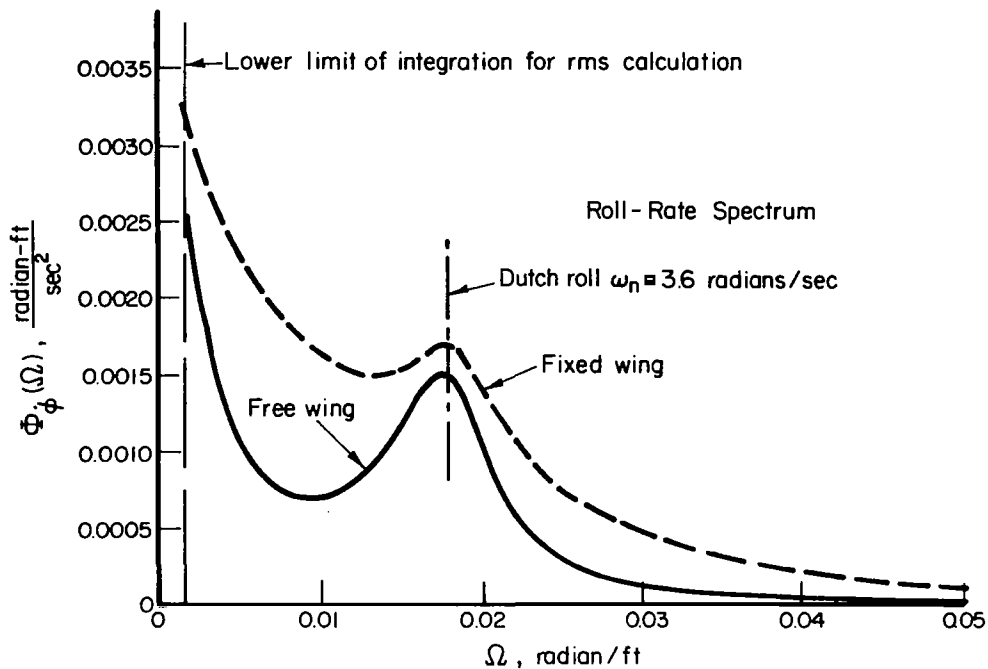
FIGURE 21.   LATERAL-DIRECTIONAL OUTPUT SPECTRA,
UNIT TURBULENCE INTENSITY

Aircraft A_1, Cruise

Roll-Angle Spectrum

Lateral-Load-Factor Spectrum
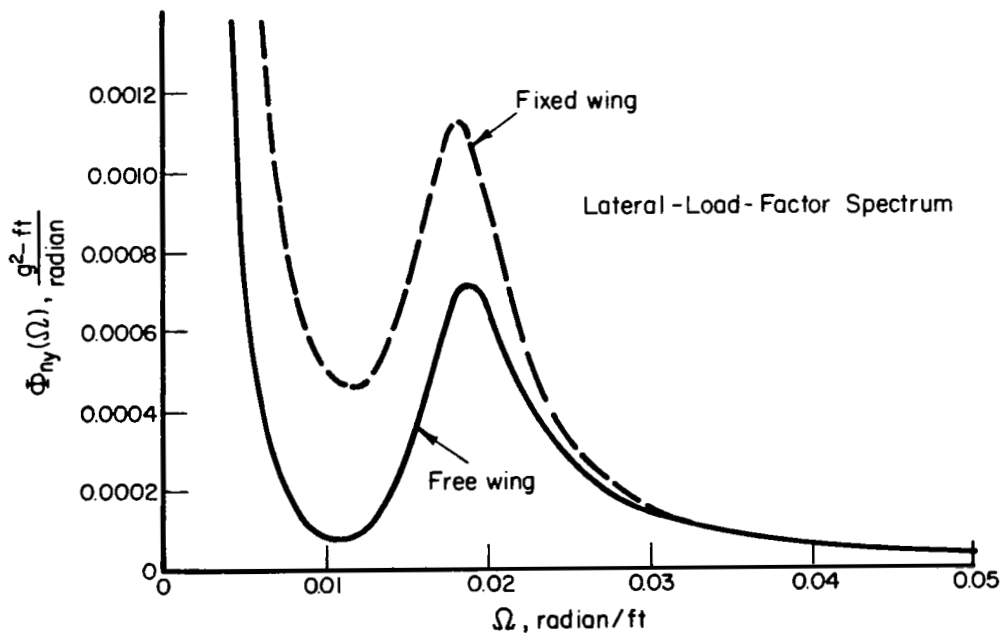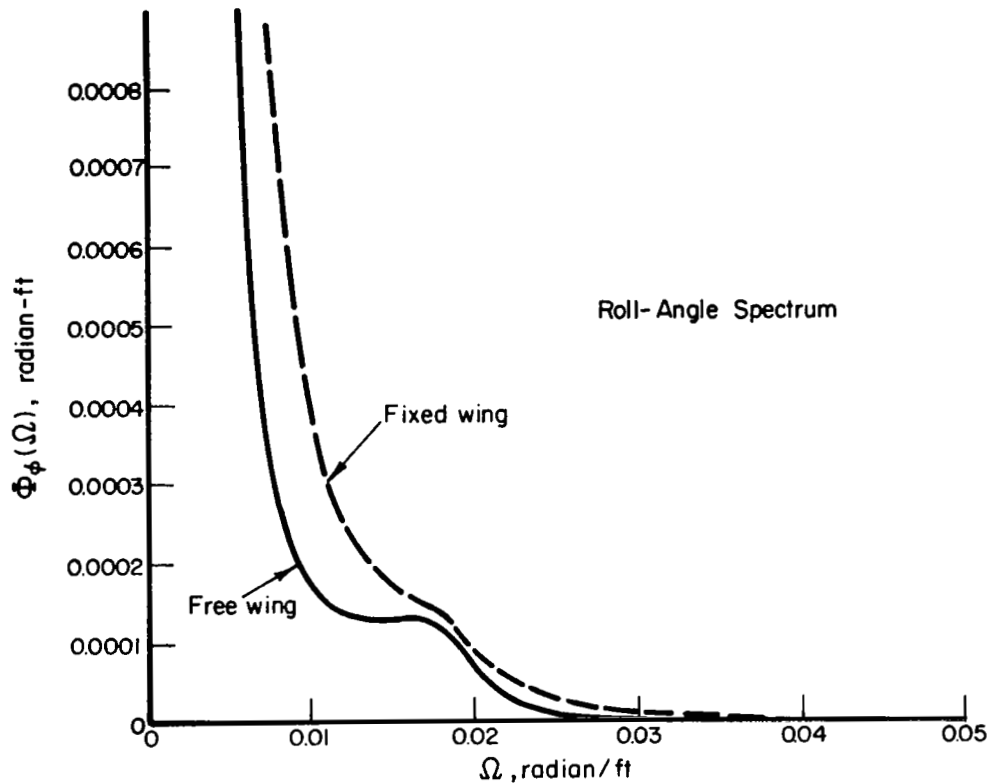
FIGURE 21. CONCLUDED
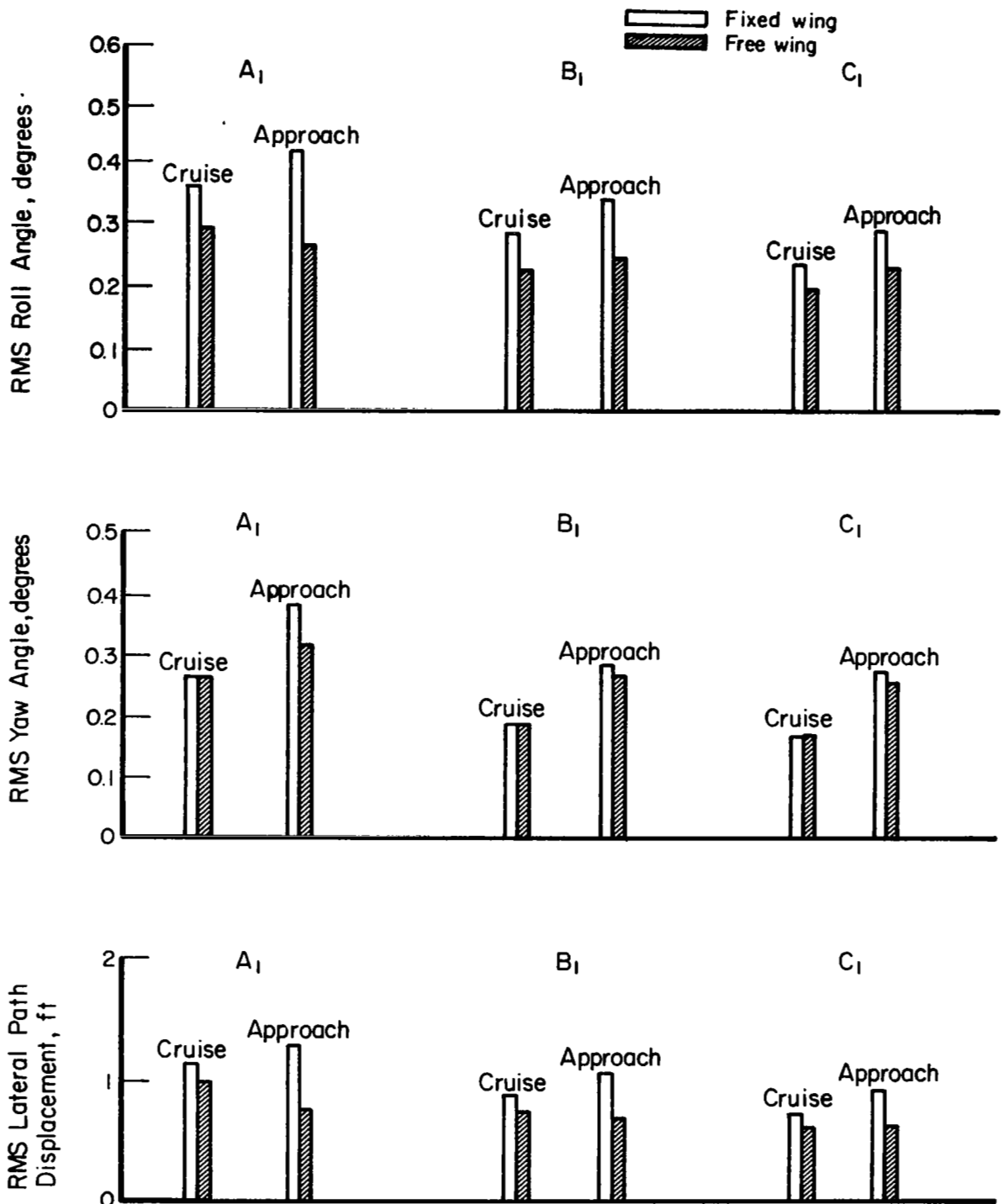
FIGURE 22. COMPARISON OF LATERAL-DIRECTIONAL
TURBULENCE RESPONSES

59
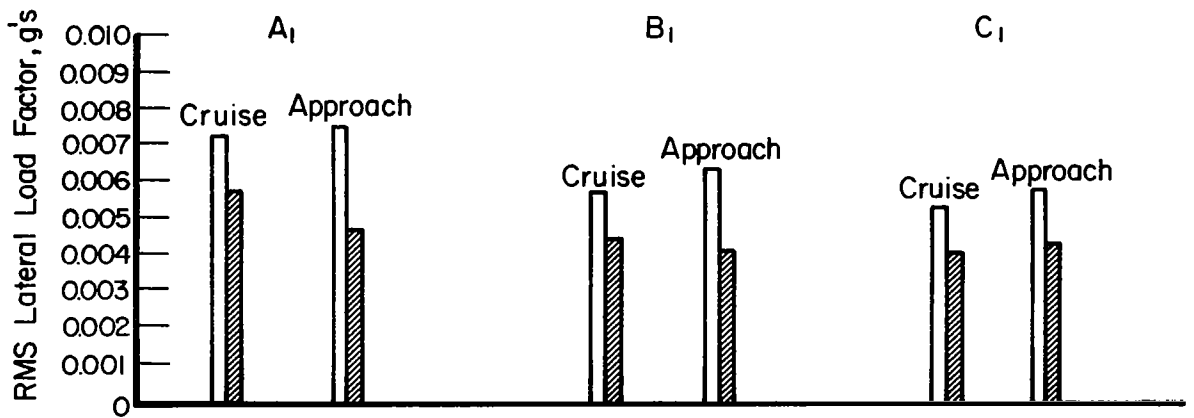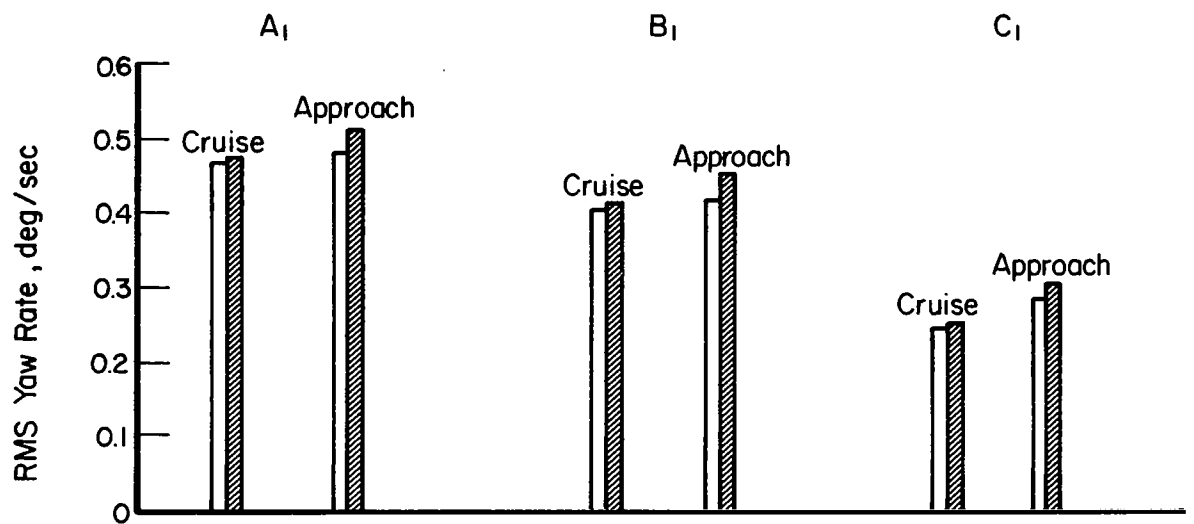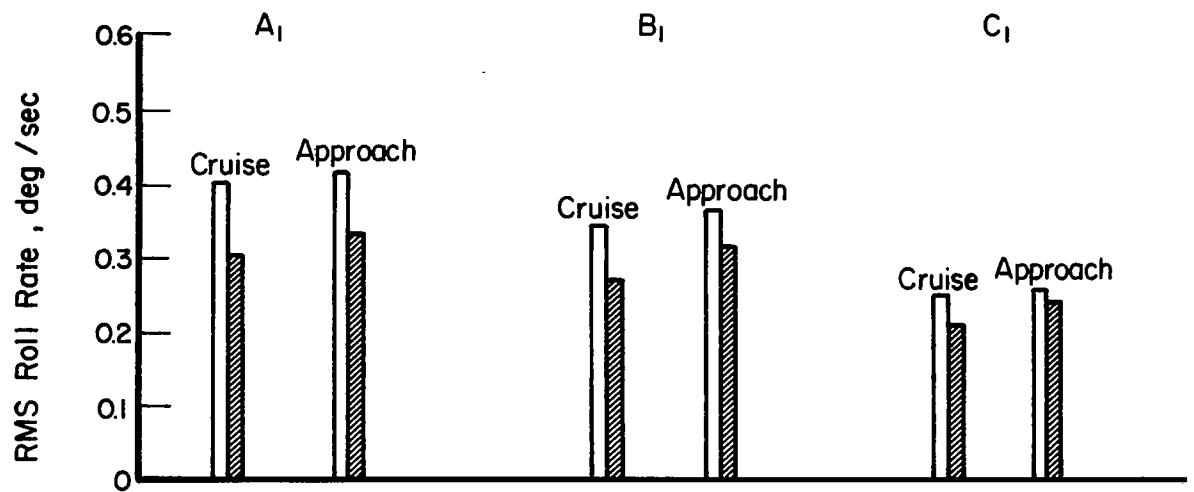
FIGURE 22. CONCLUDED

This is because the primary contributor to lateral perturbations is the span-wise gradient of vertical gust velocity, and this "rolling gust" disturbs the airplane in proportion to the aerodynamic roll damping coefficient, L_p. If the natural aerodynamic roll damping is small, the forcing function is reduced. The evidence is quite convincing that the combination of low gust sensitivity and powerful roll control provides the augmented free-wing aircraft with truly remarkable flying qualities, particularly during low-speed approaches.

TABLE IX.   COMPARISON OF RMS LATERAL-DIRECTIONAL
RESPONSES TO UNIT TURBULENCE INTENSITY

Aircraft A_1, Approach

C_p = -. 06 sec for augmented aircraft.

Aircraft	Roll Angle, deg	Yaw Angle, deg	Roll Rate, deg/sec	Yaw Rate, deg/sec	Lateral Displacement, ft	Lateral Load Factor, g units
Fixed wing	0.412	0.382	0.413	0.482	1.30	.00748
Free wing	0.270	0.316	0.335	0.511	0.766	.00470
Free wing with roll damper	0.112	0.305	0.234	0.462	0.252	.00335

Conclusions

From the results of this investigation, the following conclusions may be drawn:

(1) Atmospheric turbulence effects are greatly reduced by the free-wing concept at all flight conditions examined. The most dramatic improvements are in the root-mean-square normal load factor and vertical path displacement responses, but important alleviation effects are also obtained for rolling disturbances. On the other hand, the fuselage pitching motion response can be degraded substantially in comparison with equivalent fixed-wing aircraft.

(2) All stick fixed modes of motion of free-wing aircraft are stable, except for the spiral mode. The rates of spiral divergence are mild for cruise flight but may be excessively high for the approach configuration. In addition, a dynamic instability in roll is possible if the wing panel center of gravity is permitted to lie well aft of the hinge axis.

(3) The lateral handling qualities are unsatisfactory because of the combination of low roll damping and spiral divergence for the unaugmented free-wing aircraft, although the aircraft appears to be controllable by pilot effort.

(4) Artificial stability augmentation, in the form of a simple roll damper, provides excellent lateral control and turbulence penetration characteristics. The augmented free-wing aircraft is characterized by very powerful roll control by virtue of the differential wing-panel deflections. This unique feature can permit a relatively constant maximum roll rate capability, up to any reasonable value, over the entire speed range. This feature, coupled with the reduced gust sensitivity, can provide exceptionally good lateral handling qualities, particularly during low-speed approaches in rough air.

(5) Longitudinal handling qualities appear to be satisfactory. Pilot control of long term phugoid motion can be exercised exactly as with a conventional aircraft by employing longitudinal control feedback in response to fuselage pitch-attitude cues. In addition, the free-wing aircraft has far more rapid short term normal acceleration response to control inputs; but, because of the unconventional separation between normal load factor and fuselage pitching motion, a moving base piloted simulation may be required to ensure pilot acceptance of the longitudinal maneuvering characteristics.

With regard to fuselage pitching and lateral control improvements, the most obvious approach would be to provide an active stability-augmentation system. The possibility of using purely passive mechanical devices such as pivot springs or dampers or control interconnects should be considered, although they were not examined in this study.

REFERENCES

1. Anon., "Military Specification – Flying Qualities of Piloted Airplanes", MIL-F-008785A(USAF) (October 31, 1968).

2. Abbot and Von Doenhoff, Theory of Wing Sections, McGraw-Hill Book Company (1949).

3. Rainey, A. G., "Measurements of Aerodynamic Forces for Various Mean Angles of Attack on an Airfoil Oscillating in Pitch and on Two Finite-Span Wings Oscillating in Bending With Emphasis on Damping in the Stall", NACA TN 3643 (1956).

4. Runyan, H. L., "Single-Degree-of-Freedom Flutter Calculations for a Wing in Subsonic Potential Flow and Comparison With an Experiment", NACA Report 1089 (1952).

5. Jones, Robert T., "The Unsteady Lift of a Wing of Finite Aspect Ratio", NACA Report 681 (1940).

6. Seckel, Edward, Stability and Control of Airplanes and Helicopters, Academic Press, New York (1964).

7. O'Hara, F., "Handling Criteria", Journal of the Royal Aeronautical Society, 71 (April, 1967).

8. Taylor, L. W., Jr., "Analysis of a Pilot-Airplane Lateral Instability Experienced With the X-15 Airplane", NASA TN D-1059 (1961).

APPENDIX A

DEVELOPMENT OF EQUATIONS OF MOTION

Introduction

In deriving the equations of motion, each wing panel and the fuselage assembly are initially considered as free bodies. After the individual sets of equations with respect to the most convenient axis systems are written, they are combined into a single set, referred to standard aircraft stability axes. The consolidation of equations is accomplished by eliminating the common forces and moments acting between the various components. The equations are then linearized for convenience in the analysis.

Symbols

Symbols that are defined explicitly each time they are used have been omitted from this list.

b = wing span, feet

$\bar{c}$ = mean aerodynamic chord length, feet

C_D = drag coefficient

C_{D_α} = $\partial C_D / \partial \alpha$, per radian

C_L = lift coefficient

C_{L_α} = $\partial C_L / \partial \alpha$, per radian

$C_{L_{\delta_e}}$ = $\partial C_L / \partial \delta_e$, per radian

C_ℓ = rolling-moment coefficient, positive for right roll

C_{ℓ_p} = $\partial C_\ell / \partial \left(\dfrac{pb}{2U_o} \right)$, per radian

$C_{\ell_{p_w}}$ = wing contribution to C_{ℓ_p}

C_{ℓ_r} = $\partial C_\ell / \partial \left(\dfrac{rb}{2U_o} \right)$, per radian

$$C_{\ell_\beta} = \partial C_\ell / \partial \beta \, , \text{ per radian}$$

$$C_{\ell_{\delta_{t_R}}}, \; C_{\ell_{\delta_{t_L}}} = \partial C_\ell / \partial \, \delta_{t_R} \text{ or } \partial C_\ell / \partial \delta_{t_L}, \text{ respectively, per radian}$$

$$C_{\ell_{\delta_P}} = \partial C_\ell / \partial \delta_P \, , \text{ per radian}$$

$$C_{\ell_{\delta_L}} = \partial C_\ell / \partial \delta_L, \text{ per radian}$$

C_m = pitching-moment coefficient on fuselage assembly, positive nose up

C_{m_R} = pitching-moment coefficient on right wing panel, positive L. E. up

$$C_{m_{R_p}} = \partial C_{m_R} / \partial \left(\frac{pb}{2U_o} \right), \text{ per radian}$$

$$C_{m_{R_{\delta_P}}} = \partial C_{m_R} / \partial \delta_P, \text{ per radian}$$

$$C_{m_{R_{\dot{\delta}_P}}} = \partial C_m / \partial \left(\frac{\dot{\delta}_P \bar{c}}{2U_o} \right), \text{ per radian}$$

$$C_{m_{R_{\delta_{t_R}}}}, \; C_{m_{R_{\delta_{t_L}}}} = \partial C_{m_R} / \partial \delta_{t_R}, \; \partial C_{m_R} / \partial \delta_{t_L}, \text{ respectively, per radian}$$

$$C_{m_\beta} = \partial C_{m_R} / \partial \beta, \text{ per radian}$$

C_n = yawing moment coefficient, positive nose right

$$C_{n_p} = \partial C_n / \partial \left(\frac{pb}{2U_o} \right), \text{ per radian}$$

$$C_{n_{p_w}} = \text{wing contribution to } C_{n_p}$$

$$C_{n_r} = \partial C_n / \partial \left(\frac{rb}{2U_o} \right), \text{ per radian}$$

$$C_{n_\beta} = \partial C_n / \partial \beta \, , \text{ per radian}$$

$$C_{n_{\delta_P}} = \partial C_n / \partial \delta_P, \text{ per radian}$$

$$C_{n_{\delta_{t_R}}} = \partial C_n / \partial \delta_{t_R} \text{ , per radian}$$

C_p = gain constant, aileron deflection per unit roll rate, seconds

C_T = thrust coefficient

C_y = sideforce coefficient, positive to right

$$C_{y_p} = \partial C_y / \partial \left(\frac{pb}{2U_o} \right), \text{ per radian}$$

$$C_{y_r} = \partial C_y / \partial \left(\frac{rb}{2U_o} \right), \text{ per radian}$$

$$C_{y_\beta} = \partial C_y / \partial \beta \text{ , per radian}$$

$$C_{y_\delta} = \partial C_y / \partial \delta_P \text{ , per radian}$$

C_φ = gain constant, aileron deflection per unit roll angle

D_y = lateral path displacement, feet, positive to right

E = ratio of wing semiperimeter to span

F_x, F_y, F_z = force components along X, Y, and Z stability axes, respectively, pounds

$F_{x_{h_R}}, F_{y_{h_R}}, F_{z_{h_R}}$ = forces components along hinge axes system associated with acceleration of right wing panel, pounds

g = acceleration of gravity, feet/second^2

G_1 = transfer function relating lift coefficient to angle of attack

G_2 = transfer function relating lift coefficient to vertical gust velocity

h = altitude increment, feet

$\overline{H}$ = moment of momentum vector, feet-pound-seconds

$\overline{i}$ = unit vector along x axis

$I_{x'}, I_{y'}, I_{z'}$ = moments of inertia of right wing panel measured in panel axis system, slug-feet^2

$I_{xy'}, I_{xz'}, I_{yz'}$ = products of inertia of right wing panel measured in panel axis system, slug-feet^2

$I_{x_f}, I_{y_f}, I_{z_f}$ = moments of inertia of fuselage assembly measured in the stability axes system, slug-feet^2

$I_{xy_f}, I_{xz_f}, I_{yz_f}$ = products of inertia of fuselage assembly measured in the stability axes system, slug-feet^2

$I_{XX_T}, I_{YY_T}, I_{ZZ_T}$ = moments of inertia of total aircraft, measured in the stability axes system, slug-feet^2

I_{Y_P} = component of right-panel pitching moment of inertia defined by Equation (A-39), slug-feet^2

I_{XZ_T} = product of inertia of total aircraft, measured in the stability axes system, slug-feet^2

I_{XY_P}, I_{YZ_P} = components of right-wing-panel products of inertia defined by Equations (A-40) and (A-41), slug-feet^2

$\bar{j}$ = unit vector along Y axis

$\bar{k}$ = unit vector along Z axis

K_θ = gain constant, elevator deflection per unit pitch-angle error

$$L_p = \frac{\rho U_o S b^2}{4 I_{xx_T}} \, C_{\ell_p}$$

$$L_{p_w} = \frac{\rho U_o S b^2}{4 I_{xx_T}} \, C_{\ell_{p_w}}$$

$$L_r = \frac{\rho U_o S b^2}{4 I_{xx_T}} \, C_{\ell_r}$$

$$L_\beta = \frac{\rho U_o^2 S b}{2 I_{xx_T}} \, C_{\ell_\beta}$$

68

L_c = lift due to circulation, pounds

L_m = lift due to apparent mass of air, pounds

$$L_{\delta_e} = \frac{\rho U^2 S}{2}\ C_{L_{\delta_e}}$$

m = total mass of aircraft, slugs

m_f = mass of aircraft minus wings, slugs

m_p = mass of one wing panel, slugs

$M_{(i)}$ = fuselage-assembly pitching-moment coefficients defined by Equation (A-81)

$$M_{R_p} = \frac{\rho U_o S \bar{c} b}{4 I_{y'}}\ C_{m_{R_p}}$$

$$M_{R_\beta} = \frac{\rho U_o^2 S \bar{c}}{2 I_{y'}}\ C_{m_\beta}$$

$M_{x_{h_{R,L}}}$ = moment about x_h axis caused by inertial reactions of right, or left, wing panel, foot-pounds

$M_{y_{h_{R,L}}}$ = moment about y_h axis caused by inertial reactions of right, or left, wing panel, foot-pounds

$M_{z_{h_{R,L}}}$ = moments about z_h axis caused by inertial reactions of right, or left, wing panel, foot-pounds

$M_{x_f}, M_{y_f}, M_{z_f}$ = moments applied to fuselage assembly, measured in stability axes system, foot-pounds

$M_{X_{aero}}, M_{Z_{aero}}$ = aerodynamic moments acting on total aircraft, about roll and yaw stability axes, respectively, foot-pounds

$M_{Y_{aero}}$ = aerodynamic pitching moment acting on fuselage assembly, foot-pounds

$$N_p = \frac{\rho U_o S b^2}{4 I_{zz_T}}\ C_{n_p}$$

69

$$N_{p_w} = \frac{\rho U_o S b^2}{4 I_{zz_T}} C_{n_{p_w}}$$

$$N_r = \frac{\rho U_o S b^2}{4 I_{zz_T}} C_{n_r}$$

$$N_\beta = \frac{\rho U_o^2 S b}{2 I_{zz_T}} C_{n_\beta}$$

p = roll rate about X stability axis, radians/second

P = area of one free wing panel, feet^2

$P_{(i)}$ = coefficients of panel pitching equation, given by Equation (A-83)

q = pitching rate of fuselage, radians/second

Q = dynamic pressure, $\dfrac{\rho U_o^2}{2}$, pounds/foot^2

r = yawing rate about Z stability axis, radians/second

$\overline{R}$ = vector defining spatial position of origin of hinge axes system

$\overline{R}_o$ = vector defining spatial position of total aircraft center of gravity

S = total wing area, feet^2

$u = \dfrac{\Delta U}{U_o}$

u_h = component of velocity of hinge axis origin lying along x_h axis, feet/second

U = component of velocity of aircraft center of gravity along X stability axis, feet/second

v_h = component of velocity of hinge axis origin lying along y_h axis, feet/second

V = component of velocity of aircraft center of gravity along Y stability axis, feet/second

V_g = vertical gust velocity, positive upward, feet/second

w_h = component of velocity of hinge axis origin lying along z_h axis, feet/second

W = component of velocity of aircraft center of gravity along Z stability axis, feet/second

$\hat{x}$ = distance from hinge axis to half-chord point, a negative number, feet

x_h, y_h, z_h = coordinate axes in hinge system

x', y', z' = coordinate axes in wing-panel-fixed system

X, Y, Z = primary coordinate axes of stability axes system

$x'_{cg}, y'_{cg}, z'_{cg}$ = coordinates of wing-panel center of gravity measured in panel-fixed axes

$X_{f_{cg}}$ = longitudinal coordinate of fuselage center of gravity measured in stability axes system, feet

$\overline{X}$ = longitudinal coordinate of hinge axis measured in stability axes system, feet

$X_{(i)}$ = coefficients defined by Equation (A-87)

$$Y_p = \frac{\rho S b}{4m} C_{y_p}$$

$$Y_r = \frac{\rho S b}{4m} C_{y_r}$$

$$Y_\beta = \frac{\rho U_o S}{2m} C_{y_\beta}$$

$z_{f_{cg}}$ = coordinate of fuselage center of gravity measured along Z stability axis, feet

$Z_{(i)}$ = coefficients defined by Equation (A-72)

$\overline{Z}$ = coordinate of hinge axis measured along Z stability axis, feet

α_f = inertial angle of attack measured upward from inertial velocity vector to X stability axis, radians

β = sideslip angle, radians

δ_a = asymmetric tab displacement defined by Equation (A-47)

δ_e = symmetrical tab displacement, positive trailing edge down, radians

δ_P = displacement of right wing panel with respect to fuselage, positive leading edge up, radians

δ_L = displacement of left wing panel with respect to fuselage, positive leading edge up, radians

$\delta_{t_{R,L}}$ = displacement of right and left control tabs, respectively, positive trailing edge down, radians

θ = pitch angle of longitudinal fuselage axis with respect to horizon, radians

λ = Laplace operator, 1/second

φ = roll angle, positive right wing down, radians

ρ = atmospheric density, slugs/ft^3

ρ_x, ρ_y, ρ_z = components of position vector from origin to wing panel center of gravity measured in hinge axis system, feet

ψ = yaw angle, positive nose right, radians

$\overline{\omega}$ = angular velocity vector

Subscripts:

On unit vectors, h and p denote hinge axes and panel axes, respectively.

o = equilibrium value

* = measured with respect to earth-fixed reference

g = gust

w = wing

f = fuselage.

Coordinate Systems

Three coordinate systems were employed:

(1) Conventional stability axis system. Following standard practice, the basic set of coordinates for describing the aircraft motion has its origin at the center of gravity of the complete aircraft. The X axis is aligned with the velocity vector of the aircraft in the reference condition, the Y axis extends to the right of the plane of symmetry, and the Z axis completes the right-hand set. These coordinates are fixed in the aircraft and rotate with it.

   The orientation of the stability axis system with respect to an inertially fixed reference is defined by three standard Euler angles. The sequence of rotation used to define these angles is (1) rotation about the Z axis through the yaw angle ψ, (2) rotation about the Y axis through the pitch angle θ, and (3) rotation about the X axis through the roll angle φ.

   A sketch of the stability axis system is shown in Figure A-1.

(2) Hinge axis system. The hinge system of axes, x_h, y_h, z_h, has its origin in the plane of symmetry of the aircraft. The positive y_h axis coincides with the axis of rotation of the right wing panel. For simplicity, the wing panels are assumed to have no geometric dihedral. Consequently, z_h lies in the plane of symmetry and the negative y_h axis coincides with the axis of rotation of the left wing panel. The hinge axis system is parallel to the stability axis system, and is therefore fixed in the fuselage assembly for a given flight condition.

   Figure A-1 shows the hinge axis system.

(3) Panel axis system. The panel axis system, x', y', z', is similar to the hinge axis system but rotates with the wing panel under consideration. When dealing with the right wing panel, the panel axis system is rotated about the y_h axis through the displacement angle δ_P; whereas for the left panel the displacement angle is δ_L.

   The panel axis system is also illustrated in Figure A-1.
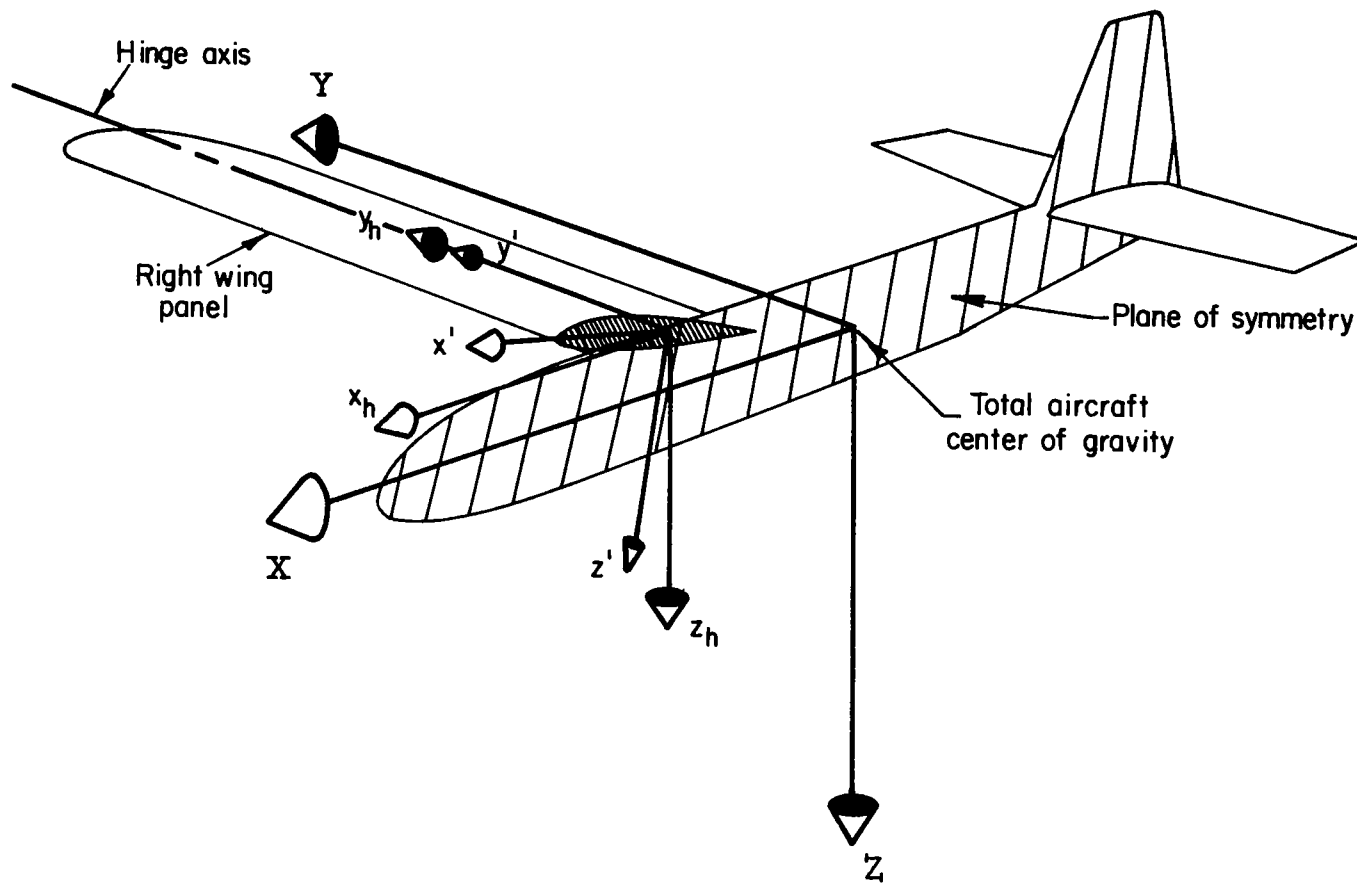
FIGURE A-1. ILLUSTRATION OF AXIS SYSTEMS

Free-Body Equations

Wing-Panel Force Equations

Force equations were developed for each wing panel separately, but only the right-wing-panel equation is discussed. A similar set of equations can be written for the left panel, differing only in the use of δ_L to denote panel displacement and the fact the y'_{cg} has the opposite sign for the left panel.

In the hinge axis system of Figure A-1, the position vector of the panel center of gravity is given by

$$\rho'_{cg} = \rho_x \bar{i}_h + \rho_y \bar{j}_h + \rho_z \bar{k}_h \quad , \tag{A-1}$$

where

$$\left.\begin{aligned}
\rho_x &= x'_{cg} \cos \delta_P + z'_{cg} \sin \delta_P \\
\rho_y &= y'_{cg} \\
\rho_z &= -x'_{cg} \sin \delta_P + z'_{cg} \cos \delta_P \quad .
\end{aligned}\right\} \tag{A-2}$$

If u_h, v_h, and w_h are the components of the inertial velocity of the origin of the hinge axis system, measured in that system, the inertial velocity of the panel center of gravity is

$$\begin{aligned}
\bar{V}_p = {}& (u_h + \dot{\rho}_x) \; \bar{i}_h + (v_h + \dot{\rho}_y) \; \bar{j}_h + (w_h + \dot{\rho}_z) \; \bar{k}_h \\
& + (\bar{\omega}_h \times \bar{\rho}'_{cg}) \quad .
\end{aligned} \tag{A-3}$$

The velocity of the hinge axis origin can be expressed in terms of the velocity of the aircraft center of gravity as

$$\left.\begin{aligned}
u_h &= U + q\bar{Z} \\
v_h &= V + r\bar{X} - p\bar{Z} \\
w_h &= W - q\bar{X} \quad .
\end{aligned}\right\} \tag{A-4}$$

Since the hinge axis system is parallel to the stability axes in which p, q, and r are defined,

$$\bar{\omega}_h = p\bar{i}_h + q\bar{j}_h + r\bar{k}_h \quad .$$

(A-5)

Differentiating once again, the inertial acceleration of the right-wing-panel center of gravity is obtained:

$$\bar{a}_p = a_{p_x}\bar{i}_h + a_{p_j}\bar{j}_h + a_{p_z}\bar{k}_h \quad ,$$

(A-6)

where

$$
\left.
\begin{aligned}
a_{p_x} &= \dot{u}_h - y'_{cg}(\dot{r} - pq) - rv_h + qw_h - \rho_z(\ddot{\delta}_P + \dot{q} + pr) \\
&\quad - \rho_x[(q + \dot{\delta}_P)^2 + r^2] \\[2mm]
a_{p_y} &= \dot{v}_h - y'_{cg}(r^2 + p^2) + ru_h - pw_h + \rho_x(\dot{r} + 2p\dot{\delta}_P + pq) \\
&\quad - \rho_z(\dot{p} - 2r\dot{\delta}_P - qr) \\[2mm]
a_{p_z} &= \dot{w}_h + y'_{cg}(\dot{p} + qr) + pv_h - qu_h + \rho_x(pr - \dot{q} - \ddot{\delta}_P) \\
&\quad - \rho_z[(q + \dot{\delta}_P)^2 + p^2] \quad .
\end{aligned}
\right\}
$$

(A-7)

Then, applying the fundamental Newtonian law, the three equations describing the forces existing at the origin of the hinge axis system that are associated with acceleration of the right wing panel are

$$
\left.
\begin{aligned}
F_{x_{h_R}} &= m_p a_{p_x} \\[2mm]
F_{y_{h_R}} &= m_p a_{p_y} \\[2mm]
F_{z_{h_R}} &= m_p a_{p_z}
\end{aligned}
\right\}
$$

(A-8)

Wing-Panel Moment Equations

The wing-panel moment equations are written most conveniently in the panel axes system (shown in Figure A-1) because in this system, the moments and products of inertia are constants. The moments are then transformed to the hinge axis system for later use.

An unusual feature of the panel axes is that the origin is displaced from the panel center of gravity. Because of this, the more general form of the principle of the conservation of moment of momentum must be used. This is

$$\bar{M} = \dot{\bar{H}} + (\rho \times m_p \ddot{\bar{R}}) \quad . \tag{A-9}$$

The components of the $\dot{\bar{H}}$ vector are the inertial terms found in the conventional Euler equations for the rotation of a rigid body. These are not rederived here because they are developed in many texts.

The second term, caused by the offset center of gravity, requires the development outlined below.

In the panel axis system, the position vector to the panel center of gravity, $\bar{\rho}$, is constant, and is given by

$$\bar{\rho} = x'_{cg} \bar{i}_p + y'_{cg} \bar{j}_p + z'_{cg} \bar{k}_p \quad . \tag{A-10}$$

The inertial velocity of the origin of the panel axis system may be expressed in that system by noting that the origins of the hinge and panel axes coincide. So

$$\dot{\bar{R}} = u_h \bar{i}_h + v_h \bar{j}_h + w_h \bar{k}_h \quad . \tag{A-11}$$

This velocity vector may be transformed to the panel axes by a simple rotation transformation through the angle δ_p, for the right panel.

$$\begin{bmatrix} \bar{i}_h \\ \bar{j}_h \\ \bar{k}_h \end{bmatrix} = \begin{bmatrix} \cos \delta_P & 0 & \sin \delta_P \\ 0 & 1 & 0 \\ -\sin \delta_P & 0 & \cos \delta_P \end{bmatrix} \begin{bmatrix} \bar{i}_p \\ \bar{j}_p \\ \bar{k}_p \end{bmatrix} \qquad (A-12)$$

So

$$\dot{\bar{R}} = (u_h \cos \delta_P - w_h \sin \delta_P) \bar{i}_p + v_h \bar{j}_p + (u_h \sin \delta_P + w_h \cos \delta_P) \bar{k}_p \qquad (A-13)$$

and

$$\ddot{\bar{R}} = \frac{d}{dt}(u_h \cos \delta_P - w_h \sin \delta_P) \bar{i}_p + \dot{v}_h \bar{j}_p + \frac{d}{dt}(u_h \sin \delta_P$$
$$+ w_h \cos \delta_P) \bar{k}_p + (\bar{\omega}_R \times \dot{\bar{R}}) \qquad . \qquad (A-14)$$

The rotational rate of the right panel, $\bar{\omega}_R$, can be expressed in the hinge axis system as

$$\bar{\omega}_R = p \, \bar{i}_h + (q + \dot{\delta}_P) \bar{j}_h + r \, \bar{k}_h \qquad . \qquad (A-15)$$

Applying the transformation of Equation (A-12),

$$\bar{\omega}_R = (p \cos \delta_P - r \sin \delta_P) \bar{i}_p + (q + \dot{\delta}_P) \bar{j}_p$$
$$+ (p \sin \delta_P + r \cos \delta_P) \bar{k}_p \qquad . \qquad (A-16)$$

This can be written as

$$\bar{\omega}_R = \omega_{x'} \, \bar{i}_p + \omega_{y'} \, \bar{j}_p + \omega_{z'} \, \bar{k}_p \qquad . \qquad (A-17)$$

Using these equations, Equation (A-9) may be expressed in the panel axis system and then transformed, by means of Equation (A-11), into the hinge axis system. The components of the moment are, for the right panel:

$$
\begin{aligned}
M_{x_{h_R}} ={} & -m_p\, \rho_z\, (\dot{v}_h + ru_h - pw_h) + y'_{cg}\, m_p\, (\dot{w}_h + pv_h - qu_h) \\
& + I_{x'}\, \dot{\omega}_{x'} \cos \delta_P + I_{z'}\, \dot{\omega}_{z'} \sin \delta_P + I_{xy'}\, [(\omega_{x'}\, \omega_{z'} \\
& - \dot{\omega}_{y'}) \cos \delta_p + (\omega^2_{y'} - \omega^2_{x'}) \sin \delta_p] - I_{xz'}\, [(\dot{\omega}_{z'} \\
& + \omega_{x'}\, \omega_{y'}) \cos \delta_P + (\dot{\omega}_{x'} - \omega_{y'}\, \omega_{z'}) \sin \delta_P] + I_{y'z'} \\
& [(\omega^2_{z'} - \omega^2_{y'}) \cos \delta_P - (\dot{\omega}_{y'} + \omega_{x'}\, \omega_{z'}) \sin \delta_P] \\
& + (I_{z'} - I_{y'})\, \omega_{z'}\, \omega_{y'} \cos \delta_P + (I_{y'} - I_{x'})\, \omega_{x'}\, \omega_{y'} \sin \delta_P
\end{aligned}
\Bigg\} \quad \text{(A-18)}
$$

$$
\begin{aligned}
M_{y_{h_R}} ={} & m_p\, \rho_z\, (\dot{u}_h - rv_h + qw_h) - m_p\, \rho_x\, (\dot{w}_h - qu_h + pv_h) + I_{y'}\, \dot{\omega}_{y'} \\
& + I_{y'z'}\, (\omega_{x'}\, \omega_{y'} - \dot{\omega}_{z'}) - I_{x'y'}\, (\dot{\omega}_{x'} + \omega_{y'}\, \omega_{z'}) + I_{x'z'} \\
& (\omega^2_{x'} - \omega^2_{z'}) + (I_{x'} - I_{z'})\, \omega_{x'}\, \omega_{z'}
\end{aligned}
\Bigg\} \quad \text{(A-19)}
$$

$$
\begin{aligned}
M_{z_{h_R}} ={} & m_p\, \rho_x\, (\dot{v}_h + ru_h - pw_h) - y'_{cg}\, m_p\, (\dot{u}_h + qw_h - rv_h) \\
& - I_{x'}\, \dot{\omega}_{x'} \sin \delta_P + I_{z'}\, \dot{\omega}_{z'} \cos \delta_P - I_{x'y'}\, [(\omega_{x'}\, \omega_{z'} \\
& - \dot{\omega}_{y'}) \sin \delta_P\, (\omega^2_{y'} - \omega^2_{x'}) \cos \delta_P] + I_{x'z'}\, [(\dot{\omega}_{z'} \\
& + \omega_{x'}\, \omega_{y'}) \sin \delta_P + (\omega_{y'}\, \omega_{z'} - \dot{\omega}_{x'}) \cos \delta_P] - I_{y'z'} \\
& [(\omega^2_{z'} - \omega^2_{y'}) \sin \delta_P + (\dot{\omega}_{y'} + \omega_{x'}\, \omega_{z'}) \cos \delta_P] \\
& + (I_{y'} - I_{z'})\, \omega_{z'}\, \omega_{y'} \sin \delta_P + (I_{y'} - I_{x'})\, \omega_{x'}\, \omega_{y'} \cos \delta_P
\end{aligned}
\quad \text{(A-20)}
$$

For the left wing panel, the equations are identical in form. They may be written by simply changing the sign of every term containing y'_{cg} as a factor. It should also be noted that moments of inertia are the same for each panel, but the products of inertias containing the y component change sign.

$$I_{xy'_R} = -I_{xy'_L}$$

$$I_{yz'_R} = -I_{yz'_L} \qquad\qquad \text{(A-21)}$$

Fuselage Moment Equations

The fuselage moment equations are written in the stability axis system whose origin lies at the center of gravity of the complete aircraft. Since the center of gravity of the fuselage assembly free-body does not, in general, coincide with that of the entire aircraft, the general form of the equation for the conservation of angular momentum must be used.

$$\bar{M}_f = \dot{\bar{H}}_f + (\bar{\rho}_f \times m_f \ddot{\bar{R}}_o) \qquad . \qquad\qquad \text{(A-22)}$$

Since the fuselage center of gravity is assumed to lie in the aircraft's plane of symmetry,

$$\bar{\rho}_f = x_{f_{cg}} \bar{i} + z_{f_{cg}} \bar{k} \qquad\qquad \text{(A-23)}$$

Since the velocity of the origin is the velocity of the aircraft's center of gravity,

$$\dot{\bar{R}}_o = U\bar{i} + V\bar{j} + W\bar{k} \qquad\qquad \text{(A-24)}$$

and

$$\ddot{\bar{R}}_o = \dot{U}\bar{i} + \dot{V}\bar{j} + \dot{W}\bar{k} + (\bar{\omega} \times \dot{\bar{R}}_o) \qquad , \qquad\qquad \text{(A-25)}$$

where

$$\bar{\omega} = p\bar{i} + q\bar{j} + r\bar{k} \qquad . \qquad\qquad \text{(A-26)}$$

So the second term on the right of Equation (A-22) becomes

$$
\begin{aligned}
\bar{\rho}_f \times m_f \ddot{\bar{R}}_o = & -m_f \, z_{f_{cg}} (\dot{V} - pW + rU) \, \bar{i} + m_f \, [(\dot{U} + qW \\
& - rV) \, z_{f_{cg}} - (\dot{W} + pV - qU) \, x_{f_{cg}}] \, \bar{j} \\
& + m_f \, x_{f_{cg}} (\dot{V} - pW + rU) \, \bar{k} \quad .
\end{aligned}
\qquad (A\text{-}27)
$$

The remaining terms on the right side of Equation (A-22) are, as before, the inertial terms found in the conventional Euler equations for the rotation of a rigid body.

The components of the applied fuselage moment defined by Equation (A-22) becomes

$$
\begin{aligned}
M_{x_f} = & -m_f \, z_{f_{cg}} (\dot{V} - pW + rU) + I_{x_f} \dot{p} + I_{xy_f} (pr - \dot{q}) \\
& - I_{xz_f} (\dot{r} + pq) + I_{yz_f} (r^2 - q^2) + (I_{z_f} - I_{y_f}) \, rq \quad .
\end{aligned}
$$

$$
\begin{aligned}
M_{y_f} = & \; m_f \, [(\dot{U} + qW - rV) \, z_{f_{cg}} - (\dot{W} + pV - qU) \, x_{f_{cg}}] \\
& + I_{y_f} \dot{q} + I_{yz_f} (pq - \dot{r}) - I_{xy_f} (\dot{p} + qr) \\
& + I_{xz_f} (p^2 - r^2) + (I_{x_f} - I_{z_f}) \, pr \quad .
\end{aligned}
\qquad (A\text{-}28)
$$

$$
\begin{aligned}
M_{z_f} = & \; m_f \, x_{f_{cg}} (\dot{V} - pW + rU) + I_{z_f} \dot{r} + I_{xz_f} (qr - \dot{p}) \\
& - I_{yz_f} (\dot{q} + pr) + I_{xy_f} (q^2 - p^2) + (I_{y_f} - I_{x_f}) \, pq \quad .
\end{aligned}
$$

The moments applied to the fuselage assembly, represented by the sides to the left in Equation (A-28), contain contributions from the reversed effective forces and moments of the wing panels. In actuality, they also contain gravity moments due to the weight of the fuselage and wing panels; however,

since the origin is at the total aircraft center of gravity, these weight moments must add to zero.

Total Aircraft Equations

The translational equations describing the motion of the mass center of the aircraft are the conventional expression of Newtons law of motion expressed in a rotating axis system. In the stability axes system these are

$$
\left.\begin{aligned}
F_x &= m\,(\dot{U} + qW - rV) \\[2mm]
F_y &= m\,(\dot{V} - pW + rU) \\[2mm]
F_z &= m\,(\dot{W} + pV - qU)\quad.
\end{aligned}\right\} \tag{A-29}
$$

The gravity-force contributions can be expressed as

$$
\left.\begin{aligned}
F_{x_{gravity}} &= -mg \sin\theta \\[2mm]
F_{y_{gravity}} &= mg \cos\theta \sin\varphi \\[2mm]
F_{z_{gravity}} &= mg \cos\theta \cos\varphi\quad.
\end{aligned}\right\} \tag{A-30}
$$

Finally, the complete set of equations defining the translation and rotation of the stability axes system may be written:

$$
\left.\begin{aligned}
F_{x_{aero}} &= m\,(\dot{U} + qW - rV) + mg \sin\theta \\[2mm]
F_{y_{aero}} &= m\,(\dot{V} + pV - rU) - mg \cos\theta \sin\varphi \\[2mm]
F_{z_{aero}} &= m\,(\dot{W} + pV - qU) - mg \cos\theta \cos\varphi
\end{aligned}\right\} \tag{A-31}
$$

and

$$M_{x_{aero}} = M_{x_f} + (M_{x_{h_R}} + M_{x_{h_L}}) - (F_{y_{h_R}} + M_{y_{h_L}})\,\overline{Z}$$

$$M_{y_{aero}} = M_{y_f} + (F_{x_{h_R}} + F_{x_{h_L}})\,\overline{Z} - (F_{z_{h_R}} + F_{z_{h_L}})\,\overline{X} \qquad (A-32)$$

$$M_{z_{aero}} = M_{z_f} + (M_{z_{h_R}} + M_{z_{h_L}}) + (F_{y_{h_R}} + M_{y_{h_L}})\,\overline{X} \;.$$

Here, M_{x_f}, M_{y_f}, and M_{z_f} come from Equation (A-28), and the remaining terms are the reversed effective forces and moments which may be evaluated from Equations (A-8) and (A-18) and equivalent expressions for the contributions of the left wing panel.

Two additional equations are necessary to describe the complete system. These are the expressions representing the rotational degrees of freedom of the two wing panels. One of these was written previously as Equation (A-19) for the right wing panel.

Linearization of Equations

The equations are linearized, using conventional techniques, about an equilibrium flight condition of straight and level flight with no angular rates or accelerations. The equilibrium panel deflections are not assumed to be zero, but they are assumed to be identical. In the following equations, all variables are considered as small perturbations from the reference condition.

Translational equations:

$$m\dot{U} = \Delta F_x - (mg)\,\theta$$

$$m\dot{V} = \Delta F_y - (mU_o)\,r - (mg)\,\varphi \qquad (A-33)$$

$$m\dot{W} = \Delta F_z + (mU_o)\,q \;.$$

Rotational equations (fuselage assembly):

$$I_{XX_T} \dot{p} = I_{XZ_T} \dot{r} + I_{XY_P} (\ddot{\delta}_P - \ddot{\delta}_L) + M_{X_{aero}}$$

$$I_{YY_T} \dot{q} = I_{Y_P} (\ddot{\delta}_P + \ddot{\delta}_L) + \overline{Z} \left(\Delta F_{x_{aero, wings}} \right)$$

$$- \overline{X} \left(\Delta F_{z_{aero, wings}} \right)$$

$$I_{ZZ_T} \dot{r} = I_{XZ_T} \dot{p} + I_{YZ_P} (\ddot{\delta}_P - \ddot{\delta}_L) + \Delta M_{Z_{aero}} \quad \Bigg\}$$

$$\left. \right\} \quad \text{(A-34)}$$

Wing panel rotational equations:

$$I_{y'} \ddot{\delta}_P = (- I_{y'} - \overline{Z} m_p \rho_z - \overline{X} m_p \rho_x) \dot{q} - (U_o m_p \rho_x) q$$

$$+ (-m_P \rho_z) \dot{U} + (m_p \rho_x) \dot{W} + I_{XY_P} \dot{p} + I_{YZ_P} \dot{r}$$

$$+ \Delta M_{y_{h_R}} \quad .$$

$$I_{y'} \ddot{\delta}_L = (-I_{y'} - \overline{Z} m_p \rho_z - \overline{X} m_p \rho_x) \dot{q} - (U_o m_p \rho_x) q$$

$$- (m_p \rho_z) \dot{U} + (m_p \rho_x) \dot{W} - I_{XY_P} \dot{p} - I_{YZ_P} \dot{r}$$

$$+ \Delta M_{y_{h_L}} \quad .$$

$$\left. \right\} \quad \text{(A-35)}$$

The total moments and products of inertia used in Equations (A-34) and (A-35) are computed from:

$$I_{XX_T} = I_{x_f} + 4m_p \overline{Z} \rho_z + 2I_{x'} \cos^2 \delta_o + 2I_{z'} \sin^2 \delta_o$$

$$- 4I_{xz'} \sin \delta_o \cos \delta_o + 2\overline{Z}^2 m_p$$

$$\text{(A-36)}$$

$$I_{YY_T} = I_{y_f} + 2m_p \, \overline{Z} \, (\overline{Z} + \rho_z) + 2m_p \, \overline{X} \, (\overline{X} + \rho_x) \qquad (A\text{-}37)$$

$$I_{ZZ_T} = I_{z_f} + 4m_p \, \overline{X} \, \rho_x + 2I_{x'} \sin^2 \delta_o + 2I_{z'} \cos^2 \delta_o$$
$$+ 4I_{xz'} \sin \delta_o \cos \delta_o + 2\overline{X}^2 \, m_p \qquad (A\text{-}38)$$

$$I_{XZ_T} = I_{xz_f} + 2m_p \, (\overline{X} \, \rho_z + \overline{Z} \, \rho_x) + (I_{x'} - I_{z'}) \sin 2\delta_o$$
$$+ 2I_{xz'} \cos 2\delta_o + 2m_p \, \overline{X} \, \overline{Z} \qquad (A\text{-}39)$$

$$I_{Y_P} = m_p \, (\overline{Z} \, \rho_z - \overline{X} \, \rho_x) \qquad (A\text{-}40)$$

$$I_{XY_P} = I_{xy'} \cos \delta_o + I_{yz'} \sin \delta_o \qquad (A\text{-}41)$$

$$I_{YZ_P} = I_{yz'} \cos \delta_o - I_{xy'} \sin \delta_o \quad . \qquad (A\text{-}42)$$

The Lateral-Directional Equations

Examination of the wing-panel displacement terms in Equation (A-34) shows that symmetrical wing-panel motion, $(\delta_p = \delta_L)$, has no effect upon the rolling and yawing equations. Furthermore, in Equation (A-35), rolling and yawing accelerations are seen to cause only asymmetric panel displacements, since the terms containing these variables have the same coefficient, but opposite sign, in the two equations. In addition, the aerodynamic derivatives are such that no coupling exists between lateral-directional variables and symmetrical wing-panel displacements. Because of this separation, the linearized equations can be split into two uncoupled sets, just as with a conventional aircraft.

Since only asymmetric displacement is significant, let

$$\delta_L = -\delta_P \quad . \qquad (A\text{-}43)$$

The lateral-directional equations then become

$$I_{XX_T} \dot{p} = I_{XZ_T} \dot{r} + 2I_{XY_P} \ddot{\delta}_P + M_{X_{aero}}$$

$$I_{ZZ_T} \dot{r} = I_{XZ_T} \dot{p} + 2I_{YZ_P} \ddot{\delta}_P + M_{Z_{aero}}$$

$$m\dot{V} = \Delta F_Y - (mU_o) r - (mg) \varphi \qquad\qquad\qquad (A-44)$$

$$I_{y'} \ddot{\delta}_P = I_{XY_P} \dot{p} + I_{YZ_P} \dot{r} + M_{y_{h_R}} \qquad .$$

The aerodynamic rolling moment is expressed as follows:

$$M_{x_{aero}} = \Delta C_\ell \frac{\rho U_o^2 Sb}{2} \qquad\qquad (A-45)$$

if

$$C_\ell = C_\ell \left(\frac{pb}{2U_o}, \frac{rb}{2U_o}, \beta, \delta_P, \delta_L, \delta_{t_R}, \delta_{t_L} \right) \qquad . \qquad (A-46)$$

The rolling moment coefficient may be expanded in a Taylors series about the equilibrium zero value. If only the first-order terms are retained, these become the rolling-moment stability derivatives.

Equation (A-45) then becomes

$$M_{x_{aero}} = \frac{\rho U_o Sb^2}{4} \left[C_{\ell_p} p + C_{\ell_r} r \right] + \frac{\rho U_o^2 Sb}{2} \left[C_{\ell_\beta} \beta + C_{\ell_{\delta_P}} \delta_P \right.$$
$$\left. + C_{\ell_{\delta_L}} \delta_L + C_{\ell_{\delta_{t_R}}} \delta_{t_R} + C_{\ell_{\delta_{t_L}}} \delta_{t_L} \right] \qquad . \qquad (A-47)$$

For control-tab displacements, only asymmetric control is of interest for lateral-directional motion. Because of this, define:

$$\delta_a = \delta_{t_R} = -\delta_{t_L} \qquad . \tag{A-48}$$

Using Equations (A-48) and (A-43), and the fact that

$$\left. \begin{array}{l} C_{\ell_{\delta_L}} = -C_{\ell_{\delta_P}} \\[2ex] C_{\ell_{\delta_{t_L}}} = C_{\ell_{\delta_{t_R}}} \end{array} \right\} \quad , \tag{A-49}$$

the rolling moment becomes

$$M_{x_{aero}} = \frac{\rho U_o S b^2}{4} \left[C_{\ell_p} p + C_{\ell_r} r \right] + \frac{\rho U^2_o S b}{2} \left[C_{\ell_\beta} \beta \right.$$
$$\left. + 2 C_{\ell_{\delta_P}} \delta_P + 2 C_{\ell_{\delta_{t_R}}} \delta_a \right] \qquad . \tag{A-50}$$

By similar development, it can be shown that

$$M_{Z_{aero}} = \frac{\rho U_o S b^2}{4} \left[C_{n_p} p + C_{n_r} r \right] + \frac{\rho U^2_o S b}{2} \left[C_{n_\beta} \beta + \right.$$
$$\left. + 2 C_{n_{\delta_P}} \delta_P + 2 C_{n_{\delta_{t_R}}} \delta_a \right] \tag{A-51}$$

and

$$\Delta F_y = \frac{\rho U_o S b}{4} \left[C_{y_p} p + C_{y_r} r \right] + \frac{\rho U^2_o S}{2} \left[C_{y_\beta} \beta + 2 C_{y_\delta} \delta \right] \qquad . \tag{A-52}$$

Similarly,

$$M_{y_{h_R}} = \Delta C_{m_R} Q S \bar{c} \qquad , \tag{A-53}$$

and let

$$C_{m_R} = C_{m_R}\left(\frac{pb}{2U_o}, \frac{\dot{\delta}_p \bar{c}}{2U_o}, \beta, \delta_P, \delta_L, \delta_{t_R}, \delta_{t_L} \right) \quad . \quad (A\text{-}54)$$

The Taylors series expansion of this function, along with Equations (A-43) and (A-48), yields

$$M_{y_{h_R}} = \frac{\rho U_o S \bar{c} b}{4} \left[C_{m_{R_p}} p \right] + \frac{\rho U_o S \bar{c}^2}{4} \left[C_{m_{R_{\dot{\delta}_P}}} \dot{\delta}_P \right]$$

$$+ \frac{\rho U_o^2 S \bar{c}}{2} \left[2C_{m_{R_{\delta_P}}} \delta_P + C_{m_\beta} \beta + \left(C_{m_{R_{\delta_{t_R}}}} \right. \right. \qquad (A\text{-}55)$$

$$\left. \left. - C_{m_{R_{\delta_{t_L}}}} \right) \delta_a \right] \quad .$$

Sideslip angle is introduced as the dependent variable in the third equation of Equation (A-43) by the substitution,

$$\dot{\beta} = \frac{\dot{V}}{U_o} \qquad (A\text{-}56)$$

The set of linear equations describing the lateral-directional motion in still air can now be written as:

$$\dot{p} = \frac{I_{XZ_T}}{I_{XX_T}}\,\dot{r} + 2\,\frac{I_{XY_P}}{I_{XX_T}}\,\ddot{\delta}_P + \frac{\rho U_o Sb^2}{4I_{XX_T}}\left[C_{\ell_p}\,p + C_{\ell_r}\,r\right]$$

$$+ \frac{\rho U_o^2 Sb}{2I_{XX_T}}\left[C_{\ell_\beta}\,\beta + 2C_{\ell_{\delta_P}}\,\delta_P + 2C_{\ell_{\delta_{t_R}}}\,\delta_a\right]$$

$$\dot{r} = \frac{I_{XZ_T}}{I_{ZZ_T}}\,\dot{p} + 2\,\frac{I_{YZ_P}}{I_{ZZ_T}}\,\ddot{\delta}_P + \frac{\rho U_o Sb^2}{4I_{ZZ_T}}\left[C_{n_p}\,p + C_{n_r}\,r\right]$$

$$+ \frac{\rho U_o^2 Sb}{2I_{ZZ_T}}\left[C_{n_\beta}\,\beta + 2C_{n_{\delta_P}}\,\delta_P + 2C_{n_{\delta_{t_R}}}\,\delta_a\right]$$

$$\dot{\beta} = \frac{\rho Sb}{4m}\,C_{y_p}\,p + \left[\frac{\rho Sb}{4m}\,C_{y_r} - 1\right]r - \frac{g}{U_o}\,\phi \qquad \Bigg\}\ (\text{A-57})$$

$$+ \frac{\rho U_o S}{2m}\left[C_{y_\beta}\,\beta + 2C_{y_\delta}\,\delta_P\right]$$

$$\ddot{\delta}_P = \frac{I_{XY_P}}{I_{y'}}\,\dot{p} + \frac{I_{YZ_P}}{I_{y'}}\,\dot{r} + \left[\frac{\rho U_o S\bar{c}b}{4I_{y'}}\,C_{m_{R_p}}\right]p$$

$$+ \left[\frac{\rho U_o S\bar{c}^2}{4I_{y'}}\,C_{m_{R_{\dot{\delta}_P}}}\right]\dot{\delta}_P + \frac{\rho U_o^2 S\bar{c}}{2I_{y'}}\left[2C_{m_{R_{\delta_P}}}\,\delta_P + C_{m_\beta}\,\beta\right.$$

$$\left. + (C_{m_{R_{\delta_{t_R}}}} - C_{m_{R_{\delta_{t_L}}}})\,\delta_a\right].$$

$$\dot{\phi} = p$$

$$\dot{\psi} = r$$

$$\dot{D}y = U_o\,(\psi + \beta)\qquad .$$

89

To these equations, a feedback control expression was added to permit simulation of bank-angle control by a pilot or augmentation system. To perform this function, aileron deflection is considered as a linear function of roll angle and roll rate, with no actuator lags.

$$\delta_a = C_\phi \; \phi + C_p \, p \quad .$$

(A-58)

When flying in turbulence, the air mass is in motion. The relative velocities, both linear and angular, of the aircraft with respect to the local air mass is considered to be made up of two parts: one caused by motion of the aircraft with respect to an earth-fixed reference, and the other caused by air movement.

$$p = \dot{\phi} = \dot{\phi}_* + \dot{\phi}_g$$

$$r = \dot{\psi} = \dot{\psi}_* + \dot{\psi}_g$$

(A-59)

$$\beta = \beta_* + \beta_g \quad .$$

In Equation (A-59), the subscript (*) denotes displacement with respect to the Earth-fixed frame of reference, and the subscript (g) denotes effective rolling, yawing, and sideslip gusts, respectively.

If the set of equations in Equation (A-59) is substituted into the set in Equation (A-57), and proper distinction is made between inertial and aerodynamic displacements, the set of equations can be written as

$$
[B]
\begin{bmatrix}
\phi_* \\
\psi_* \\
\beta_* \\
\delta_P \\
\delta_a \\
D_y
\end{bmatrix}
= [G]
\begin{bmatrix}
\dot{\phi}_g \\
\psi_g \\
\beta_g \\
0 \\
0 \\
0
\end{bmatrix}
$$

(A-60)

90

where [B] is given by Equation (4) in the main body of this report and

$$[G] = \begin{bmatrix} L_p & L_r & L_\beta & 0 & 0 & 0 \\ N_p & N_r & N_\beta & 0 & 0 & 0 \\ Y_p & Y_r & Y_\beta & 0 & 0 & 0 \\ M_{R_p} & 0 & 2M_{R_\beta} & 0 & 0 & 0 \\ 0 & 0 & 0 & 0 & 0 & 0 \\ 0 & 0 & 0 & 0 & 0 & 0 \end{bmatrix} \qquad (A\text{-}61)$$

The rolling gusts of Equation (A-59) result, in reality, from the span-wise gradient of the vertical gust velocity. Similarly, the yawing gust is related to the gradient of side gust velocity along the length of the aircraft. The yawing gust is therefore related to the sideslip gust, whereas both of these are unrelated to the rolling gust.

It should be mentioned at this point that the use of equivalent rolling and yawing gusts, operating through fixed coefficients to provide the turbulence forcing function, is an approximation to the more rigorous technique outlined in Reference A-1. In that work, use was made of power spectra of rolling- and yawing-moment coefficients on wings subjected to continuous isotropic turbulence. These spectra take into account the random distribution of gusts across the span and along the flight path. Furthermore, the sideslip-dependent coefficients in the third column of Equation (A-61) become frequency-dependent if lateral gust penetration effects are incorporated as in Reference A-1.

The effective yawing gust of Equation (A-60) includes two independent effects. One is the spanwise gradient of the head-on longitudinal gust velocity which acts predominantly to cause rolling moments through the L_r coefficient, and the other is the gradient of the side gust velocity which acts upon the fuselage and vertical tail as an aerodynamic yawing rate.

The results of Reference A-1 show that the spanwise gradient of longitudinal gust velocity has a negligible contribution to the total motion; for this reason the L_r term in the G matrix may be ignored. Furthermore, the side force caused by the yawing gust, Y_r, is generally a much smaller effect than the yawing moment, and may also be omitted. As an additional and important simplification, the side gust forcing-function coefficients are not treated as

frequency-dependent stability derivatives. Instead, the lateral gust penetration effects are included only by allowing for the equivalent aerodynamic yawing-rate forcing function in the yawing-moment equation.

With these simplifications, Equation (A-58) becomes

$$
[B] \begin{bmatrix} \phi_* \\ \psi_* \\ \beta_* \\ \delta_P \\ \delta_a \\ D_y \end{bmatrix} = \begin{bmatrix} -L_{P_w} \\ -N_{P_w} \\ 0 \\ -M_{R_p} \\ 0 \\ 0 \end{bmatrix} \dot{\phi}_g + \begin{bmatrix} -L_\beta \\ -N_\beta - N_r \lambda \\ -Y_\beta \\ -2M_{R_\beta} \\ 0 \\ 0 \end{bmatrix} \beta_g \qquad (A-62)
$$

In Equation (A-62), the subscript w has been added to the coefficients of the rolling and yawing moments caused by the rolling gust. This is in accordance with the rationale of Reference A-1, which recognizes that the spanwise gradient of vertical gust velocity acts almost exclusively on the wing, and not on other parts of the aircraft, such as the vertical tail, which normally contribute to these derivatives.

The Longitudinal Equations

For the longitudinal motion, only symmetrical wing-panel displacement need be considered:

$$
\delta_L = \delta_P \quad . \qquad (A-63)
$$

Similarly, only symmetrical control-tab displacement is included. Because of this, let

$$
\delta_e = \delta_{t_R} = \delta_{t_L} \quad . \qquad (A-64)
$$

The longitudinal equations from Equations (A-33), (A-34), and (A-35) then become

$$m\dot{W} = \Delta F_z + (mU_o) q$$

$$I_{YY_T} \dot{q} = 2I_{YP} \ddot{\delta}_P + \overline{Z} (\Delta F_{x_{aero,\,wings}}) - \overline{X} (\Delta F_{z_{aero,\,wings}})$$

$$+ \Delta M_{y_{aero}}$$

(A-65)

$$I_{y'} \ddot{\delta}_P = [-I_{y'} - \overline{Z} m_p \rho_z - \overline{X} m_p \rho_x] \dot{q} + (-U_o m_p \rho_x) q$$

$$+ (-m_p \rho_z) \dot{U} + (m_p \rho_x) \dot{W} + \Delta M_{y_{h_R}}$$

$$m\dot{U} = \Delta F_x + (-mg) \theta \quad .$$

The first of these equations can be written in terms of the fuselage angle of attack by noting that

$$\dot{\alpha}_f = \frac{\dot{w}}{U_o} \quad . \tag{A-66}$$

The equation becomes

$$\dot{\alpha}_f = \frac{\Delta F_z}{mU_o} + q \quad . \tag{A-67}$$

The increment in normal force, ΔF_z, involves components due to circulatory lift and apparent mass effects, as shown in Appendix B. In fact,

$$\Delta F_z = L_c + L_m + L_{\delta_e} \delta_e \quad . \tag{A-68}$$

L_c is the circulatory lift, and from Appendix B, is

$$L_c = QS \left\{ G_1 \left[\alpha_f + \delta_P + \left(\frac{\overline{c}}{rU_o} - \frac{\overline{X}}{U_o} - \frac{\hat{x}}{U_o} \right) q + \left(\frac{\overline{c}}{rU_o} - \frac{\hat{x}}{U_o} \right) \dot{\delta}_P \right] + G_2 \left(\frac{v_g}{U_o} \right) \right\} \tag{A-69}$$

93

Where G_1 and G_2 are complex lift-curve-slope derivatives which for aspect ratios near 6 may be written as the following transfer functions:

$$G_1 (\lambda) = C_{L_{\alpha_w}} \left[1 - \frac{0.361\lambda}{\lambda + 0.598 \frac{U}{\bar{c}}} \right] \qquad \text{(A-70)}$$

$$G_2 (\lambda) = C_{L_{\alpha_w}} \left[1 - \frac{0.488\,\lambda}{\lambda + 0.455 \frac{U}{\bar{c}}} - \frac{0.272\,\lambda}{\lambda + 1.04 \frac{U}{\bar{c}}} - \frac{0.193\,\lambda}{\lambda + 4.71 \frac{U}{\bar{c}}} \right] . \qquad \text{(A-71)}$$

The factor in the brackets of Equation (A-70) describes the lag in circulatory lift following a change in the angle of attack due to wing motion, whereas the bracketed factor in Equation (A-71) represents the transient effects of angle-of-attack changes associated with vertical gusts.

From Appendix B, the lift increment due to apparent mass effects is

$$L_m = QS \frac{2\bar{c}}{EU} \left[\alpha_f + \dot{\delta} - \left(\frac{\overline{X}}{U_o} - \frac{\hat{x}}{U_o} \right) \dot{q} - \frac{x}{U_o} \ddot{\delta} \right] . \qquad \text{(A-72)}$$

After appropriate substitutions, Equation (A-67) becomes

$$Z_{\dot{\alpha}_f} \dot{\alpha}_f = Z_\alpha \alpha_f + Z_q q + Z_{\dot{q}} \dot{q} + Z_{\delta_P} \delta_P + Z_{\dot{\delta}_P} \dot{\delta}_P + Z_{\ddot{\delta}_P} \ddot{\delta}_P$$

$$\qquad \text{(A-73)}$$

$$+ Z_u u + Z_{V_g} V_g + Z_{\delta_e} \delta_e \quad ,$$

where

$$Z_{\dot{\alpha}_f} = 1 + \frac{\rho S \bar{c}}{mE}$$

$$Z_\alpha = -\frac{\rho U_o S}{2m}$$

$$Z_q = 1 - \frac{\rho S \bar{c}}{2m}\left(\frac{1}{\pi} - \frac{\overline{X}}{\bar{c}} - \frac{\hat{x}}{\bar{c}}\right)G_1$$

$$Z_{\dot{q}} = \frac{\rho S \bar{c}}{mEU}(\overline{X} + \hat{x})$$

$$Z_{\delta_P} = -\frac{\rho U S}{2m}G_1$$

$$Z_{\dot{\delta}_P} = \frac{\rho S \bar{c}}{2m}\left(\frac{\hat{x}}{\bar{c}} - \frac{\rho S \bar{c}}{mE} - \frac{1}{\pi}\right)G_1 \qquad\qquad \text{(A-74)}$$

$$Z_{\ddot{\delta}_P} = \frac{\rho S \bar{c}}{mEU_o}\hat{x}$$

$$Z_u = -\frac{2g}{U_o}$$

$$Z_{V_g} = -\frac{\rho S}{2m}G_2$$

$$Z_{\delta_e} = -\frac{\rho U S}{m}C_{L_{\delta_e}} \qquad .$$

The pitching motion of the fuselage assembly is given by the second equation of the set in Equation (A-65). For simplicity, unsteady aerodynamic effects are not included in the wing-force terms.

If the wing-force increments are assumed to be linearly related to wing angle-of-attack and airspeed changes,

$$\Delta F_{x_{aero_{wings}}} = -QS[C_{D_{\alpha_w}} \alpha_w + 2 C_{D_w} u] \tag{A-75}$$

$$\Delta F_{z_{aero_{wings}}} = -QS[C_{L_{\alpha_w}} \alpha_w + 2 C_{L_w} u] \quad , \tag{}$$

where

$$u = \frac{\Delta U}{U_o} \quad . \tag{A-76}$$

The wing angle of attack is

$$\alpha_w = \alpha_f + \delta_P + \frac{V_g}{U_o} \quad . \tag{A-77}$$

The aerodynamic pitching moment on the fuselage assembly is

$$\Delta M_{y_{aero}} = \Delta C_m QS\bar{c} \quad . \tag{A-78}$$

The vertical gust influences the aerodynamic angle of attack of the fuselage assembly since

$$\alpha = \alpha_f + \frac{V_g}{U_o} \quad . \tag{A-79}$$

Furthermore, following Reference A-2, the vertical gust imposes an effective pitching rate equal to

$$q_g = -\frac{\dot{V}_g}{U_o} \tag{A-80}$$

The influence of the variation in downwash at the horizontal tail caused by wing-panel deflections must also be considered in evaluating the increment in the fuselage pitching-moment coefficient. Equation (A-78) becomes

$$\Delta M_{y_{aero}} = Q S \bar{c} \left[C_{m_\alpha} \left(\alpha_f + \frac{V_g}{U_o} \right) + C_{m_q} \left(q - \frac{\dot{V}_{gV}}{U_o} \right) \frac{\bar{c}}{2U_o} \right.$$

$$\left. + C_{m_{\dot\alpha}} \left(\dot\alpha_f + \frac{\dot{V}_{gV}}{2U} \right) \frac{\bar{c}}{2U} + C_{m_{f_\delta}} \delta_P \right] . \tag{A-81}$$

With appropriate substitutions, then, the fuselage pitching equation may be written

$$\dot{q} = M_{\alpha_f} \alpha_f + M_{\dot\alpha_f} \dot\alpha_f + M_q q + M_{\ddot\delta_P} \ddot\delta_P + M_{\delta_P} \delta_P + M_{V_g} V_g$$

$$+ M_{\dot{V}_g} \dot{V}_g \quad , \tag{A-82}$$

where

$$\left. \begin{aligned}
M_{\alpha_f} &= \frac{\rho U^2 S \bar{c}}{2 I_{YY_T}} \left[C_{m_\alpha} + \frac{\overline{X}}{\bar{c}} C_{L_{\alpha_w}} - \frac{\overline{Z}}{\bar{c}} C_{D_{\alpha_w}} \right] \\[2mm]
M_{\dot\alpha_f} &= \frac{\rho U S \bar{c}^2}{4 I_{YY_T}} C_{m_{\dot\alpha}} \\[2mm]
M_q &= \frac{\rho U S \bar{c}^2}{4 I_{YY_T}} C_{m_q} \\[2mm]
M_{\delta_P} &= \frac{\rho U^2 S \bar{c}}{2 I_{YY_T}} \left[\frac{\overline{X}}{\bar{c}} C_{L_{\alpha_w}} - \frac{\overline{Z}}{\bar{c}} C_{D_{\alpha_w}} + C_{m_{f_\delta}} \right] \\[2mm]
M_{\ddot\delta_P} &= \frac{2 I_{Y_P}}{I_{YY_T}} \\[2mm]
M_{V_g} &= \frac{\rho U S \bar{c}}{2 I_{YY_T}} \left[C_{m_\alpha} + \frac{\overline{X}}{\bar{c}} C_{L_{\alpha_w}} - \frac{\overline{Z}}{\bar{c}} C_{D_{\alpha_w}} \right] \\[2mm]
M_{\dot{V}_g} &= \frac{\rho S \bar{c}^2}{4 I_{YY_T}} \left[C_{m_{\dot\alpha}} - C_{m_q} \right]
\end{aligned} \right\} \tag{A-83}$$

97

The third equation of the set in Equation (A-65) describes the pitching motion of one wing panel. The aerodynamic moment which appears in that equation involves the unsteady aerodynamics effects. After substitution, the equation may be written as

$$\ddot{\delta} = P_{\alpha_f} \alpha_f + P_{\dot{\alpha}_f} \dot{\alpha}_f + P_q q + P_{\dot{q}} \dot{q} + P_{\delta_P} \delta_P + P_{\dot{\delta}_P} \dot{\delta}_P$$

$$+ P_{\ddot{\delta}_P} \ddot{\delta}_P + P_{\dot{u}} \dot{u} + P_{\delta_e} \delta_e + P_{V_g} V_g \qquad , \tag{A-84}$$

where

$$P_{\alpha_f} = \frac{\rho U_o^2 P}{2 I_{y'}} \; (\hat{x} + \frac{\bar{c}}{4}) \, G_1$$

$$P_{\dot{\alpha}_f} = U m_p \frac{\rho_x}{I_{y'}} + \frac{\rho U_o P \bar{c}}{I_{y'}} \; \frac{\hat{x}}{E}$$

$$P_q = -U m_p \frac{\rho_x}{I_{y'}} + \frac{\rho U_o P}{2 I_{y'}} \; (\hat{x} + \frac{\bar{c}}{4}) \, (\frac{\bar{c}}{\pi} - x_h - \hat{x}) \, G_1$$

$$P_{\dot{q}} = -1 - \bar{Z} m_p \frac{\rho_z}{I_{y'}} - \bar{x} m_p \frac{\rho_x}{I_{y'}} - \frac{\rho P \bar{c}}{I_{y'}} \; \frac{\hat{x}}{E} (x_h + \hat{x})$$

$$P_{\delta_P} = \frac{\rho U_o^2 P}{2 I_{y'}} \; (\hat{x} + \frac{\bar{c}}{4}) \, G_1$$

$$P_{\dot{\delta}_P} = \frac{\rho U_o P}{2 I_{y'}} \; [(\hat{x} + \frac{\bar{c}}{4}) \, (\frac{\bar{c}}{\pi} - \hat{x}) \, G_1 + \frac{2\bar{c}}{E} (\hat{x} - \frac{\bar{c}}{4})]$$

$$P_{\ddot{\delta}_P} = \frac{\rho P \bar{c}}{I_{y'}} \; \frac{\hat{x}^2}{E}$$

$$P_{\dot{u}} = -U m_p \frac{\rho_z}{I_{y'}}$$

$$P_{\delta_e} = \frac{\rho U^2 P \bar{c}}{2 I_{y'}} \; (C_{m_{R_{\delta_{t_R}}}} + C_{m_{R_{\delta_{t_L}}}})$$

$$P_{V_g} = \frac{\rho U P}{2 I_{y'}} \; (\hat{x} + \frac{\bar{c}}{4}) \, G_2 \quad .$$

\qquad\qquad (A-85)

The last of the longitudinal equations of the set in Equation (A-65) can be written

$$\dot{u} = \frac{\Delta F_x}{mU_o} - \frac{g}{U_o} \theta \quad .$$

(A-86)

Here, F_x is one component of the total applied force vector which is composed of the lift force acting normal to the aerodynamic velocity vector and the drag and thrust forces which act parallel to the aerodynamic velocity.

The force term can be written

$$\frac{\Delta F_x}{mU_o} = \frac{g}{U_o} \alpha_f + \frac{g}{U_o^2} V_g + \frac{\rho US}{2m} [\Delta (C_T - C_D)] \quad .$$

(A-87)

Equation (A-86) becomes

$$u = X_{\alpha_f} \alpha_f + X_\theta \theta + X_{\delta_P} \delta_P + X_u u + X_{V_g} V_g \quad ,$$

(A-88)

where

$$\left. \begin{aligned} X_{\alpha_f} &= - \frac{\rho U_o S}{2m} \left(C_{D_{\alpha_w}} + C_{D_{\alpha_f}} \right) + \frac{g}{U_o} \\[2mm] X_\theta &= - \frac{g}{U_o} \\[2mm] X_{\delta_P} &= - \frac{\rho U_o S}{2m} C_{D_{\alpha_w}} \\[2mm] X_u &= \frac{\rho U_o^2 S}{2m} \frac{\partial C_T}{\partial U} \\[2mm] X_{V_g} &= \frac{g}{U_o^2} - \frac{\rho S}{2m} C_{D_{\alpha_w}} \quad . \end{aligned} \right\}$$

(A-89)

Two additional equations, associated with longitudinal motion, were used in the analysis. The first describes a simple feedback of fuselage pitch attitude to elevator (symmetrical tab) displacement:

$$\delta_e = K_\theta \theta$$

(A-90)

The second is the kinematic relationship required to compute altitude deviations:

$$\dot{h} = U_o (\theta - \alpha_f) \quad . \tag{A-91}$$

The complete set of linear longitudinal equations, composed of Equations (A-73), (A-82), (A-84), (A-88), (A-90), and (A-91), appears in matrix operational form as Equation (1) in the main body of this report.

References

A-1. Eggleston, John M., and Phillips, William H., "The Lateral Response of Airplanes to Random Atmospheric Turbulence", NASA Technical Report R-74 (1960).

A-2. Etkin, Bernard, Dynamics of Flight, John Wiley and Sons, Inc., New York (1959).

AERODYNAMIC CHARACTERISTICS OF FREE WINGS

Introduction

The unique character of the free-wing concept required certain preliminary tasks to (1) define the control-tab geometry; (2) assess the general nature of the pitching motion, including unsteady aerodynamics effects; and (3) compute the additional lateral-directional stability derivatives which arise because of the independent movement of the left and right wing panels.

Symbols

a_O = two-dimensional lift-curve slope, 1/radian

A_n = coefficients of Fourier series

b = wing span, feet

c = local chord length, feet

C_{t_1} = chord length at inboard end of control tab, feet

C_{t_2} = chord length at outboard end of control tab, feet

$\bar{c}$ = mean aerodynamic chord length, feet

C_D = drag coefficient

C_ℓ = rolling-moment coefficient

C_L = lift coefficient

$C_{L_\alpha} = \dfrac{\partial C_L}{\partial \alpha}$

C_{L_m} = lift coefficient caused by transient apparent mass effects

C_m = Free-wing-panel pitching-moment coefficient on each panel about hinge axis

C_{m_R} = Free-wing-panel pitching-moment coefficient on right panel

C_{m_L} = Free-wing-panel pitching-moment coefficient on left panel

C_n = yawing-moment coefficient

$$C_{\ell_{\delta_{t_R}}}, \ C_{\ell_{\delta_{t_L}}} = \frac{\partial C_\ell}{\partial \delta_{t_R}}, \ \frac{\partial C_\ell}{\partial \delta_{t_L}}$$

$$C_{\ell_{\delta_P}}, \ C_{\ell_{\delta_L}} = \frac{\partial C_\ell}{\partial \delta_P}, \ \frac{\partial C_\ell}{\partial \delta_L}$$

$$C_{\ell_p} = \frac{\partial C_\ell}{\partial \left(\frac{pb}{2U_o}\right)}$$

$$C_{\ell_r} = \frac{\partial C_\ell}{\partial \left(\frac{rb}{2U_o}\right)}$$

$$C_{n_{\delta_{t_R}}}, \ C_{n_{\delta_{t_L}}} = \frac{\partial C_n}{\partial \delta_{t_R}}, \ \frac{\partial C_n}{\partial \delta_{t_L}}$$

$$C_{n_{\delta_P}}, \ C_{n_{\delta_L}} = \frac{\partial C_n}{\partial \delta_P}, \ \frac{\partial C_n}{\partial \delta_L}$$

$$C_{n_p} = \frac{\partial C_n}{\partial \left(\frac{pb}{2U_o}\right)}$$

$$C_{m_{\delta_e}} = \frac{\partial C_m}{\partial \delta_e}$$

$$C_{m_\alpha} = \frac{\partial C_m}{\partial \alpha}$$

$$C_{m_{R_{\delta_{t_R}}}}, \ C_{m_{L_{\delta_{t_L}}}} = \frac{\partial C_{m_R}}{\partial \delta_{t_R}}, \ \frac{\partial C_{m_L}}{\partial \delta_{t_L}}$$

$$C_{m_{L_{\delta_{t_R}}}}, \quad C_{m_{R_{\delta_{t_L}}}} = \frac{\partial C_{m_L}}{\partial \delta_{t_R}}, \quad \frac{\partial C_{m_R}}{\partial \delta_{t_L}}$$

$$C_{m_{R_{\delta_P}}}, \quad C_{m_{L_{\delta_L}}} = \frac{\partial C_{m_R}}{\partial \delta_P}, \quad \frac{\partial C_{m_L}}{\partial \delta_L}$$

$$C_{m_{L_{\delta_P}}}, \quad C_{m_{R_{\delta_L}}} = \frac{\partial C_{m_L}}{\partial \delta_P}, \quad \frac{\partial C_{m_R}}{\partial \delta_L}$$

$$C_{m_{R_p}}, \quad C_{m_{L_p}} = \frac{\partial C_{m_R}}{\partial \left(\frac{pb}{2U_o}\right)}, \quad \frac{\partial C_{m_L}}{\partial \left(\frac{pb}{2U_o}\right)}$$

E = ratio of semiperimeter of wing to span length

G_1 = complex lift-curve slope, 1/radian

$\overline{G}_1$ = Laplace transform of G_1

g_{12}, g_{13} = constants appearing in $\overline{G}_1$

$\overline{h}$ = distance, in mean aerodynamic chord length, from quarter-chord point to hinge axis, feet

$I_{y'}$ = pitching moment of inertia of each panel about hinge axis, slug-ft^2

$\overline{I}$ = mass parameter of wing panel, Equation (B-21)

L_m = transient lift force caused by apparent mass effects, pounds

L_c = lift force caused by circulation, pounds

M = total pitching moment of wing panel about hinge axis, foot-pounds

$(M)_{\delta_t}$ = pure pitching moment caused by tab deflection, foot-pounds

$(M)_{L, D}$ = pitching moment caused by lift and drag forces, foot-pounds

P = area of one free panel

r = yaw rate, radians/second; also number of span segments used for lifting-line calculations

s = distance traveled, in half-chord lengths

t = time, seconds

U = local airspeed, feet/second

U_o = trim airspeed, feet/second

$w_{\frac{c}{2}}$ = velocity of free stream normal to half-chord point, feet/second

$\hat{x}$ = distance from origin of hinge axis system forward to half-chord point, feet

y_r = distance from center span to inboard end of free-wing panel, feet

y_{t_1} = distance from center span to inboard end of control tab, feet

y_{t_2} = distance from center span to outboard end of control tab, feet

α = angle of attack, degrees or radians

α_i = induced angle of attack, degrees

β_{mk} = multipliers for induced-angle-of-attack calculations

δ_{t_R}, δ_{t_L} = right and left control tab deflections, respectively, positive trailing edge down, radians

δ_P, δ_L = right and left wing panel deflections, respectively, positive leading edge up, radians

λ = Laplace operator, 1/second

$\hat{\lambda}$ = nondimensional Laplace operator, Equation (B-20)

ρ = atmospheric density, slugs/ft^3

θ = pitch angle, positive leading edge up, radians.

Control-Tab Geometry

For simplicity, the tab is considered to run the full span of the free-wing portions, and to be a plain flap design with a sealed gap.

With an arbitrarily chosen tab-chord ratio of 0.1, the section tab effectiveness, $C_{L_{\delta_t}}$, as given by Figure 96 of Reference B-1, is 0.3. The pitching moment effectiveness of the tab is taken from Figure 97 of the same reference, where

$$(C_{m_{\delta_t}})_{\frac{\bar{c}}{4}} = -0.55 \quad . \tag{B-1}$$

Since the airfoil section is assumed to be without camber, the lift coefficient is related to angle of attack and tab deflection through

$$C_L = C_{L_\alpha} \left[1 + C_{L_{\delta_t}} \left(\frac{\delta_t}{\alpha} \right) \right] \alpha \quad . \tag{B-2}$$

The ratio of tab deflection to angle of attack within Equation (B-2) is determined from a balance of moments about the hinge axis:

$$\frac{\delta_t}{\alpha} = \frac{\bar{h} (C_{L_\alpha} + C_D)}{(C_{m_{\delta_t}})_{\frac{\bar{c}}{4}} - \bar{h} \, C_{L_{\delta_t}} \, C_{L_\alpha}} \quad . \tag{B-3}$$

Using the last two equations, the two-dimensional trim characteristics in Figure 3 of this report were computed using

$$\left. \begin{array}{l} C_{L_\alpha} = 6.28/\text{radian} \\[2ex] C_D = .006 \quad . \end{array} \right\} \tag{B-4}$$

A similar approach is used for finite wings. The data in Figure 4 of this report were computed using the lift-curve slope and pitching moment due to tab deflection from the results of the finite wing analysis presented later in this appendix.

Pitch Dynamics of Isolated Free Wing

Following Reference B-2, a wing of aspect ratio 6 was considered to be free only to rotate in pitch about a spanwise axis. The physical situation is depicted in Figure B-1, where for convenience in the derivation, the hinge axis is shown in a far aft position to make ℓ a positive quantity. In practice, the hinge axis must be forward of the quarter-chord point for static stability.
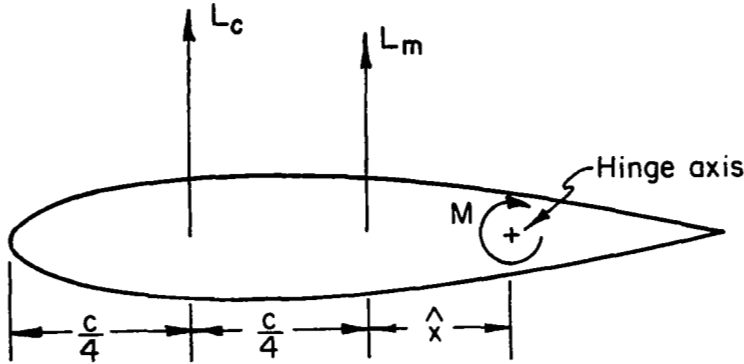
Note: Hinge axis placed in aft
position only for convenience
in derivations

FIGURE B-1. PITCHING-MOMENT ARMS

Equation (29) of Reference B-2 provides an approximate expression for the indicial response of lift coefficient to a step angle-of-attack change for an elliptic wing of aspect ratio 6.

$$C_{L_\alpha}(s) = C_{L_\alpha} [1. - 0.361 e^{-0.381s}] \quad . \tag{B-5}$$

This expression is assumed to be a sufficiently accurate approximation for other aspect ratios and planforms, with the only adjustment being to use the appropriate values of C_{L_α}.

The independent variable of Equation (B-5) is the distance traveled in half-root-chord lengths. This variable may be related to time, in seconds, by using

$$s = \frac{2U}{c} t$$

$$c = \frac{4}{\pi} \bar{c} \quad . \tag{B-6}$$

In the last equation, the mean aerodynamic chord, $\bar{c}$, is taken to be identical to the average chord length of the elliptical wing.

Equation (B-5) then becomes

$$C_{L_\alpha}(t) = C_{L_\alpha} [1. - 0.361 e^{-0.598 \frac{U}{\bar{c}} t}] \quad . \tag{B-7}$$

The corresponding transfer function relating lift coefficient to angle of attack may be obtained, as outlined in Reference B-3, by taking the Laplace transform of the time derivative of the indicial response of Equation (B-7).

$$\overline{C}_{L_\alpha} = C_{L_\alpha} \left[\frac{1}{\lambda} - \frac{0.361}{\lambda + 0.598 \frac{U}{\overline{c}}} \right] \quad . \tag{B-8}$$

The desired transfer function is, then,

$$\overline{G}_1 = \overline{C}_{L_\alpha} (\lambda) = C_{L_\alpha} \left[1 - \frac{0.361\lambda}{\lambda + 0.598 \frac{U}{\overline{c}}} \right] \quad . \tag{B-9}$$

According to Reference B-2, the circulatory lift is determined by G_1 acting on the angle of attack as defined by the normal velocity at the half-chord point, plus an incremental angle of attack caused by the effective camber due to pitching:

$$\alpha = \delta - \frac{\hat{x}}{U} \dot{\delta} + \frac{1}{2} \frac{d\delta}{ds} \quad . \tag{B-10}$$

The last term is converted to time dependence as

$$\frac{1}{2} \frac{d\delta}{ds} = \frac{\overline{c}}{\pi U} \dot{\delta} \quad . \tag{B-11}$$

The circulatory-lift contribution for one wing panel then becomes

$$L_c = \frac{\rho U^2 P}{2} G_1 \left[\delta + \left(\frac{\overline{c}}{\pi U} - \frac{\hat{x}}{U} \right) \dot{\delta} \right] \quad . \tag{B-12}$$

The lift coefficient arising from the acceleration of the apparent mass of air surrounding the wing is given in Reference B-2 as

$$C_{L_m} = \frac{\pi}{E} \frac{d\alpha}{ds} \quad . \tag{B-13}$$

Again converting to time units,

$$C_{L_m} = \frac{2 \overline{c}}{EU} \dot{\alpha} \quad . \tag{B-14}$$

The angle-of-attack rate is again based upon the local rate of change of normal velocity at the half-chord point.

Since

$$w_{\frac{c}{2}} = - \hat{x}\, \dot{\delta} + U\delta \quad , \tag{B-15}$$

then

$$\dot{\alpha} = - \frac{\hat{x}}{U}\, \ddot{\delta} + \dot{\delta} \quad . \tag{B-16}$$

Substituting Equation (B-16) into Equation (B-14), the total lift force caused by apparent mass effects is

$$L_m = \frac{\rho U \bar{P} \bar{c}}{E}\, \dot{\delta} - \frac{\rho \bar{P} \bar{c}}{E}\, x\, \ddot{\delta} \quad . \tag{B-17}$$

In Chapter 5 of Reference B-4 it is implied that the pitching moments of the wing panel may be computed by considering the circulatory lift force to act at the quarter-chord point. In addition, the L_m force is divided into two parts for the moment calculation. The first term in Equation (B-17) acts at the three-quarter-chord point, whereas the remaining term acts very near the half-chord position.

Using these moment arms, the equation describing the pitching motion about the hinge axis is

$$I_{y'}\, \ddot{\delta} = L_c \left(\hat{x} + \frac{\bar{c}}{4} \right) + \frac{\rho U \bar{P} \bar{c}}{E} \left(\hat{x} - \frac{\bar{c}}{4} \right) \dot{\delta} - \frac{\rho \bar{P} \bar{c}}{E}\, \hat{x}^2\, \ddot{\delta} \quad . \tag{B-18}$$

The characteristic equation used to compute the modes of the pitching motion is obtained by taking the Laplace transform of Equation (B-18). Then, G_1 is written as

$$\bar{G}_1 = C_{L_\alpha} \left[\frac{(1 - g_{12})\, \lambda + g_{13}\, \frac{U}{\bar{c}}}{\lambda + g_{13}\, \frac{U}{\bar{c}}} \right] \quad . \tag{B-19}$$

Multiplying the transformed version of Equation (B-18) through by the denominator of Equation (B-19), a characteristic equation is obtained which is the product of a cubic polynomial and the first-order denominator of

Equation (B-19). The first-order factor is disregarded because it describes an uncoupled stable real root. The cubic factor, on the other hand, will generally yield one stable real root and a complex conjugate pair.

The complexity of the cubic equation is reduced by employing a dimensionless form of the Laplace operator defined by

$$\lambda = \frac{2U}{\bar{c}}\,\hat{\lambda} \quad . \tag{B-20}$$

Furthermore, a mass parameter is defined as

$$\bar{I} = \frac{8I_{y'}}{\rho P \bar{c}^3} \quad . \tag{B-21}$$

The nondimensional form of the cubic characteristic equation becomes

$$\left[\bar{I} + \frac{8}{E}\left(\frac{\hat{x}}{\bar{c}}\right)^2\right]\hat{\lambda}^3 + \left[\frac{g_{13}}{2}\,\bar{I} + \frac{4g_{13}}{E}\left(\frac{\hat{x}}{\bar{c}}\right)^2 - 2\,C_{L_\alpha}\,(1 - g_{12})\left(\frac{1}{\pi} - \frac{\hat{x}}{\bar{c}}\right)\left(\frac{\hat{x}}{\bar{c}} + \frac{1}{4}\right)\right.$$
$$\left. - \frac{4}{E}\left(\frac{\hat{x}}{\bar{c}} - \frac{1}{4}\right)\right]\hat{\lambda}^2 + \left[- C_{L_\alpha}\,(1 - g_{12})\left(\frac{\hat{x}}{\bar{c}} + \frac{1}{4}\right) - g_{13}\,C_{L_\alpha}\left(\frac{1}{\pi} - \frac{\hat{x}}{\bar{c}}\right)\left(\frac{\hat{x}}{\bar{c}} + \frac{1}{4}\right)\right.$$
$$\left. - \frac{2g_{13}}{E}\left(\frac{\hat{x}}{\bar{c}} - \frac{1}{4}\right)\right]\hat{\lambda} + \left[- C_{L_\alpha}\,\frac{g_{13}}{2}\left(\frac{\hat{x}}{\bar{c}} + \frac{1}{4}\right)\right] \quad . \tag{B-22}$$

Free-Wing Aerodynamic Derivatives

Wing Geometry

The wing is considered to be composed of a short center section of constant chord, with a free-wing panel on either side. The quarter-chord lines of all sections of the wing are aligned in the spanwise direction with no sweep, and the hinge axis is parallel to the quarter-chord line.

The purpose of the center section is to approximate the effect of the fuselage between the two free panels, and the chosen span of this section, 12.5 percent, is an arbitrary value. For symmetrical deflections of the free-wing panels, the center-section geometrical angle of attack is taken to be the same as that of the outer panels; but, for asymmetric conditions, the angle of attack varies linearly between the values at the root sections of the deflected panels.

109

Application of Lifting-Line Theory

Reference (B-5) provides a convenient formulation of the application of classical lifting-line theory to the determination of the circulation distribution on finite wings of arbitrary planform and twist. The approach used in Reference (B-5) is followed closely in this study, except that the method is expanded to permit spanwise variation of airspeed caused by yawing rates and spanwise variation of geometrical angle of attack caused by roll rates. The expanded approach is outlined briefly below.

If y is the spanwise distance measured positive from the plane of symmetry to the right wing tip, a substitution of variables can be made as

$$\frac{b}{2} \cos \theta = y \quad .$$

A Fourier series can now be written in terms of θ to define the spanwise distribution of circulation. At any spanwise location, the strength of the bound vortex is related to,

$$\left(\frac{C_L c}{b} \frac{U}{U_o} \right)_k = \sum_{n=1}^{r-1} A_n \sin n \, \theta_k \quad . \tag{B-23}$$

Furthermore, the local lift coefficient is, by definition,

$$C_{L_k} = a_o (\alpha - \alpha_i)_k \quad . \tag{B-24}$$

The induced angle of attack, however, depends upon the entire circulation distribution through

$$\alpha_{i_k} = \sum_{m=1}^{r-1} \left(\frac{C_L c}{b} \frac{U}{U_o} \right)_m \beta_{mk} \quad . \tag{B-25}$$

Here, the β_{mk} are multipliers which depend only upon the number of spanwise segments, r. An expression for these multipliers is contained in Reference (B-5).

In brief, the computational process begins with assuming an initial C_L distribution. Combining this with a knowledge of wing geometry, flight

speed, and angular rates, the induced angle of attack is computed at each station by means of Equation (B-25). Then, a revised raw estimate of local C_L at each station is obtained from Equation (B-24). This raw estimate is refined through a smoothing scheme described in Reference (B-5) and the process is repeated until the change in C_L becomes less than 0.1 percent of the previous value at all wing stations.

Having found the circulation distribution, the left side of Equation (B-23) is known, and the coefficients of the Fourier series can be found as

$$A_n = \frac{2}{r} \sum_{k=1}^{r-1} \left(\frac{C_L c}{b} \frac{U}{U_o} \right)_k \sin \left(n \frac{k\pi}{r} \right) . \qquad \text{(B-26)}$$

For this study, 29 Fourier coefficients were obtained in all cases. For each wing planform and angle of attack, the lift distribution was computed six times:

(1) The first distribution was for zero tab and wing-panel deflections, and no rolling or yawing velocities. This established the wing lift coefficient, lift-curve slope, and free-wing-panel pitching moments at the reference angle of attack.

(2) Following this, the control tabs were displaced symmetrically, and by comparison with the first computation, the contribution of symmetrical tab displacement to the wing lift coefficient and the panel pitching-moment coefficients was evaluated.

(3) Next, only the right tab was deflected. From this, the direct rolling-moment and yawing-moment contributions from single tab displacement were determined, and the direct effect of single tab displacement upon the pitching moment coefficient of each panel was evaluated.

(4) With the control-tab displacements once again set to zero, the right wing panel was displaced and its contribution to the rolling, yawing, and individual panel pitching moments was determined.

(5) Following this, the panel displacements were again set to zero, and a rolling velocity was assumed. As before, the rolling-velocity contribution to the rolling, yawing, and individual panel pitching moments was established.

(6) Finally, the rolling velocity was returned to zero, but a yawing velocity was assumed to evaluate the roll-due-to-yaw rate derivative and the effects on each of the wing-panel pitching moments.

Concise expressions were derived for each of the aerodynamic parameters, in terms of the series coefficients of Equation (B-26), obviating the need for numerical integration of the forces and moments.

Wing lift coefficient:

$$C_L = \frac{\pi b^2}{4S} \left[A_1 - \frac{rb}{2U_o} \frac{A_2}{2} \right] \; . \qquad \text{(B-27)}$$

Roll-damping derivative:

$$C_{\ell_p} = - \frac{bU_o \pi}{8Sp} A_2 \; . \qquad \text{(B-28)}$$

Roll-due-to-yaw rate derivative:

$$C_{\ell_r} = \frac{\pi b}{8S} \left[- \frac{U_o}{r} A_2 + \frac{b}{4} (A_1 + A_3) \right] \; . \qquad \text{(B-29)}$$

If the input is a panel deflection or a tab deflection, δ_i,

$$C_{\ell_{\delta_i}} = - \frac{b^2 \pi}{16S\delta_i} A_2 \; . \qquad \text{(B-30)}$$

The yaw-due-to-roll derivative is,

$$C_{n_p} = - \frac{b^2 \pi}{32S} \left[A_1 + A_3 - \frac{U_o}{2pb} \sum (2n + 1) A_n A_{n+1} \right] \; . \qquad \text{(B-31)}$$

If a panel or tab deflection is the input,

$$C_{n_{\delta_i}} = \frac{b^2 \pi}{128S\delta_i} \sum (2n + 1) A_n A_{n+1} \; . \qquad \text{(B-32)}$$

The pitching moment on each free panel is composed of a pure pitching moment caused by tab deflection and the contributions of the lift and drag forces (some of which may be caused by tab deflection) acting through their respective moment arms about the hinge axis.

By direct integration, the pure pitching moment caused by tab deflection on the right panel is

$$(M)_{\delta_t} = C_{m_{\delta_t}} \frac{\rho U_o^2}{2} \delta_t [e^2 (y_{t_2} - y_{t_1}) + ef (y_{t_2} - y_{t_1})^2] \quad , \quad \text{(B-33)}$$

where

$$\left. \begin{array}{c} e = C_{t_1} - y_{t_1} \dfrac{C_{t_2} - C_{t_1}}{y_{t_2} - y_{t_1}} \\[4mm] f = \dfrac{C_{t_2} - C_{t_1}}{y_{t_2} - y_{t_1}} \end{array} \right\} \qquad \text{(B-34)}$$

The pitching moment caused by lift and drag forces is, for the right panel,

$$(M)_{L, D_R} = \bar{x} \left(1 + \frac{C_{D_o}}{a_o} \right) \frac{\rho b^2 U_o^2}{4} \left\{ A_1 \left(\frac{\sin 2\gamma}{4} - \frac{\gamma}{2} \right) + \right.$$

$$\left. \sum_{n=2}^{r-1} A_n \left[\frac{\sin (n+1)\gamma}{2(n+1)} - \frac{\sin (n-1)\gamma}{2(n-1)} \right] \right\} \quad , \qquad \text{B-35)}$$

where

$$\gamma = \cos^{-1} \left(\frac{y_r}{b/2} \right) \quad . \qquad \text{(B-36)}$$

For the left panel, the equivalent expression is

$$(M)_{L, D_L} = \bar{x} \left(1 + \frac{C_{D_o}}{a_o} \right) \frac{\rho b^2 U_o^2}{4} \left\{ A_1 \left[- \frac{\gamma}{2} - \frac{\sin 2 (\pi - \gamma)}{4} \right] + \right.$$

$$\left. \sum_{n=2}^{r-1} A_n \left[\frac{\sin (n-1)(\pi - \gamma)}{2(n-1)} - \frac{\sin (n+1)(\pi - \gamma)}{2(n+1)} \right] \right\} \quad . \qquad \text{B-37)}$$

113

The total pitching moment on either panel is

$$M = (M)_{\delta_t} + (M)_{L, D} \quad ,$$ (B-38)

from which the total pitching moment coefficient is

$$C_m = \frac{2M}{\rho U_o^2 S \bar{c}} \quad .$$ (B-39)

Each pitching-moment derivative is then obtained by dividing the pitching-moment coefficient by the appropriate variable.

For each combination of aspect ratio and taper ratio, the preceding computational procedure was performed for three angles of attack and two hinge line positions. The results of the calculations are listed in Table B-I.

References

B-1. Abbott, Ira H., and Von Doenhoff, Albert E., Theory of Wing Sections, Dover Publications, Incorporated, New York (1959).

B-2. Jones, Robert T., "The Unsteady Lift of a Wing of Finite Aspect Ratio", NACA Report 681 (1940).

B-3. Etkin, Bernard, Dynamics of Flight, John Wiley and Sons, Inc., New York (1959).

B-4. Bisplinghoff, Raymond L., Ashley, Holt, and Halfman, Robert L., Aeroelasticity, Addison-Wesley Publishing Company, Cambridge, Massachusetts (1955).

B-5. Sivells, James C., and Neely, Robert H., "Method for Calculating Wing Characteristics by Lifting-Line Theory Using Nonlinear Section Lift Data", NACA TN 1269 (1947).

TABLE B-I. COMPUTED WING AERODYNAMIC CHARACTERISTICS

All Dimensions per Radian

10 Percent Sealed Plain Control Tabs, Full Span of Free Panels

	Aspect Ratio = 6		Aspect Ratio = 8	
	Taper Ratio		Taper Ratio	
	0.6	1.0	0.6	1.0
Lift Derivatives				
C_{L_α}	4.75	4.53	4.95	4.84
$C_{L_{\delta_e}}$	1.428	1.36	1.485	1.45
Rolling-Moment Derivatives				
$C_{\ell_{\delta_{t_R}}},\ -C_{\ell_{\delta_{t_L}}}$	-0.121	-0.124	-0.133	-0.139
$C_{\ell_{\delta_P}},\ -C_{\ell_{\delta_L}}$	-0.415	-0.423	-0.454	-0.474
C_{ℓ_p}	-0.505	-0.523	-0.556	-0.593
C_{ℓ_r}	$0.206C_L$	$0.216C_L$	$0.218C_L$	$0.229C_L$
Yawing-Moment Derivatives				
$C_{n_{\delta_{t_R}}},\ -C_{n_{\delta_{t_L}}}$	$0.0007 +$ $0.0103C_L$	$0.0008 +$ $0.0115C_L$	$0.0006 +$ $0.0087C_L$	$0.0007 +$ $0.0101C_L$
$C_{n_{\delta_P}},\ -C_{n_{\delta_L}}$	$0.0082 +$ $0.0351C_L$	$0.0081 +$ $0.040C_L$	$0.0072 +$ $0.0292C_L$	$0.0084 +$ $0.0336C_L$
C_{n_p}	$-0.0867C_L$	$-0.0881C_L$	$-0.0949C_L$	$-0.0967C_L$

| | Aspect Ratio = 6 | | Aspect Ratio = 8 | |
| | Taper Ratio | | Taper Ratio | |
	0.6	1.0	0.6	1.0
Free-Wing-Panel Pitching-Moment Derivatives[a] (Hinge axis 10 percent root chord forward of quarter-chord line)				
$C_{m_{\delta_e}}$	-0.416	-0.292	-0.298	-0.296
C_{m_α}	-0.335	-0.194	-0.254	-0.208
$C_{m_{R_{\delta_{t_R}}}}$, $C_{m_{L_{\delta_{t_L}}}}$ [b]	-0.408	-0.289	-0.294	-0.293
$C_{m_{L_{\delta_{t_R}}}}$, $C_{m_{R_{\delta_{t_L}}}}$	-0.00711	-0.00385	-0.00428	-0.00315
$C_{m_{R_{\delta_P}}}$, $C_{m_{L_{\delta_L}}}$	-0.286	-0.169	-0.223	-0.185
$C_{m_{L_{\delta_P}}}$, $C_{m_{R_{\delta_L}}}$	-0.0315	-0.0166	-0.0194	-0.0143
$C_{m_{R_p}}$, $- C_{m_{L_p}}$	-0.136	-0.0837	-0.108	-0.0935

(a) All of the pitching moment derivatives, except those dependent on control tab deflection, are directly proportional to hinge margin.

(b) These derivatives are linear with hinge margin and have a value at zero hinge margin equal to the two-dimensional pitching moment due to tab deflection multiplied by the ratio of free panel area to total wing area.

APPENDIX C

DESCRIPTIONS OF HYPOTHETICAL AIRCRAFT

Introduction

Three aircraft, designated A, B, and C, were considered in this study. These aircraft range in gross weight from 3000 to 50,000 pounds. This range of weights was used to uncover any unusual characteristics which might depend upon mass and inertia properties. In addition, four wing planforms were postulated for use with each aircraft. A subscript ranging from 1 to 4 denotes the planform.

These hypothetical aircraft are patterned in a general way after existing aircraft. The design effort has been limited to the selection of the gross arrangement of components to provide a rational basis for the estimation of weights and inertias. Although the outboard hinge axis is externally supported in all three designs, no engineering details regarding support strength, etc., were considered.

Descriptions of Aircraft

Aircraft A

Aircraft A is in the light observation class and is patterned after the Cessna family of aircraft. The high wing configuration seems well suited to a simple type of external support for the outer axis bearing.

In Figure C-1, the A_1 version of this aircraft is shown, with aspect ratio of 8 and taper ratio of 1. As in the other aircraft, conventional arrangements have been preserved as much as possible to provide a meaningful comparison between the free-wing and fixed-wing counterparts.

Aircraft B

Aircraft B is a twin-engine utility aircraft, patterned loosely after the Short Skyvan utility transport, although a single vertical tail is used and

Nominal hinge axis

Full-span control tabs

Nominal total center of gravity

Nominal center of gravity wings off
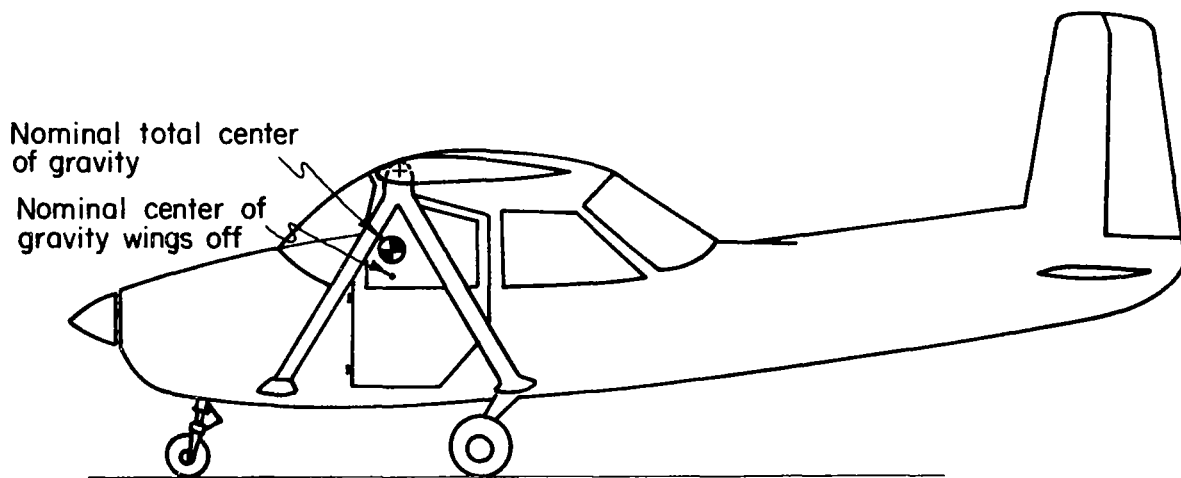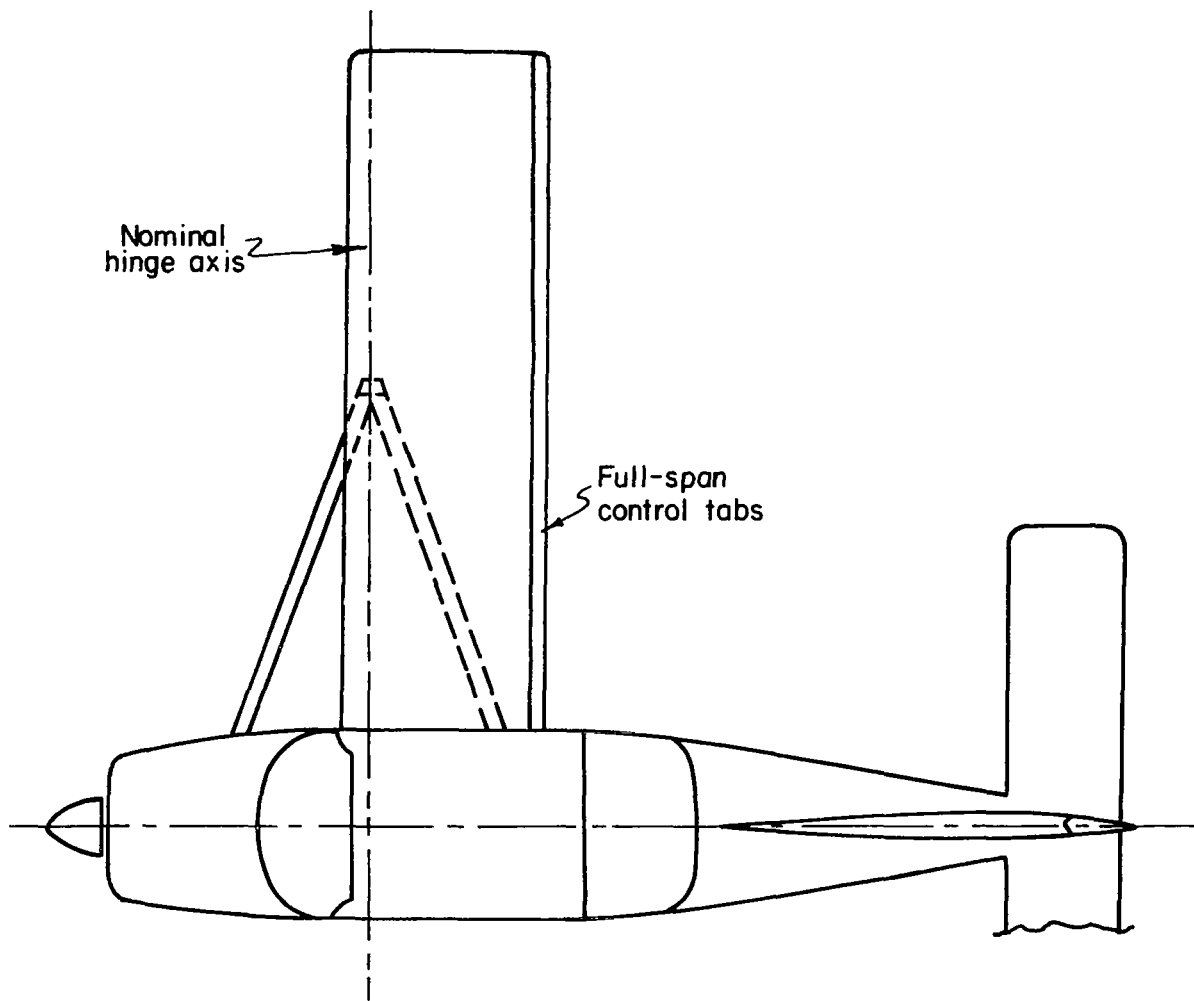
FIGURE C-1. AIRCRAFT A_1 – LIGHT OBSERVATION AIRCRAFT

the engines have been moved from wing to fuselage mounting. The overall length, general fuselage configuration, wing loading, and gross weight of 12,500 pounds are similar to those of the Skyvan. Aircraft B$_1$ is shown in Figure C-2.

Aircraft C

Aircraft C is a transport/freighter aircraft with a gross weight of 50,000 pounds, patterned roughly after the Bristol Type 170 Mk 32 freighter, although turboprop engines mounted beneath the wings are assumed. (See Figure C-3.)

Weights and Inertia Parameters

The estimation of component weights and inertia parameters was required for inclusion in the equations of motion.

Gross estimates of wing weights and structural weights were obtained from Reference C-1. These were then used with the approximate method outlined in Reference C-2 to obtain the inertia parameters.

Table C-I is a listing of the significant parameters describing each of the aircraft.

References

C-1.   Wood, K. D., Aerospace Vehicle Design, Volume I, Aircraft Design, Johnson Publishing Company, Boulder, Colorado (1963).

C-2.   USAF Stability and Control Datcom, Air Force Flight Dynamics Laboratory, Wright-Patterson Air Force Base, Ohio, Revised November, 1965.
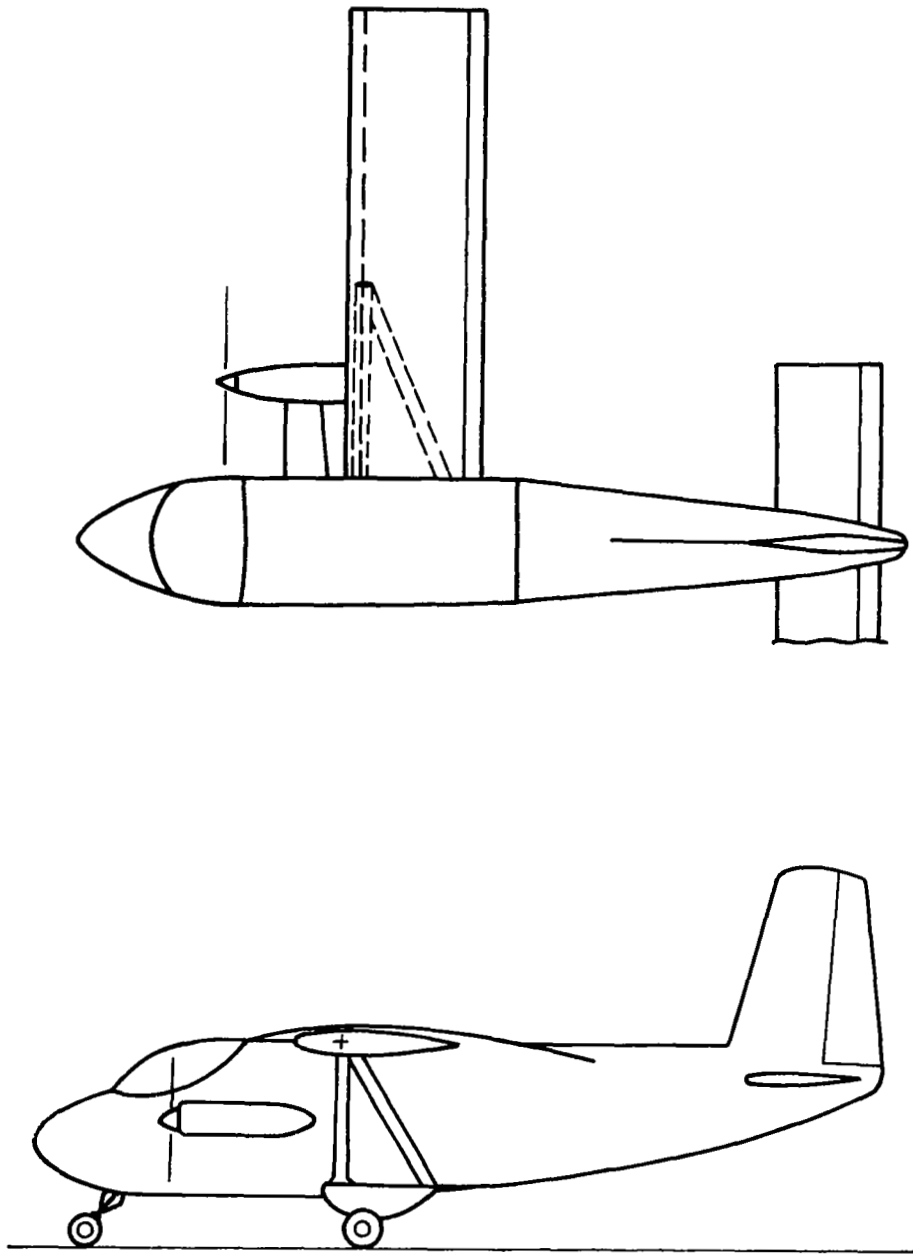
FIGURE C-2. AIRCRAFT B$_1$ — MEDIUM UTILITY AIRCRAFT
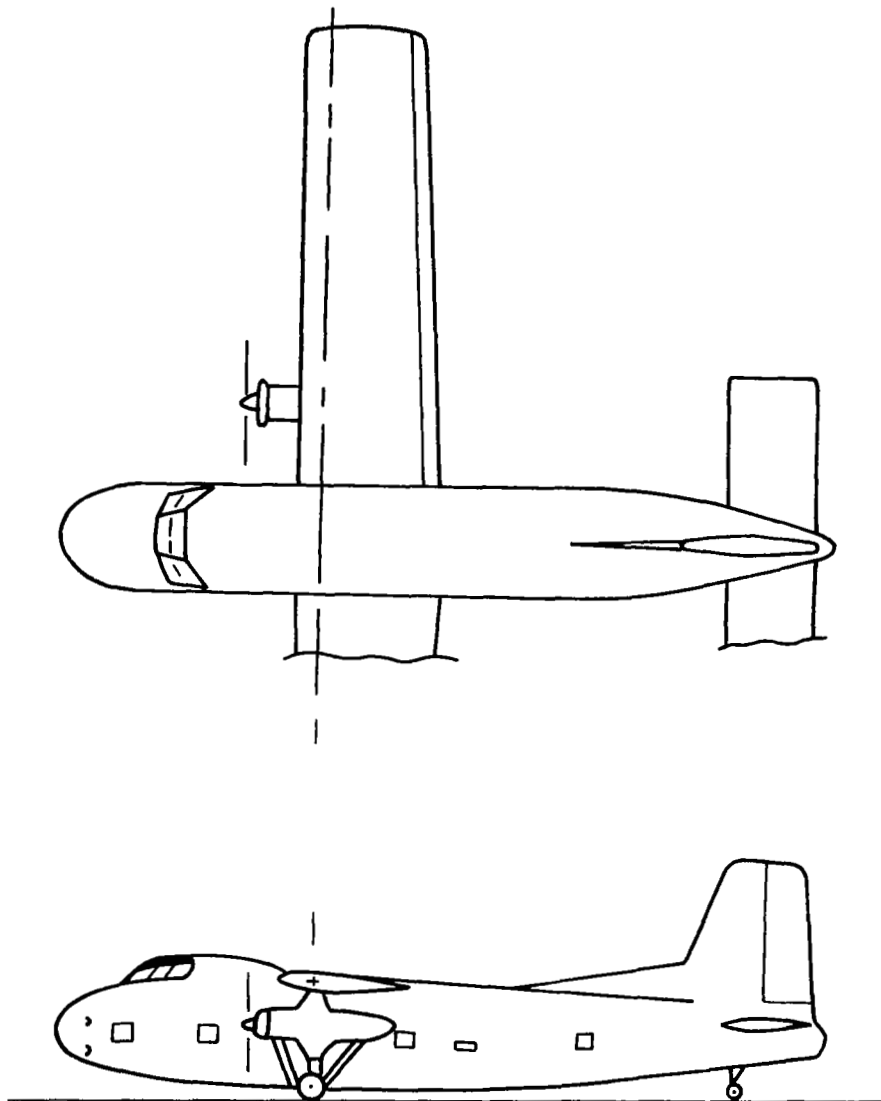
FIGURE C-3. AIRCRAFT C_2 – TRANSPORT/FREIGHTER AIRCRAFT

TABLE C-I. BASIC CHARACTERISTICS OF THREE SAMPLE FREE WING AIRCRAFT

Aircraft	Gross Weight, lb	Wing Area, ft²	Aspect Ratio	Taper Ratio	Wing Span, ft	Chords Root Tip, ft	Y'_{cg}, ft	I_{x_f}, slug-ft²	I_{y_f}, slug-ft²	I_{z_f}, slug-ft²	I_x', slug-ft²	I_y, slug-ft²	I_z', slug-ft²	$I_{x',y'}$, slug-ft²
Planform 1	3,000	214	8	1.0	41.4	5.18 5.18	$\frac{Span}{4}$	461	2,502	2,502	1,420	$31.2 + 10\,x'_{cg}{}^2$	$1451 + 10\,x'_{cg}{}^2$	$90.6\,x'_{cg}$
2	3,000	214	8	0.6	41.4	6.27 3.76	$\frac{Span}{4}$	461	2,502	2,502	1,242	--	$1271 + 10\,x'_{cg}{}^2$	$81.7\,x'_{cg}$
A 3	3,000	214	6	1.0	35.8	5.97 5.97	$\frac{Span}{4}$	461	2,502	2,502	1,089	$39.8 + 10\,x'_{cg}{}^2$	$1123 + 10\,x'_{cg}{}^2$	$78.5\,x'_{cg}$
4	3,000	214	6	0.6	35.8	7.22 4.34	$\frac{Span}{4}$	461	2,502	2,502	--	--	--	--
Planform 1	12,500	373	8	1.0	54.6	6.83 6.83	$\frac{Span}{6.0}$	8,000	22,700	22,850	4,640	$80.8 + 28.7\,x'_{cg}{}^2$	$4721 + 28.7\,x'_{cg}{}^2$	$261\,x'_{cg}$
2	12,500	373	8	0.6	54.6	8.27 4.96	$\frac{Span}{6.66}$	8,000	22,700	22,850	3,980	$85.0\,x + 28.7\,x'_{cg}{}^2$	$4065 + 28.7\,x'_{cg}{}^2$	$235\,x'_{cg}$
B 3	12,500	373	6	1.0	47.3	7.88 7.88	$\frac{Span}{6.0}$	8,000	22,700	22,850	3,485	$105.0 + 28.7\,x'_{cg}{}^2$	$3590 + 28.7\,x'_{cg}{}^2$	$226\,x'_{cg}$
4	12,500	373	6	0.6	47.3	9.5 5.7	$\frac{Span}{6.66}$	8,000	22,700	22,850	3,050	$90.5 + 28.7\,x'_{cg}{}^2$	$3141 + 28.7\,x'_{cg}{}^2$	$204\,x'_{cg}$
Planform 1	50,000	1690	8	1.0	116.3	14.52 14.52	$\frac{Span}{6.0}$	35,567	373,512	384,900	119,300	$2055 + 163\,x'_{cg}{}^2$	$121,355 + 163\,x'_{cg}{}^2$	$3160\,x'_{cg}$
2	50,000	1690	8	0.6	116.3	17.7 10.61	$\frac{Span}{6.66}$	35,567	373,512	384,900	104,600	$2120 + 163\,x'_{cg}{}^2$	$106,720 + 163\,x'_{cg}{}^2$	$2845\,x'_{cg}$
C 3	50,000	1690	6	1.0	100.7	16.8 16.8	$\frac{Span}{6.0}$	35,567	373,512	384,900	89,500	$2525 + 163\,x'_{cg}{}^2$	$92,025 + 163\,x'_{cg}{}^2$	$2740\,x'_{cg}$
4	50,000	1690	6	0.6	100.7	20.4 12.21	$\frac{Span}{6.66}$	35,567	373,512	384,900	79,300	$2980 + 163\,x'_{cg}{}^2$	$82,280 + 163\,x'_{cg}{}^2$	$2460\,x'_{cg}$

APPENDIX D

AERODYNAMIC CHARACTERISTICS OF COMPLETE AIRCRAFT

Introduction

For simplicity, and to delineate the effects of aircraft size more vividly, the nondimensional stability derivatives are assumed to be the same for all aircraft with a given wing planform. All differences in dynamic characteristics are therefore dependent upon mass and inertia effects as well as the equilibrium flight condition. Furthermore, to reduce the number of parameters to be computed, the cruise and approach lift coefficients were held fixed, respectively, for all aircraft.

Those aerodynamic parameters that are dependent only upon the wing, and which are discussed in Appendix B, are not treated in this appendix.

Symbols

A = aspect ratio

a_t = slope of lift curve for tail surface, 1/radian

b = wing span, feet

$\bar{c}$ = mean aerodynamic chord length, feet

C_D = total drag coefficient

C_{D_o} = profile drag coefficient

$C_{D_\alpha} = \dfrac{\partial C_D}{\partial \alpha}$, 1/radian

C_L = lift coefficient

$C_{L_\alpha} = \dfrac{\partial C_L}{\partial \alpha}$, 1/radian

C_ℓ = rolling moment coefficient

$$C_{\ell_p} = \frac{\partial C_\ell}{\partial \left(\frac{pb}{2U_o} \right)} \;,\; 1/\text{radian}$$

$$C_{\ell_r} = \frac{\partial C_\ell}{\partial \left(\frac{rb}{2U_o} \right)} \;,\; 1/\text{radian}$$

$$C_{\ell_\beta} = \frac{\partial C_\ell}{\partial \beta} \;,\; 1/\text{radian}$$

$$C_{\ell_{\delta_P}} = \frac{\partial C_\ell}{\partial \delta_P} \;,\; 1/\text{radian}$$

C_m = pitching-moment coefficient

$$C_{m_q} = \frac{\partial C_m}{\partial \left(\frac{q\bar{c}}{2U_o} \right)} \text{ for fuselage assembly, } 1/\text{radian}$$

$$C_{m_{f_\delta}} = \frac{\partial C_m}{\partial \delta_P} \text{ for fuselage assembly, } 1/\text{radian}$$

C_{m_R} = pitching moment of right wing panel about hinge axis

$$C_{m_{R\delta_P}} = \frac{\partial C_{m_R}}{\partial \delta_P} \;,\; 1/\text{radian}$$

$$C_{m_{R\delta_L}} = \frac{\partial C_{m_R}}{\partial \delta_L} \;,\; 1/\text{radian}$$

$$C_{m_{R\dot\delta}} = \frac{\partial C_{m_R}}{\partial \left(\frac{\dot\delta\bar{c}}{2U_o} \right)} \;,\; 1/\text{radian}$$

$$C_{m_\beta} = \frac{\partial C_{m_R}}{\partial \beta} \;,\; 1/\text{radian}$$

C_n = yawing moment coefficient

$$C_{n_p} = \frac{\partial C_n}{\partial \left(\dfrac{pb}{2U_o} \right)} \quad , \quad 1/\text{radian}$$

$$C_{n_r} = \frac{\partial C_n}{\partial \left(\dfrac{rb}{2U_o} \right)} \quad , \quad 1/\text{radian}$$

$$C_{n_\beta} = \frac{\partial C_n}{\partial \beta} \quad , \quad 1/\text{radian}$$

$$C_T = \text{thrust coefficient}$$

$$C_y = \text{sideforce coefficient}$$

$$C_{y_p} = \frac{\partial C_y}{\partial \left(\dfrac{pb}{2U_o} \right)} , \quad 1/\text{radian}$$

$$C_{y_r} = \frac{\partial C_y}{\partial \left(\dfrac{rb}{2U_o} \right)} \quad , \quad 1/\text{radian}$$

$$C_{y_{\delta_p}} = \frac{\partial C_y}{\partial \delta_p} \quad , \quad 1/\text{radian}$$

$$C_{y_\beta} = \frac{\partial C_y}{\partial \beta} \quad , \quad 1/\text{radian}$$

$$e = \text{span efficiency factor}$$

$$\overline{I} = \text{mass parameter defined in Appendix B}$$

$$\ell_t = \text{tail moment arm, feet}$$

$$p = \text{roll rate, radians/second}$$

$$q = \text{pitching rate, radian/second}$$

$$r = \text{yaw rate, radians/second}$$

$$S = \text{wing area, ft}^2$$

U_o = trim airspeed, feet/second

V_H = horizontal tail volume, $\dfrac{S_t \ell_t}{S \bar{c}}$

V_V = vertical tail volume, $\dfrac{S_t \ell_t}{S b}$

Z_{vt} = height of vertical tail center of pressure above roll axis, feet

α = angle of attack, radians

β = sideslip angle, radians

δ_P = deflection of right wing panel, L.E. up positive, radians

δ_L = deflection of left wing panel, L.E. up positive, radians

ϵ = downwash angle at horizontal tail

λ = Laplace operator, 1/sec

$\hat{\lambda}$ = dimensionless operator

$\hat{\lambda}_R$ = real component of complex root.

Subscripts,

int = interference of wing and body

f = fuselage

vt = vertical tail

w = wing.

Longitudinal Coefficients

C_D

A simple parabolic drag polar was assumed:

$$C_D = C_{D_o} + \frac{C_L^2}{\pi Ae} \quad , \qquad (D-1)$$

where

$$C_{D_o} = .027$$

$$e = 0.8$$

$$C_L = 0.343 \text{ for cruise, } 0.77 \text{ for approach.}$$

$C_{D_{\alpha_f}}$

This derivative could conceivably be zero if the equilibrium attitude of the fuselage is for minimum drag, but an arbitrary small value of .0029 was selected for all cases.

$C_{D_{\alpha_w}}$

It is assumed that the profile drag coefficient is independent of angle of attack over a small range about the trim point. Consequently, all drag changes are associated with the induced drag,

$$C_{D_{\alpha_w}} = \frac{2C_L}{\pi Ae} \quad . \qquad (D-2)$$

C_{m_α}

The neutral point of the wing alone would be at the quarter-chord point. If the influence of the body is considered, less horizontal tail, the neutral point is shifted forward because of the destabilizing influence of the fore-body and propeller effects.

The forward shift caused by the fuselage is estimated from Figure B.8.1 of Reference D-1, and was computed to be approximately 5.8 percent of the mean aerodynamic chord. A further shift of 5 percent was arbitrarily selected to account for propeller effects, placing the aerodynamic center of the wing-body combination at $0.14\,\bar{c}$. By definition, then, any pitching-moment changes with angle of attack about this point are caused by the horizontal tail.

Since $0.14\,\bar{c}$, as a hinge location, gives an 11 percent hinge margin, the C_{m_α} for the fuselage and tail assembly can be computed for this near-nominal location by simply calculating the horizontal tail contribution.

This is

$$C_{m_{\alpha_f}} = - a_t V_H \left(1 - \frac{d\epsilon}{d\alpha} \right) \quad . \tag{D-3}$$

Values used throughout were: $a_t = 4.35/\text{radian}$

$$\frac{d\epsilon}{d\alpha} = 0.4$$

The nominal value of horizontal tail volume, V_H, was 0.68.

$C_{m_{\dot\alpha}}$

From Reference D-1, assuming that horizontal tail is sole contributor,

$$C_{m_{\dot\alpha}} = - 2\, a_t V_H \frac{\ell_t}{\bar{c}} \frac{d\epsilon}{d\alpha} \quad . \tag{D-4}$$

C_{m_q}

From Reference D-1, assuming that all damping is provided by the horizontal tail,

$$C_{m_q} = - 2\, a_t V_H \frac{\ell_t}{\bar{c}} \quad . \tag{D-5}$$

$C_{m_{f_\delta}}$

It can be easily shown that the downwash effect of wing-panel deflection is

$$C_{m_{f_\delta}} = a_t V_H \frac{d\epsilon}{d\alpha} \quad . \tag{D-6}$$

$\partial C_T / \partial U$

Since all aircraft being considered are propeller driven, the assumption is made that the engine delivers constant power over the limited speed range near trim. This leads to

$$\frac{\partial C_T}{\partial U} = -3 \frac{C_D}{U} \quad . \tag{D-7}$$

Lateral-Directional Coefficients

C_{ℓ_p}

It is assumed that the entire roll-damping derivative is due to the wing contribution. Accordingly C_{ℓ_p} is obtained from Table B-I in Appendix B.

C_{ℓ_r}

Similarly, the wing contribution to the rolling moment due to yaw rate is assumed to predominate. These values were taken from Table B-I in Appendix B.

Error

An error occurred while processing this page. See the system log for more details.

The total value of the dihedral-effect derivative is obtained by summing the results of Equations (D-8), (D-9), and (D-12).

The selected nominal value of V_V was .0683.

C_{n_p}

The wing and vertical tail are both important contributors to the yawing moment due to roll rate. The wing contribution given in Table B-1 of Appendix B includes only the effect of the tilting of the lift vector. To this must be added the profile drag component which is obtained from Figure B.12.2 of Reference D-1. If the wing-profile drag coefficient is taken to be .006, this component becomes

$$C_{n_{p_{wdrag}}} = .054 \qquad . \qquad \text{(D-13)}$$

The derivation of the vertical-tail contribution is similar to that of the dihedral effect, but in this case,

$$C_{n_{p_{vt}}} = 6.6 \frac{Z_{vt}}{b} V_V \qquad . \qquad \text{(D-14)}$$

Since the span changes with aspect ratio, for fixed area, two expressions are obtained:

$$C_{n_{p_{vt}}} = 0.319\ V_V \text{ for } A = 8$$

$$C_{n_{p_{vt}}} = 0.379\ V_V \text{ for } A = 6 \qquad \text{(D-15)}$$

The total derivative is obtained by summing the value from Table B-I of Appendix B with the results of Equations (D-13) and (D-15).

C_{n_r}

It is assumed that all yaw-rate damping comes from the side force on the vertical tail induced by the yawing rate. This is estimated to be

$$C_{n_r} = -2.72\ V_V \text{ for } A = 8$$

$$C_{n_r} = -2.98\ V_V \text{ for } A = 6 \qquad \text{(D-16)}$$

$$C_{n_\beta}$$

The procedure used to compute the directional-stability parameter was to compute the effect of the side force on the vertical tail only, and then to reduce this value by 10 percent to allow for the destabilizing influence of other components of the aircraft. This approach yielded

$$C_{n_\beta} = 2.96 \, V_V \quad . \tag{D-17}$$

$$C_{y_p}$$

Only the vertical-tail contribution was considered in computing the side force due to roll rate. This became

$$C_{y_p} = -0.734 \, V_V \quad . \tag{D-18}$$

$$C_{y_r}$$

The side-force derivative due to yawing rate is computed by again considering only the vertical-tail contribution:

$$C_{y_r} = 6.6 \, V_V \quad . \tag{D-19}$$

$$C_{y_{\delta_P}}$$

Although this derivative may exist because of pressure differences on the fuselage with asymmetric panel deflections, no convenient means is available to compute its value. It was therefore assumed to be zero.

$$C_{y_\beta}$$

The side force due to sideslip was assumed to be dominated by the vertical-tail force so this derivative was estimated as

$$C_{y_\beta} = -7.57 \, V_V \text{ for } A = 8$$

$$C_{y_\beta} = -6.57 \, V_V \text{ for } A = 6 \tag{D-20}$$

$$C_{m_\beta}$$

This derivative is peculiar to the free-wing aircraft and represents the pitching moment on the wing panel (right panel) due to sideslip. As explained in the main body of this report, a nominal value of this derivative was selected. This nominal value was sized to provide steady-state cancellation of the wing contribution to $C\ell_\beta$. From the requirement for equilibrium in both the rolling-moment and pitching-moment equations, the expression for the nominal value is

$$C_{m_\beta} = \frac{C_{\ell_{\beta_w}} + C_{\ell_{\beta_{int}}}}{4C_{\ell_{\delta_P}}} \left(C_{m_{R_{\delta_P}}} - C_{m_{R_{\delta_L}}} \right) \quad . \tag{D-21}$$

$$C_{m_{R_{\dot\delta}}}$$

To approximate the damping derivative of the wing panel for asymmetric motion, a technique was developed to make use of the symmetrical-oscillatory-mode data in Figure 5 of the main body of this report.

If the stability derivatives used for asymmetric motion were used to describe the symmetric oscillation of the wing, the characteristic motion of the isolated symmetrical panel mode would be

$$-\lambda^2 + M_{R_{\dot\delta}}\lambda + (M_{R_{\delta_P}} - M_{R_{\delta_L}}) \quad . \tag{D-22}$$

The roots of this equation are

$$\lambda = \frac{2U}{\bar c} \frac{1}{2\bar I} \left[C_{m_{R_{\dot\delta}}} + j\sqrt{4\bar I\,(-C_{m_{R_{\delta_L}}} - C_{m_{R_{\delta_P}}}) - C^2_{m_{R_{\dot\delta}}}} \right] \quad . \tag{D-23}$$

The real component of the corresponding dimensionless root is

$$\hat\lambda_R = \frac{C_{m_{R_{\dot\delta}}}}{2\bar I} \quad . \tag{D-24}$$

Since the primary effect of the damping derivative is upon the real component, the selected value of the derivative is

$$C_{m_{R_{\dot\delta}}} = 2\bar I\,\hat\lambda_R \quad . \tag{D-25}$$

133

References

D-1.   Etkin, Bernard, <u>Dynamics of Flight</u>, John Wiley and Sons, Inc.,
       New York (1959).

D-2.   Campbell, John P., and McKinney, Marian O., "Summary of
       Methods for Calculating Dynamic Lateral Stability and Response
       and for Estimating Lateral Stability Derivatives", NACA
       Report 1098 (1952).

APPENDIX E

METHOD OF COMPUTING TURBULENCE RESPONSES

Symbols

b = wing span, feet

$\bar{c}$ = length of mean aerodynamic chord, feet

g_{13} = coefficient defined in Appendix B

g = quantity defined by Equation (E-11)

L = scale length of turbulence, feet

U = airspeed, feet/second

Δ = numerical value of determinant

λ = Laplace operator, 1/second

σ_x = rms value of variable x

Φ = power spectral density function

$\Phi_{\dot{\varphi}g}$ = power spectrum of rolling gust, feet/second^2

$\Phi_{\beta g}$ = power spectrum of sideslip gust, feet

Ω = spatial frequency, radius 1 foot.

Longitudinal Responses

Equation (1) of the main text of this report describes the deterministic response of the longitudinal system to the vertical gust velocity.

For random turbulence responses it is necessary to derive transfer functions for the response of each variable to the gust, and to use these transfer functions to compute the spectrum of the response in each variable of interest. The output spectrum for a variable , x, is given by

$$\Phi_x (\Omega) = \left| \frac{x}{V_g} \right|^2 \Phi(\Omega) , \qquad (E-1)$$

where $\frac{x}{V_g}$ is the modulus of a frequency response function which defines the response of the variable to the gust velocity.

The root-mean-square response of the variable is

$$\sigma_x = \left[\int_o^\infty \Phi_x(\Omega) \, d\Omega \right]^{1/2} . \qquad \text{(E-2)}$$

Expressions for the transfer functions of interest can be developed using standard techniques. For example, the transfer function relating pitch angle to vertical gust velocity is

$$\frac{\theta}{V_g}(\lambda) = \frac{\left| [A^1] \right| (\lambda)}{\left| [A] \right| (\lambda)} , \qquad \text{(E-3)}$$

where $\left| [A^1] \right|$ is the determinant of the matrix obtained by substituting the column matrix on the right side of Equation (1) for the second column of the matrix $[A]$.

Expressions for any of the other transfer functions are obtained in a similar fashion, and for the variables related by a differentiation through, for instance,

$$\frac{q}{V_g}(\lambda) = \lambda \frac{\theta}{V_g}(\lambda) . \qquad \text{(E-4)}$$

Because of the algebraic complexity of the transfer functions, no analytical derivations of these expressions were performed. Instead, the determinants of the respective matrices for the numerators and denominator were expressed in polynomials of the operator λ, by purely numerical means.

Assume, for example, that the determinant of the matrix of coefficients in the denominator of Equation (E-3) can be expressed as an nth-order polynomial, with n+1 coefficients. The technique consists of selecting n+1 arbitrary values of λ. Then, for each one of these, a unique value of the determinant of the matrix is found using a standard computer library subroutine for determinant expansion. After a value of the determinant has been found for each of the n+1 values of λ, a set of n+1 linear simultaneous algebraic equations can be formed and solved for the coefficients of the characteristic polynomial.

This technique was employed, with some modification as described below, for the numerators and the denominator of each of the transfer functions.

Then, setting $\lambda = j\omega$, the transfer functions were converted into the complex frequency response functions.

A complication exists in applying the basic technique to the longitudinal set of equations because some of the elements in the first and third rows of matrix [A] include the complex lift-curve slope function G, which contains a denominator that is, itself, a first-order polynomial in λ. Because all elements of the determinant are not simple polynomials, the determinant cannot be expressed as a simple polynomial. Instead, the determinant is,

$$\Delta = \frac{\text{Polynomial}}{\left(\lambda + g_{13} \dfrac{U}{\bar{c}}\right)^2} \ . \tag{E-5}$$

Since the same factor appears in all numerators as well as the denominator of the transfer functions, only the ratio of the polynomials is significant. For this reason, for each numerical value of λ, the corresponding value of Δ was multiplied by the denominator of Equation (E-5) to obtain

$$(\text{Polynomial})_i = \Delta_i \left(\lambda_i + g_{13} \frac{U}{\bar{c}}\right)^2 \tag{E-6}$$

The unsteady aerodynamics effects of the buildup of aerodynamic lift following penetration of a vertical gust were approximated by multiplying the vertical gust velocity by a smoothing transfer function which approximates the Kussner lift growth function.

The approximation was obtained by taking the Laplace transform of the time derivative of the indicial response to a vertical gust. The indicial-response function was obtained from Reference E-1, and although it was given therein for aspect ratio 6, it was used for aspect ratio 8 as well in this study.

$$G_2 = 1 - \frac{0.448 \, \lambda}{\lambda + 0.455 \, \dfrac{U}{\bar{c}}} - \frac{0.272 \, \lambda}{\lambda + 1.04 \, \dfrac{U}{\bar{c}}} - \frac{0.193 \, \lambda}{\lambda + 4.71 \, \dfrac{U}{\bar{c}}} \tag{E-7}$$

Lateral-Directional Responses

Equation (3) of the main body of the report describes the deterministic response of the system to rolling and sideslip gusts. Two forcing functions are present in Equation (3), and these functions are uncorrelated in the statistical sense.

Since the turbulence is assumed to be homogeneous isotropic, the vertical and side gust components measured at the same point on the airplane have the same spectrum, and both components have the same rms value. The sideslip gust is directly related to the side gust velocity, but the rolling gust is based upon the spanwise gradient of the vertical gust velocity.

Because the side and vertical gust components are uncorrelated, the total response of the aircraft, in a variable x, is computed from

$$\Phi_x (\Omega) = \left| \frac{x}{\dot{\varphi}_g} \right|^2 \Phi_{\dot{\varphi}_g} (\Omega) + \left| \frac{x}{\beta_g} \right|^2 \Phi_{\beta_g} (\Omega) \quad , \qquad (E-8)$$

where $\left| \dfrac{x}{\dot{\varphi}_g} \right|$ and $\left| \dfrac{x}{\beta_g} \right|$ are the moduli of frequency-response functions for the response of the variable x to the rolling and sideslip gusts, respectively. The spectrum of the sideslip gust is simply related to the PSD function plotted in Figure 2 of the main body of this report, and is, for unit gust intensity,

$$\Phi_{\beta_g} = \frac{L}{\pi U_o^2} \frac{1 + 3 \Omega^2 L^2}{[1 + \Omega^2 L^2]^2} \quad . \qquad (E-9)$$

The power spectrum of the rolling gust was obtained from Reference E-3, wherein a quantity, φ_2, is derived which is equivalent to one-half the rolling gust PSD function used in Equation (E-8). This rolling-gust spectrum is, for unit intensity,

$$\Phi_{\dot{\varphi}_g} (\Omega) = \frac{1}{\pi L} \left(\frac{L^2 \Omega^2}{1 + L^2 \Omega^2} \right) g^3 +$$

$$\frac{3}{2} \frac{1}{\pi L} \left[\ln \left(\frac{1 + g}{1 - g} \right) - 2g - \frac{2}{3} g^3 \right] \quad , \qquad (E-10)$$

where

$$g = \frac{\pi L/b}{\sqrt{1 + L^2 \Omega^2 + (\pi L/B)^2}} \quad . \qquad (E-11)$$

The frequency-response functions needed for Equation (E-8) are obtained by the numerical method outlined earlier, and the root-mean-square responses are computed from Equation (E-2).

References

E-1. Jones, Robert T., "The Unsteady Lift of a Wing of Finite Aspect Ratio", NACA Report 681 (1940).

E-2. Eggleston, John M., and Phillips, William H., "The Lateral Response of Airplanes to Random Atmospheric Turbulence", NASA Technical Report R-74 (1960).

E-3. Etkin, B., "A Theory of the Response of Airplanes to Random Atmospheric Turbulence", Journal of the Aero/Space Sciences (July, 1959).

APPENDIX F

TABULATED NUMERICAL RESULTS

Introduction

To provide a complete record, the results of each of the computer runs for the longitudinal and lateral-directional turbulence responses are tabulated in this appendix. For longitudinal cases, results are given for the fixed-wing aircraft and four versions of the free-wing counterpart. For lateral-directional responses, results are tabulated for the fixed-wing aircraft and the nominal free-wing equivalent. This nominal free-wing aircraft has the same vertical-tail volume as the fixed-wing aircraft and a hinge margin of 10 percent of the root chord.

All rms values are per unit turbulence intensity.

Symbols

V_H = horizontal tail volume

Longitudinal Responses

σ_{n_z} = rms load factor, g's

σ_q = rms pitch rate, degrees/second

$\sigma_{\dot{q}}$ = rms pitch acceleration, degrees/second^2

σ_{δ_P} = rms panel deflection, degrees

σ_h = rms altitude deviation, feet

Lateral-Directional Responses

σ_ϕ = rms roll angle, degrees

σ_ψ = rms yaw angle, degrees

$\sigma_{\dot{\phi}}$ = rms roll rate, degrees/second

$\sigma_{\dot{\psi}}$ = rms yaw rate, degrees/second

σ_{D_y} = rms lateral path displacement, feet

σ_{n_y} = rms lateral load factor, g's.

	Fixed Wing	Nominal Free Wing			
		10% Hinge Margin	20% Hinge Margin	10% Hinge Margin 1/2 Nominal V_H	10% Hinge Margin 1/4 Nominal V_H
			Cruise $\div$		
Phugoid Roots	$-0.0217 \pm j\ 0.181$	$-0.0226 \pm j\ 0.226$	$-0.0227 \pm j\ 0.226$	$-0.0225 \pm j\ 0.226$	$-0.0225 \pm j\ 0.226$
Short-Period Roots	$-4.04 \pm j\ 2.96$	$-2.59 \pm j\ 6.35$	$-2.74 \pm j\ 6.50$	$-1.33 \pm j\ 3.72$	$-0.668 \pm j\ 2.72$
Symmetric Panel Roots	$-$	$-8.96 \pm j\ 13.8$	$-10.7 \pm j\ 18.6$	$-8.75 \pm j\ 13.65$	$-8.69 \pm j\ 13.6$
Plunging Roots	$-$	$-25.2, -23.8$	$-26.4, -23.8$	$-25.8, -23.3$	$-26.0, -23.2$
σ_{n_z}	0.02476	0.00946	0.00634	0.00912	0.009
σ_q	0.134	0.474	0.486	0.381	0.367
$\sigma_{\dot{q}}$	1.46	3.37	3.63	1.74	1.15
σ_{δ_p}	$-$	0.0823	0.0899	0.119	0.148
σ_h	1.22	0.145	0.106	0.150	0.150
			Approach		
Phugoid Roots	$-0.0244 \pm j\ 0.277$	$-0.026 \pm j\ 0.362$	$-0.0266 \pm j\ 0.362$	$-0.0257 \pm j\ 0.362$	$-0.0255 \pm j\ 0.362$
Short-Period Roots	$-2.4 \pm j\ 1.69$	$-1.8 \pm j\ 4.15$	$-1.92 \pm j\ 4.26$	$-0.0926 \pm j\ 2.44$	$-0.462 \pm j\ 1.79$
Symmetric Panel Roots	$-$	$-6.19 \pm j\ 8.85$	$-7.38 \pm j\ 11.9$	$-6.04 \pm j\ 8.76$	$-5.99 \pm j\ 8.74$
Plunging Roots	$-$	$-16.5, -14.5$	$-17.4, -14.5$	$-16.6, -14.5$	$-16.6, -14.5$
σ_{n_z}	0.0191	0.00673	0.00453	0.00651	0.00651
σ_q	0.151	0.476	0.487	0.384	0.372
$\sigma_{\dot{q}}$	1.150	2.32	2.49	1.22	0.804
σ_{δ_p}	$-$	0.126	0.139	0.184	0.228
σ_h	2.37	0.377	0.284	0.400	0.403

TABLE F-II. LONGITUDINAL DATA, AIRCRAFT B_1

	Fixed Wing	Nominal Free Wing			
		10% Hinge Margin	20% Hinge Margin	10% Hinge Margin 1/2 Nominal V_H	10% Hinge Margin 1/4 Nominal V_H
			Cruise		
Phugoid Roots	$-0.0127 \pm j\ 0.121$	$-0.0137 \pm j\ 0.136$	$-0.0137 \pm j\ 0.136$	$-0.0137 \pm j\ 0.136$	$-0.0137 \pm j\ 0.136$
Short-Period Roots	$-2.07 \pm j\ 2.77$	$-1.27 \pm j\ 5.33$	$-1.33 \pm j\ 5.38$	$-0.644 \pm j\ 3.06$	$-0.321 \pm j\ 2.19$
Symmetric Panel Roots	--	$-13.1 \pm j\ 18.0$	$-16.3 \pm j\ 24.6$	$-13.1 \pm j\ 18.0$	$-13.0 \pm j\ 18.0$
Plunging Roots	--	$-34.8, -29.2$	$-34.7, -30.3$	$-34.2, -29.6$	$-34.6, -29.3$
σ_{n_z}	0.0206	0.00588	0.00365	0.00571	0.00567
σ_q	0.124	0.413	0.411	0.325	0.318
$\sigma_{\dot{q}}$	0.719	2.33	2.37	1.10	0.749
$\sigma_{\delta P}$	--	0.0829	0.0853	0.116	0.153
σ_h	0.659	0.0540	0.0411	0.056	0.0568
			Approach		
Phugoid Roots	$-0.0137 \pm j\ 0.197$	$-0.0177 \pm j\ 0.233$	$-0.0177 \pm j\ 0.233$	$-0.0176 \pm j\ 0.233$	$-0.0175 \pm j\ 0.233$
Short-Period Roots	$-0.60 \pm j\ 1.66$	$-0.964 \pm j\ 3.51$	$-1.01 \pm j\ 3.56$	$-0.488 \pm j\ 2.02$	$-0.241 \pm j\ 1.45$
Symmetric Panel Roots	--	$-9.38 \pm j\ 10.7$	$-11.5 \pm j\ 14.5$	$-9.30 \pm j\ 10.6$	$-9.28 \pm j\ 10.6$
Plunging Roots	--	$-22.05, -17.02$	$-23.05, -17.04$	$-22.1, -17.0$	$-22.1, -17.0$
σ_{n_z}	0.0154	0.00442	0.00279	0.00429	0.00427
σ_q	0.103	0.406	0.411	0.326	0.321
$\sigma_{\dot{q}}$	0.571	1.582	1.62	0.766	0.519
$\sigma_{\delta P}$	--	0.126	0.131	0.179	0.235
σ_h	1.04	0.111	0.0875	0.117	0.119

	Fixed Wing	Nominal Free Wing			
		10% Hinge Margin	20% Hinge Margin	10% Hinge Margin 1/2 Nominal V_H	10% Hinge Margin 1/4 Nominal V_H
Cruise					
Phugoid Roots	$-0.0116 \pm j\,0.102$	$-0.0123 \pm j\,0.122$	$-0.0124 \pm j\,0.122$	$-0.0123 \pm j\,0.122$	$-0.0123 \pm j\,0.122$
Short-Period Roots	$-2.04 \pm j\,1.88$	$-1.29 \pm j\,3.73$	$-1.35 \pm j\,3.79$	$-0.660 \pm j\,2.16$	$-0.332 \pm j\,1.57$
Symmetric Panel Roots	--	$-8.16 \pm j\,9.59$	$-9.95 \pm j\,13.0$	$-8.06 \pm j\,9.54$	$-8.03 \pm j\,9.52$
Plunging Roots	--	$-19.2, \; -15.2$	$-20.2, \; -15.2$	$-19.3, \; -15.2$	$-19.3, \; -15.2$
σ_{n_z}	0.0220	0.00762	0.00487	0.00763	0.00729
σ_q	0.0781	0.2727	0.277	0.212	0.202
$\sigma_{\dot{q}}$	0.516	1.17	1.23	0.574	0.372
σ_{δ_P}	--	0.0804	0.086	0.113	0.142
σ_h	0.906	0.0777	0.490	0.083	0.085
Approach					
Phugoid Roots	$-0.0174 \pm j\,0.181$	$-0.0177 \pm j\,0.248$	$-0.0180 \pm j\,0.248$	$-0.0172 \pm j\,0.248$	$-0.0170 \pm j\,0.248$
Short-Period Roots	$-1.84 \pm j\,0.938$	$-1.15 \pm j\,2.29$	$-1.21 \pm j\,2.36$	$-0.589 \pm j\,1.35$	$-0.297 \pm j\,1.00$
Symmetric Panel Roots	--	$-5.54 \pm j\,4.30$	$-6.77 \pm j\,5.78$	$-5.44 \pm j\,4.26$	$-5.40 \pm j\,4.25$
Plunging Roots	--	$-12.9, \; -7.53$	$-13.1, \; -7.53$	$-12.9, \; -7.53$	$-12.96, \; -7.53$
σ_{n_z}	0.0174	0.00618	0.00392	0.00609	0.00603
σ_q	0.0803	0.261	0.275	0.208	0.197
$\sigma_{\dot{q}}$	0.492	0.816	0.872	0.425	0.266
σ_{δ_P}	--	0.126	0.141	0.181	0.220
σ_h	1.51	0.241	0.156	0.265	0.274

TABLE F-IV. LONGITUDINAL DATA, AIRCRAFT A3

	Fixed Wing	Nominal Free Wing			
		10% Hinge Margin	20% Hinge Margin	10% Hinge Margin 1/2 Nominal V_H	10% Hinge Margin 1/4 Nominal V_H
		Cruise			
Phugoid Roots	$-0.0228 \pm j\,0.180$	$-0.0239 \pm j\,0.226$	$-0.0240 \pm j\,0.226$	$-0.0239 \pm j\,0.226$	$-0.0239 \pm j\,0.226$
Short-Period Roots	$-4.41 \pm j\,2.73$	$-2.89 \pm j\,6.65$	$-3.11 \pm j\,6.87$	$-1.49 \pm j\,5.01$	$-0.699 \pm j\,5.19$
Symmetric Panel Roots	--	$-8.90 \pm j\,12.2$	$-10.5 \pm j\,16.4$	$-8.60 \pm j\,12.04$	$-8.56 \pm j\,12.05$
Plunging Roots	--	$-22.3,\ -20.5$	$-23.4,\ -20.5$	$-22.9,\ -20.1$	$-22.7,\ -20.2$
σ_{n_z}	0.0239	0.00942	0.00627	0.00925	0.00963
σ_q	0.141	0.465	0.485	0.460	0.647
$\sigma_{\dot{q}}$	1.58	3.43	3.77	2.48	3.32
σ_{δ_P}	0.0937	0.0735	0.0834	0.0952	0.114
σ_h	1.23	0.159	0.115	0.159	0.155
		Approach			
Phugoid Roots	$-0.0282 \pm j\,0.275$	$-0.0307 \pm j\,0.362$	$-0.0311 \pm j\,0.362$	$-0.0306 \pm j\,0.362$	$-0.0309 \pm j\,0.362$
Short-Period Roots	$-3.11 \pm j\,1.41$	$-2.01 \pm j\,4.32$	$-2.18 \pm j\,4.49$	$-1.03 \pm j\,3.28$	$-0.483 \pm j\,3.41$
Symmetric Panel Roots	--	$-6.13 \pm j\,7.80$	$-7.20 \pm j\,10.4$	$-5.92 \pm j\,7.69$	$-5.88 \pm j\,7.69$
Plunging Roots	--	$-14.67,\ -12.55$	$-15.5,\ -12.6$	$-14.7,\ -12.5$	$-14.7,\ -12.5$
σ_{n_z}	0.0185	0.00671	0.00451	0.00662	0.00698
σ_q	0.157	0.466	0.485	0.461	0.645
$\sigma_{\dot{q}}$	1.24	2.36	2.59	1.68	2.20
σ_{δ_P}	--	0.113	0.129	0.146	0.172
σ_h	2.28	0.413	0.314	0.415	0.447

	Fixed Wing	Nominal Free Wing		10% Hinge Margin 1/2 Nominal V_H	10% Hinge Margin 1/4 Nominal V_H
		10% Hinge Margin	20% Hinge Margin		
			Cruise		
Phugoid Roots	$-0.0134 \pm j\,0.121$	$-0.0145 \pm j\,0.136$	$-0.0145 \pm j\,0.136$	$-0.0145 \pm j\,0.136$	$-0.0145 \pm j\,0.136$
Short-Period Roots	$-2.24 \pm j\,2.79$	$-1.43 \pm j\,5.68$	$-1.51 \pm j\,5.74$	$-0.716 \pm j\,4.1$	$-0.323 \pm j\,4.15$
Symmetric Panel Roots	--	$-12.62 \pm j\,15.5$	$-15.4 \pm j\,21.1$	$-12.5 \pm j\,15.4$	$-12.5 \pm j\,15.4$
Plunging Roots	--	$-30.1, -26.0$	$-32.2, -25.5$	$-30.9, -25.5$	$-31.0, -25.4$
σ_{n_z}	0.0196	0.00593	0.00361	0.00590	0.00630
σ_q	0.126	0.414	0.414	0.410	0.605
$\sigma_{\dot{q}}$	0.779	2.47	2.53	1.75	2.52
σ_{δ_p}	--	0.0765	0.0799	0.103	0.141
σ_h	0.660	0.059	0.0444	0.059	0.058
			Approach		
Phugoid Roots	$-0.0163 \pm j\,0.196$	$-0.0207 \pm j\,0.233$	$-0.0207 \pm j\,0.233$	$-0.0207 \pm j\,0.233$	$-0.0208 \pm j\,0.233$
Short-Period Roots	$-1.73 \pm j\,1.61$	$-1.08 \pm j\,3.74$	$-1.15 \pm j\,3.79$	$-5.41 \pm j\,2.72$	$-0.242 \pm j\,2.76$
Symmetric Panel Roots	--	$-8.84 \pm j\,8.97$	$-10.3 \pm j\,12.2$	$-8.75 \pm j\,8.92$	$-8.74 \pm j\,8.92$
Plunging Roots	--	$-20.1, -14.7$	$-20.9, -14.8$	$-20.1, -14.7$	$-20.1, -14.7$
σ_{n_z}	0.0148	0.00448	0.00283	0.00445	0.00475
σ_q	0.106	0.411	0.413	0.408	0.601
$\sigma_{\dot{q}}$	0.617	1.67	1.73	1.17	1.67
σ_{δ_p}	--	0.116	0.123	0.155	0.209
σ_h	1.06	0.128	0.102	0.128	0.124

TABLE F-VI. LONGITUDINAL DATA, AIRCRAFT C_3

	Fixed Wing	Nominal Free Wing			
		10% Hinge Margin	20% Hinge Margin	10% Hinge Margin 1/2 Nominal V_H	10% Hinge Margin 1/4 Nominal V_H
		Cruise			
Phugoid Roots	$-0.0122 \pm j\,0.101$	$-0.0130 \pm j\,0.122$	$-0.0131 \pm j\,0.122$	$-0.0130 \pm j\,0.122$	$-0.0131 \pm j\,0.122$
Short-Period Roots	$-2.22 \pm j\,1.84$	$-1.46 \pm j\,3.94$	$-1.54 \pm j\,4.03$	$-0.739 \pm j\,2.91$	$-0.344 \pm j\,2.98$
Symmetric Panel Roots	--	$-7.99 \pm j\,8.09$	$-9.68 \pm j\,10.98$	$-7.87 \pm j\,8.02$	$-7.85 \pm j\,8.02$
Plunging Roots	--	$-17.8,\; -13.2$	$-18.6,\; -13.2$	$-17.9,\; -13.2$	$-17.9,\; -13.2$
σ_{n_z}	0.0211	0.00754	0.0048	0.00746	0.00786
σ_q	0.0817	0.270	0.277	0.265	0.382
$\sigma_{\dot{q}}$	0.557	1.22	1.29	0.845	1.15
σ_{δ_p}	--	0.0728	0.0799	0.0948	0.121
σ_h	0.903	0.0855	0.0534	0.0857	0.0819
		Approach			
Phugoid Roots	$-0.0198 \pm j\,0.180$	$-0.0206 \pm j\,0.247$	$-0.0208 \pm j\,0.247$	$-0.0206 \pm j\,0.247$	$-0.0209 \pm j\,0.248$
Short-Period Roots	$-2.01 \pm j\,0.764$	$-1.30 \pm j\,2.38$	$-1.37 \pm j\,2.48$	$-0.664 \pm j\,1.83$	$-0.318 \pm j\,1.93$
Symmetric Panel Roots	--	$-5.04 \pm j\,3.43$	$-6.10 \pm j\,4.57$	$-4.90 \pm j\,3.40$	$-4.88 \pm j\,3.40$
Plunging Roots	--	$-12.8,\; -6.5$	$-13.0,\; -6.52$	$-12.9,\; -6.52$	$-12.9,\; -6.52$
σ_{n_z}	0.0168	0.00618	0.00394	0.00618	0.00637
σ_q	0.0858	0.256	0.273	0.250	0.349
$\sigma_{\dot{q}}$	0.528	0.835	0.904	0.561	0.687
σ_{δ_p}	--	0.113	0.131	0.143	0.163
σ_h	1.50	0.272	0.179	0.273	0.253

TABLE F-VII. LATERAL-DIRECTIONAL DATA, AIRCRAFT A

	A_1		A_2		A_3	
	Fixed	Free	Fixed	Free	Fixed	Free
Cruise						
Dutch-Roll Roots	$-0.0763 \pm j\ 3.58$	$-0.0759 \pm j\ 3.58$	$-0.808 \pm j\ 3.69$	$-0.812 \pm j\ 3.70$	$-0.671 \pm j\ 3.56$	$-0.664 \pm j\ 3.57$
Spiral Root	-0.000145	0.0246	-0.00116	0.0181	-0.00117	0.0224
Roll-Mode Root	-6.58	-0.639	-6.89	-0.717	-5.38	-0.463
Asymmetric Panel Root	$--$	$-10.9 \pm j\ 14.8$	$--$	$-10.7 \pm j\ 16.2$	$--$	$-10.7 \pm j\ 12.8$
σ_ϕ	0.365	0.297	0.366	0.315	0.375	0.285
σ_ψ	0.261	0.262	0.260	0.262	0.266	0.269
$\sigma_{\dot\phi}$	0.403	0.303	0.410	0.321	0.425	0.317
$\sigma_{\dot\psi}$	0.470	0.478	0.475	0.481	0.491	0.502
σ_{D_y}	1.140	1.000	1.140	1.050	1.170	0.963
σ_{n_y}	0.00724	0.00578	0.00722	0.00598	0.00735	0.00556
Approach						
Dutch-Roll Roots	$-0.523 \pm j\ 2.44$	$-0.437 \pm j\ 2.44$	$-0.554 \pm j\ 2.52$	$-0.462 \pm j\ 2.52$	$0.446 \pm j\ 2.43$	$-0.336 \pm j\ 2.411$
Spiral Root	0.0335	0.184	0.0322	0.172	0.0359	0.171
Roll-Mode Root	-4.68	-0.783	-4.90	-0.860	-3.87	-0.662
Asymmetric Panel Root	$--$	$-7.65 \pm j\ 9.77$	$--$	$-7.55 \pm j\ 10.7$	$--$	$-7.56 \pm j\ 8.41$
σ_ϕ	0.412	0.270	0.413	0.286	0.422	0.271
σ_ψ	0.382	0.316	0.381	0.330	0.391	0.344
$\sigma_{\dot\phi}$	0.413	0.335	0.421	0.363	0.436	0.368
$\sigma_{\dot\psi}$	0.482	0.511	0.487	0.520	0.506	0.553
σ_{D_y}	1.30	0.766	1.30	0.812	1.32	0.729
σ_{n_y}	0.00748	0.00470	0.00751	0.00484	0.00759	0.00445

TABLE F-VIII. LATERAL-DIRECTIONAL DATA, AIRCRAFT B

	B_1		B_2		B_3	
	Fixed	Free	Fixed	Free	Fixed	Free
Cruise						
Dutch-Roll Roots	$-0.542 \pm j\, 3.44$	$-0.537 \pm j\, 3.45$	$-0.563 \pm j\, 3.51$	$-0.564 \pm j\, 3.52$	$-0.583 \pm j\, 3.56$	$-0.581 \pm j\, 3.57$
Spiral Root	-0.000058	0.0155	-0.000701	0.0112	-0.000709	0.0146
Roll-Mode Root	-5.35	-0.554	-5.41	-0.602	-5.40	-0.473
Asymmetric Panel Root	$--$	$-15.6 \pm j\, 20.1$	$--$	$-14.9 \pm j\, 22.0$	$--$	$-12.6 \pm j\, 17.2$
σ_ϕ	0.282	0.228	0.290	0.239	0.291	0.230
σ_ψ	0.186	0.187	0.185	0.186	0.184	0.186
$\sigma_{\dot\phi}$	0.341	0.270	0.346	0.284	0.349	0.279
$\sigma_{\dot\psi}$	0.404	0.411	0.406	0.409	0.405	0.410
σ_{D_y}	0.884	0.755	0.885	0.785	0.889	0.761
σ_{n_y}	0.00577	0.00440	0.00575	0.00449	0.00573	0.00435
Approach						
Dutch-Roll Roots	$-0.398 \pm j\, 2.36$	$-0.331 \pm j\, 2.35$	$-0.412 \pm j\, 2.40$	$-0.342 \pm j\, 2.40$	$-0.322 \pm j\, 2.28$	$-0.261 \pm j\, 2.27$
Spiral Root	0.0219	0.132	0.0210	0.122	0.0234	0.122
Roll-Mode Root	-4.15	-0.675	-4.21	-0.727	-3.18	-0.545
Asymmetric Panel Root	$--$	$-11.96 \pm j\, 12.81$	$--$	$-11.5 \pm j\, 14.2$	$--$	$-11.8 \pm j\, 10.2$
σ_θ	0.345	0.248	0.346	0.261	0.355	0.250
σ_ψ	0.283	0.267	0.282	0.270	0.294	0.288
$\sigma_{\dot\phi}$	0.363	0.316	0.369	0.343	0.383	0.354
$\sigma_{\dot\psi}$	0.417	0.451	0.419	0.456	0.439	0.488
σ_{D_y}	1.07	0.701	1.07	0.733	1.08	0.649
σ_{n_y}	0.00629	0.00413	0.00623	0.00424	0.00637	0.00382

TABLE F-IX. LATERAL-DIRECTIONAL DATA, AIRCRAFT C

	C_1		C_2		C_3	
	Fixed	Free	Fixed	Free	Fixed	Free

Cruise

Dutch-Roll Roots	$-0.458 \pm j\,2.28$	$-0.458 \pm j\,2.28$	$-0.477 \pm j\,2.33$	$-0.483 \pm j\,2.33$	$-0.497 \pm j\,2.38$	$-0.506 \pm j\,2.38$
Spiral Root	-0.0000788	0.0137	-0.000629	0.010	-0.000636	0.0130
Roll-Mode Root	-5.73	-0.497	-6.00	-0.567	-6.43	-0.443
Asymmetric Panel Root	$--$	$-11.2 \pm j\,11.8$	$--$	$-11.0 \pm j\,13.05$	$--$	$-9.95 \pm j\,10.5$
σ_ϕ	0.239	0.198	0.240	0.210	0.242	0.207
σ_ψ	0.169	0.170	0.168	0.169	0.167	0.169
$\sigma_{\dot\phi}$	0.246	0.208	0.251	0.224	0.256	0.225
$\sigma_{\dot\psi}$	0.272	0.275	0.274	0.275	0.275	0.277
σ_{D_y}	0.738	0.621	0.739	0.654	0.742	0.643
σ_{n_y}	0.00530	0.00404	0.00528	0.00411	0.00528	0.00405

Approach

Dutch-Roll Roots	$-0.414 \pm j\,1.54$	$-0.340 \pm j\,1.57$	$-0.430 \pm j\,1.58$	$-0.350 \pm j\,1.60$	$-0.346 \pm j\,1.52$	$-0.273 \pm j\,1.53$
Spiral Root	0.0230	0.131	0.0221	0.123	0.0247	0.123
Roll-Mode Root	-5.16	-0.600	-5.41	-0.676	-4.36	-0.506
Asymmetric Panel Root	$--$	$-10.1 \pm j\,7.01$	$--$	$-9.93 \pm j\,8.02$	$--$	$-10.4 \pm j\,5.04$
σ_ϕ	0.293	0.235	0.295	0.250	0.307	0.250
σ_ψ	0.272	0.255	0.271	0.258	0.281	0.277
$\sigma_{\dot\phi}$	0.255	0.239	0.260	0.260	0.277	0.267
$\sigma_{\dot\psi}$	0.284	0.302	0.286	0.308	0.294	0.326
σ_{D_y}	0.937	0.637	0.939	0.664	0.961	0.627
σ_{n_y}	0.00572	0.00424	0.00572	0.00430	0.00591	0.00415